Energy Education and Research Collaboration EERC

Second Quarterly Report
Phase II
October 30, 2009

Prepared by

Prof. Nariman Farvardin, Provost

Principal Investigator and EERC Project Director

Prof. Avram Bar-Cohen, Chair

EERC Project Deputy Director

Dr. Azar Nazeri

EERC Research Manager

THE UNIVERSITY OF MARYLAND AND THE PETROLEUM INSTITUTE OF ABU DHABI, UAE

EERC Key Contributors

University of Maryland – College Park, MD, USA

Shapour Azarm
Balakumar Balachandran
David Bigio
H.A. Bruck
Nikil Chopra
Avram Bar-Cohen
Serguei Dessiatoun
Bryan Eichhorn
Ashwani K. Gupta
Satyandra K. Gupta
Yunho Hwang
Greg Jackson
P.K. Kannan
Mohammad Modarres
Reinhard Radermacher
Amir Shooshtari

Petroleum Institute – Abu Dhabi, UAE

Ahmed Abdala
Youssef Abdel-Majid
Ahmed Al Shoaibi
Ali Almansoori
Saleh Al Hashimi
Ebrahim Al-Hajri, Returning ADNOC Scholar
Valerie Eveloy
Sai Cheong Fok
Afshin Goharzadeh
Hamad Karki
Rocky Kubo
Ahmed Nafees
Michael Ohadi
Peter Rodgers
Abdennour Seibi

Table of Contents

Executive Summary

The following is a summary of the major project activities that have taken place over the completed quarter. For more details, see the individual reports in the last section of this report.

Thrust 1: Energy Recovery and Conversion

Sulfur Recovery from Gas Stream using Flameless and Flame Combustion Reactor
A.K. Gupta, A. Al Shoaibi

- Examined further the mixing characteristics and degree of mixing in the flow field of a non-reactive flow field.
- Examined for further reduction the H_2S/O_2 reaction mechanism with the 24-reduced mechanism we developed in a previous report.
- Performed equilibrium analysis for the Claus reactor and detailed kinetic analysis for the H_2S/O_2 reaction mechanism.

Solid Oxide Fuel Cell Systems for Operation on Petroleum Off-Gases with Contaminants
G. Jackson, B. Eichhorn, A. Almansoori, V. Eveloy, A. Nafees

- Began work on automated operation for long-term durability tests.
- Began joint publication on SOFC experimental studies with syngas and n-butane/H_2O direct feeds.
- Used MEA models to fit experimental data to validate models before integration into system-level models.
- Identified a system for process model development in Aspen/Hisys at PI with support from UMD.

Separate Sensible and Latent Cooling with Solar Energy
R. Radermacher, Y. Hwang, I. Kubo

- Investigated the performance of sensible vapor compression cycle using the EES.
- Investigated the hybrid solar system performance under Abu Dhabi's climate conditions.
- Explored the optimization capability of MATLAB.
- Coupled the TRNSYS with MATLAB.

Waste Heat Utilization in the Petroleum Industry
R. Radermacher, Y. Hwang, S. Al Hashimi, P. Rodgers

The following were modeled in HYSYS:
- APCI base cycle
- APCI enhanced with absorption chillers
- Gas turbine
- Different gas turbine combined cycle configurations (double pressure, triple pressure with and without reheat)

Thrust 2: Energy-Efficient Transport Process Projects

Multidisciplinary Design and Characterization of Polymer Composite Seawater Heat Exchanger Module

P. Rodgers, A. Bar-Cohen, S.K. Gupta, D. Bigio, H.A. Bruck

- Continued investigation on the mechanical and surface effects of immersing polymer composites in fresh and saltwater.
- Began investigation on effect of varying injection molding and material conditions on fiber orientation.
- Characterized the suitability of injection molding for creating thermally enhanced polymer heat exchangers.
- Began training on use of equipment for creating and using molds to validate results from Moldflow analysis.
- Integrated the mold-filling meta-model in the design process of a modular heat exchanger.
- Investigated parametrically the use of an effective isotropic thermal conductivity for fins with local anisotropy.
- Commissioned ENGEL Victory Tech 200/70 injection-molding machine at PI.

Study on Microchannel-Based Absorber/Stripper and Electrostatic Precipitators for CO^2 Separation from Flue Gas

S. Dessiatoun, A. Shooshtari, M. Ohadi, A. Goharzadeh

- Finished building the test setup.
- Generated water droplets.
- Tested the separator performance.

Microreactors for Oil and Gas Processes Using Microchannel Technologies

S. Dessiatoun, A. Shooshtari, M. Ohadi, A. Goharzadeh, E. Al-Hairi

- Performed literature survey.
- Identified target reaction.

Thrust 3: Energy System Management

Integration of Engineering and Business Decisions for Robust Optimization of Petrochemical Systems

S. Azarm, P.K. Kannan, A. Almansoori, S. Al Hashimi

- Continued the focus on integrating business and engineering decisions in the context of oil, gas and petrochemical systems.
- Applied a collaborative optimization technique to decompose business and engineering problems and obtain optimal decisions for a simple case study model.
- Studied the optimal decisions from the case study that provide insights into both business and engineering problems.

- Began research on the decision support role of dashboards for the management in the integration framework and developed a preliminary dashboard using Matlab Graphical User Interface (GUI).
- Prepared four papers based on the collaboration.

Dynamics and Control of Drill Strings
B. Balachandran, H. Karki, Y. Abdelmagid

- Conducted experiments to examine the system behavior and compare it with predictions obtained through the Hamiltonian formulation.
- Collaborated with Professor S.P. Singh on fundamental studies on the stick-slip interactions and reduced-order models.

Studies on Mobile Sensor Platforms
B. Balachandran, N. Chopra, H. Karki, S.C. Fok

- Carried out numerical simulations.
- Visited industry to get a better understanding of the inspection system, the ultrasonic and magnetic flux sensors used as a part of the inspection system, the harshness of the environment, and the complexity of the system.

Development of a Probabilistic Model for Degradation Effects of Corrosion-Fatigue Cracking in Oil and Gas Pipelines
M. Modarres, A. Seibi

- Further assessed and justified model developed by Dr. M. Chookah.
- Double-checked programs written in MATLAB.
- Ran WinBugs and Weibull analyses again to supplement data and further justify results.
- Prepared paper for submission for a journal.
- Conducted pitting corrosion experiments in a small-scale corrosion-fatigue chamber.
- Gathered information about requirements for a heating chamber.
- Used Cortest rig to further verify and reduce epistemic uncertainties associated with the corrosion-fatigue model.

Introduction

The second quarter of the collaboration has witnessed great progress across all the projects plus other achievements that are highlighted in this section. The second year of the summer internship program was a great success with more than twice the number of junior students than last year and one female graduate student participating. Professor Mikhail Anisimov completed his sabbatical at PI and several professors from both institutions had fruitful visits to each other's campuses. Moreover, two ADNOC scholars finished their PhD programs and one has started his career as a PI faculty member. We also saw the graduations of students who were supported by EERC, and new GRAs have joined the collaborations. Details about these accomplishments are presented below.

Summer Student Internships

For the second year, ten PI juniors and one graduate student participated in the UMD summer internship program. In this program, PI students visit UMD for seven weeks over the summer to work with a UMD professor and graduate students on a current EERC or other UMD research project. The EERC Summer Internship Program is an important part of the educational arm of the EERC, providing PI students with the opportunity to study with UMD professors who are world leaders in their fields, to interact with graduate students from UMD's culturally diverse Clark School of Engineering, and to experience life in the United States, if only for a short time.

The aims of the program are to provide students with valuable research and engineering skills through working on actual EERC and other UMD research projects, to give them experience collaborating with students and professionals from diverse backgrounds, to encourage them to pursue graduate education, and to expose them to a variety of cultural experiences through travel abroad. The second year of this program was highly successful, and we anticipate many more years of this fruitful exchange of students and ideas.

Group trip to Boston.

Nalah Al Amoodi at work in the lab.

Visit to Waste-to-Energy Facility

Professor A.K. Gupta took the interns to visit the Wheelabrator Baltimore waste-to-energy facility, which provides dependable, environmentally safe disposal of municipal solid waste for the City and County of Baltimore, Maryland while generating clean electricity for sale to the local utility. The Baltimore facility, designed, constructed, owned and operated by Wheelabrator Technologies Inc., processes up to 2,250 tons per day of municipal solid waste. At full capacity, the plant can generate more than 60,000 kilowatts of electrical energy for sale to Baltimore Gas & Electric Company. This is the equivalent of supplying all of the electrical needs of 50,000 homes. Steam is also supplied by the plant to Trigen Baltimore Corporation for the downtown heating loop.

UMD Nuclear Reactor and Washington D.C.
Locally, students also visited the nuclear reactor on the UMD campus, one of the few reactors on a state university campus. The reactor is used for research by university scientists as well as NASA and other industry leaders. The students also enjoyed the Smithsonian National Air and Space Museum, where they explored milestones in American flight and aerospace.

Student Suggestions
The main suggestions participants had for the program were to either extend its length or to focus the research tasks more narrowly. "The time constraints limited the application of different options and solutions for...the experiment." Alaa Khalil wrote. Bilal Sarris agreed: "It would be much better if the internship period [were] at least 10 weeks."

In addition, Saleh Al Hilali observed that "the students who had the opportunity to work on the labs had more benefits than those who worked only in the office modeling systems. We can have the simulation programs in PI, but the labs aren't there."

Student Projects
Each student worked with a UMD professor and graduate student supervisors on actual ongoing research projects. They gained practical, hands-on experience and valuable engineering skills in addition to experience working with students and professors from culturally diverse backgrounds.

Student	Professor	Project Title
Alaa Khalil	Dessiatoun	Microreactors for Oil and Gas Separation Processes Using Microchannel Technologies
Bilal Sarris	Radermacher	Waste Heat Utilization in Oil and Gas Industries
Nabil Hirzallah	Shamma	Segregation of Speech Using the Cortical Model
Waled Saeed and Alawi Abdulla	Balachandran	Dynamics and Control of Drill Strings
Ahmed Khalil	Bar-Cohen and S.K. Gupta	Thermally Enhanced Polymer Heat Exchangers
Saleh Al Hilali	Radermacher	Solar Powered Cooling Systems for Houses in Abu Dhabi
Abdallah Helal	Dessiatoun	Study on Microchannel-Based Absorber/Stripper and Electrostatic Precipitators for CO2 Separation from Flue Gas
Mohammed Abdudaga and Abdullah Tamimi	Modarres	Risk Analysis and Probabilistic Study on Corrosion on X-70 Steel
Nalah Al Amoodi	A.K. Gupta	Sulfur Recovery From Gas Stream

Professor Mikhail Anisimov Sabbatical at PI

Professor Mikhail Anisimov, who was on sabbatical from UMD's Chemical and Biomolecular Engineering Department at the PI for the last year, is back at UMD.

Professor Anisimov worked on a number of theoretical and experimental research projects, built a state-of-the-art Dynamic Scattering Lab at PI to measure submicron and nano-particle sizes in opaque liquid materials, taught three courses, and published several articles and chapters in books related to his research activities at PI, among other activities.

Professor Ali Almansoori's Visit to UMD

During the summer of 2009, Professor Ali Almansoori visited the University of Maryland (UMD) for three weeks (July 4-25). The purpose of the trip was to follow up with the projects that he has been engaged in for the past year and half. The trip allowed him to interact face-to-face with his collaborators and students and gave him the chance to visit UMD's state-of-the-art fuel cell laboratories.

Professor Almansoori is working on two projects with UMD. The first is with Dr. P.K. Kannan and Dr. Shapour Azarm, on optimization of petrochemical systems. Almansoori worked with Professor Azarm in developing an optimization course that can be offered collaboratively in the spring semester of 2010. They also explored the possibility of offering a graduate elective course, entitled Engineering Decision Making, covering both business and engineering aspects in collaboration with Dr. Kannan from the Business School.

The second project, with Dr. Greg Jackson and Bryon Eichhorn, involves designing and modeling a fuel cell system to generate power utilizing petroleum off-gases from the UAE oil and gas fields. Professor Almansoori had weekly group meetings with the students to discuss the progress of the project and its direction. He visited the fuel cell experimental facilities and had the chance to see the single-test SOFC test rigs and the fabrication process of the anode assembly. He also had a look at the state-of-the-art Ballard SOFC system to generate power using light hydrocarbons. "Having a close look at the UMD fuel cell facilities gave me a clearer picture of how the future PI fuel cell facility will look like," Professor Almansoori reports, "and we will try to duplicate the UMD facility, to allow us to build the fuel cell anode assembly here at the PI."

Professors Shapour Azarm and P.K. Kannan Visit to PI and ADNOC OpCos

Professors Azarm (UMD) and Kannan (UMD) visited PI and several ADNOC companies during the third week of August. The ADNOC companies included ADGAS, ADCO, ZADCO, Takreer, and Borouge. The professors' talks on "Integrated Business and Engineering Decisions for Optimization of Petrochemical Systems" were well received during their visit. Some of the ADNOC companies expressed interest in collaborating further on the project.

Graduation of Two ADNOC Scholars

Ebrahim Al Hajri and Mohammed Chookah, the two ADNOC scholars who have been studying at UMD for the past few years, defended their dissertations last summer and obtained their PhD degrees. Dr. Al Hajri is a member of the PI faculty at present.

Graduate Research Assistants (GRAs)

The following table lists the GRAs working on the Phase II EERC projects.

Student	UM Professor	PI Professor	Degree	Funding Source
Mohamed Chooka Mohammad Nuhi	Modarres	Seibi	Ph.D. Ph.D	Graduated Aug 2009 EERC
Mohamed Alshehhi	Dessiatoun	Ohadi, Goharzadeh,	Ph.D.	ADNOC
Ebrahim Al-Hajri	Dessiatoun	Ohadi, Goharzadeh	Ph.D.	Graduated June 2009
Weiwei Hu	Azarm	Al Hashimi, Almansoori	Ph.D.	EERC
Hatem Selim	Gupta	Al Shoaibi	Ph.D.	EERC
Juan Cevallos Tim Hall Frank Robinson William Pappas	Bar-Cohen, SK Gupta SK Gupta, Bar-Cohen Bar-Cohen, SK Gupta, Bruck Bigio	Rodgers, Abdala	Ph.D MS BS/MS MS	EERC(partial) EERC UMD Foundation UMD Foundation
Chien-Min Liao	Balachandran,	Karki Abdelmagid	Ph.D.	EERC
Hesham Ismail	Balachandran Chopra	Karki Abdelmagid	Ph.D	ADNOC
Ali Alalili	Radermacher	Al Hashimi, Rodgers,	Ph.D.	ADNOC
Amir Mortazavi Chris Somers Abdullah Alabdulkarem	Radermacher	Al Hashemi. Rodgers	MS MS Ph.D	EERC Graduated Aug 2009 EERC
Siddharth Patel	Jackson	Almansoori	MS	Graduated Oct 2009
Lei Wang	Jackson	Almansoori	Ph.D	EERC

Individual Project Reports

Thrust 1
Energy Recovery and Conversion Projects

Sulfur Recovery from Gas Stream using Flameless and Flame Combustion Reactor

UMD Investigators: Ashwani K. Gupta
GRA: Hatem Selim
PI Investigators: Ahmed Al Shoaibi
Student: Nahla Al-Amoodi
Start Date: October 2006

1. Objectives/Abstract

The main objective is to obtain fundamental information on the thermal process of sulfur recovery from sour gas by conventional flame combustion as well as flameless combustion, using numerical and experimental studies. Our ultimate goal is to determine optimal operating conditions for enhanced sulfur conversion. Therefore, an experimental study of the flameless combustion processes of the Claus furnace is proposed, and the results are compared with the normal flame process in order to determine the improved performance. In this study we will explore different operating conditions and perform exhaust gas analyses of both flame and flameless modes of reactor operation in order to attain enhanced sulfur recovery.

Specific objectives are to provide:

- A comprehensive literature review of the existing flame combustion process for sulfur removal with special reference to sulfur chemistry
- Near isothermal reactor conditions and how such conditions assist in the enhanced sulfur recovery process
- CFD simulation of the flame and flameless combustion in the furnace.
- Determination of the chemical kinetics and the major reaction pathways that result in high performance
- Design of a flameless combustion furnace for experimental verification of the numerical results
- Measurements and characterization of the flameless combustion furnace using high-temperature air combustion principles, including the conditions of flameless combustion
- Experiments with different sulfur content gas streams using the flame and flameless combustion furnace modes of operation
- Installation of the appropriate diagnostics for quantification of stable and intermediate sulfur compounds in the process
- Flow and thermal field characteristics in the reactor
- Product gas stream characteristics and evaluation of sulfur recovery and performance in the process

2. Deliverables for the Completed Quarter

- Further examination of the mixing characteristics and degree of mixing in the flow field of a non-reactive flow field. The non-reactive flow simulates the reactive flow in the Claus process, where nitrogen is used to simulate the main stream and oxygen is used to simulate the injected stream. Different geometries are investigated with different configurations. Angle of injection, main-stream bluff body, and injector orifice are incorporated as parameters to be examined in order to improve the degree of mixing.

- Further examination of the H_2S/O_2 reaction mechanism, in which the 24-reduced mechanism we developed in a previous report is examined for further reduction. The direct elementary reaction error equation is incorporated in order to find the complete effect of removing a single elementary reaction on each of the main species. Three elementary reactions are eliminated from the 24-reduced mechanism and the corresponding error was minimal.
- Equilibrium Claus reactor and detailed kinetic analyses for the H_2S/O_2 reaction mechanism. The equilibrium analysis investigates the optimum operating temperature for the Claus furnace that provides maximum sulfur recovery for different acid gas compositions. On the other hand, the chemical kinetic analysis investigates rigorously the reactions that occur in the isothermal and adiabatic Claus furnace in order to compare the behavior of both reactors.

3. Executive Summary

During the reported quarter, progress continued in the areas of investigation of non-reactive mixing characteristics of the Claus process reactants. Nitrogen and oxygen were used to non-reactively simulate the real reactive case of the Claus process. The momentum flux ratio was kept constant during the non-reactive simulations, as it was in the reactive case effect of injection angle, bluff body, and injector orifice, which were incorporated to examine their effect on improving the mixing characteristics. The results revealed an improvement in the mixing length while using an inclined injector. However, the 30° inclined injector gave a better degree of mixing than the 60° inclined injector. One the other hand, the 90° inclined injector (opposed injection) was tested with the presence of a bluff body. This configuration showed improved mixing characteristics, and poor mixture fraction uniformity.

Another examination was conducted to study the effect of the bluff body geometry and orientation. Meanwhile, the injector orifice effect was investigated. In addition, the 24-reduced mechanism presented in the quarterly report of December 2008 has been reduced further. Our novel equation for the effect of removing a specific elementary reaction on the main species (DERE) was utilized to determine the effect of removing every elementary reaction on each main species. The results show that the error generated by removing a certain elementary reaction can be compensated for by removing other reactions. Three elementary reactions were eliminated from the 24-reduced mechanism, and a comparison between the new mechanism and the 24-reduced one was conducted. The results show that both mechanisms have the same trend, but a minor error was noticed on the steady state value of some main species.

In addition, equilibrium and chemical kinetic analyses are conducted on acid gas that contains carbon dioxide, nitrogen, and water vapor along with hydrogen sulfide. The objective of the equilibrium investigation was to find the optimum operating temperature for the Claus furnace that provides maximum sulfur recovery for different acid gas compositions. On the other hand, the objective of the chemical kinetic analysis was to study rigorously the reactions that occur in isothermal and adiabatic Claus furnace in order to compare the behavior of both reactors. The equilibrium investigations indicate that the presence of contaminants decreases the optimum operating temperature and the sulfur conversion efficiency. Meanwhile, the chemical kinetic analysis revealed the main reaction responsible for the reduction of sulfur recovery in adiabatic Claus furnace and the factors that have a direct effect on this reaction. Equilibrium and chemical kinetic analyses are based on numerical simulations.

4. Progress

4.1 Mixing of Claus reactants under non-reactive conditions

To achieve such high conversion efficiencies, the Claus reactions must take place under defined and uniform temperature conditions. Furthermore, the reactants must be uniformly mixed. Our experimental facility is designed such that it can achieve uniform temperature in the reactor where the pertinent Claus reactions occur. In this report the flow patterns and mixing characteristics of different injection geometries are investigated. We started with the comparison between different angles of injections (30°, 60°, and 90°) where the angle is measured relative to the axis of the injector. It is to be noted that the effect of having a bluff body in the main stream is incorporated with the opposed injection (90° injection) scheme. Furthermore, different bluff body geometries and orientation are investigated in order to achieve better mixing characteristics. Meanwhile, injector orifice is used in order to enhance the magnitude of generated vortices so that the injected stream is introduced into the main stream with a considerable amount of eddies in order to enhance the mixing between both streams.

The primary focus of this study has been on the non-reactive case, since this directly impacts mixing, which subsequently impact sulfur conversion efficiency. The focus here is on quantifying the mass fraction of hydrogen sulfide in the main stream. The environmental regulations prohibit emission of unburned H_2S to the environment. Therefore the simulations have been carried out first to examine mixing between gases that behave similarly to the H_2S in the mixing experiments for simulating mixing during the non-reactive conditions while avoiding complexity associated with the reactive cases. The main stream is simulated with nitrogen and hydrogen sulfide with oxygen. The momentum flux ratio is kept constant between the reactive case and the corresponding non-reactive case. According to what we have presented in the quarterly report of June 2009, five non-reactive cases were simulated, in which each one represented a specific heat load for the corresponding reactive case. In this report, case 4a has been arbitrarily chosen to assess different geometries and orientations incorporated in this study. Fluent 6.2 code was used for the numerical simulations. The turbulence model used was the standard K-ε viscous model and included the buoyancy effects. The main-stream reactor diameter was 14.22 mm. The injection inlet diameters were reduced in this examination compared to those in the previous investigation (quarterly report of June 2009) to 1.5875 mm inner diameter and 6.35 mm outer diameter. This improved the penetration of the injected stream into the main stream. Due to the symmetrical geometry of the reactor, only one-quarter geometry was simulated in this study. The mesh grid independence was checked in order to ensure that the results obtained were independent of the grid mesh. The grid mesh for the different simulated geometries consisted on average of 1,600,000 cells for one quarter the geometries.

Effect of injection angle and main-stream bluff body

Different injections angles were used to assess their effect on the mixing characteristics and flow patterns. The injector angle varied between 30° and 90° with steps of 30°, where this angle is the angle between the injector centerline and the horizontal plane. According to our definition of the injection angle, the 90° injection is an opposed injection scheme. Meanwhile, the bluff body effect was investigated along with the 90° injection angle effect.

Figure 1 depicts simulated isometric of the examined geometries where the hollow parts denote the non-simulated walls, which are the tube thickness and the bluff body.

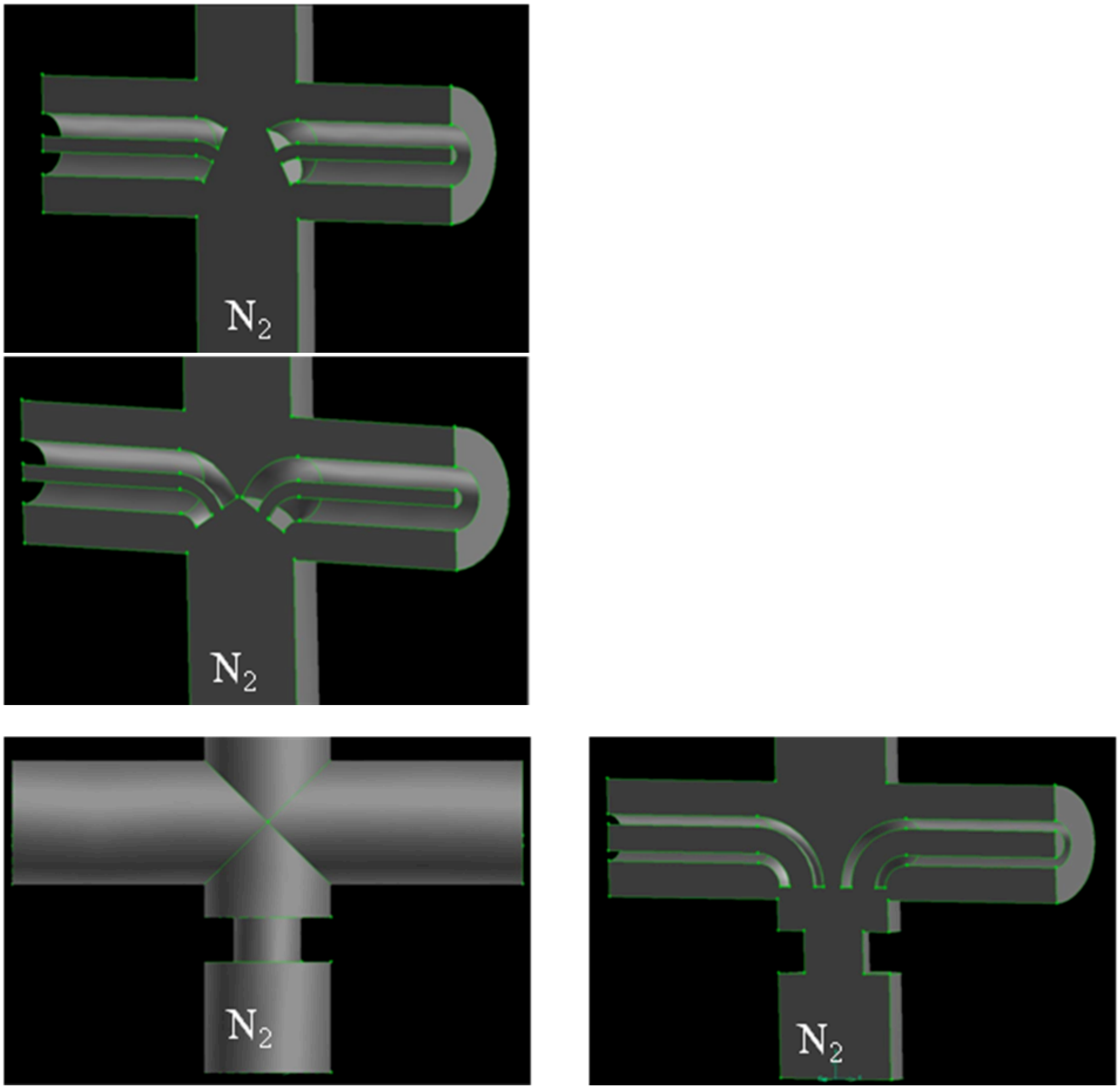

Figure 1. Sectional isometric of the simulated examined geometries, 60° injection (upper right), 30° injection (upper left), 90° injection (lower right). Full isometric of the 90° injection (lower left).

Figure 2 shows the effect of changing the injection angle on the oxygen mass fraction. Increasing the injection angle from 30° to 60° deteriorated the mixing characteristics when the mixing length was increased. On the other hand, the opposed injection (90° injection) with bluff body showed a drastic reduction in the mixing length, which translated to better mixing. However, the flow pattern of the opposed injection case showed poor oxygen mass fraction uniformity where the injected oxygen hovers inside the cross legs. Figure 3 shows the mixing length obtained at the different geometries where the mixing length is defined as:

$$l = \frac{Z_{mixing}}{D_{jet}}$$

Since the 30° injection showed the best performance in terms of both mixing length and mass fraction uniformity, the next investigation focused on the improvement of its performance. Meanwhile, the cross legs were eliminated from our geometry so that the hovering of the injected stream will be prevented.

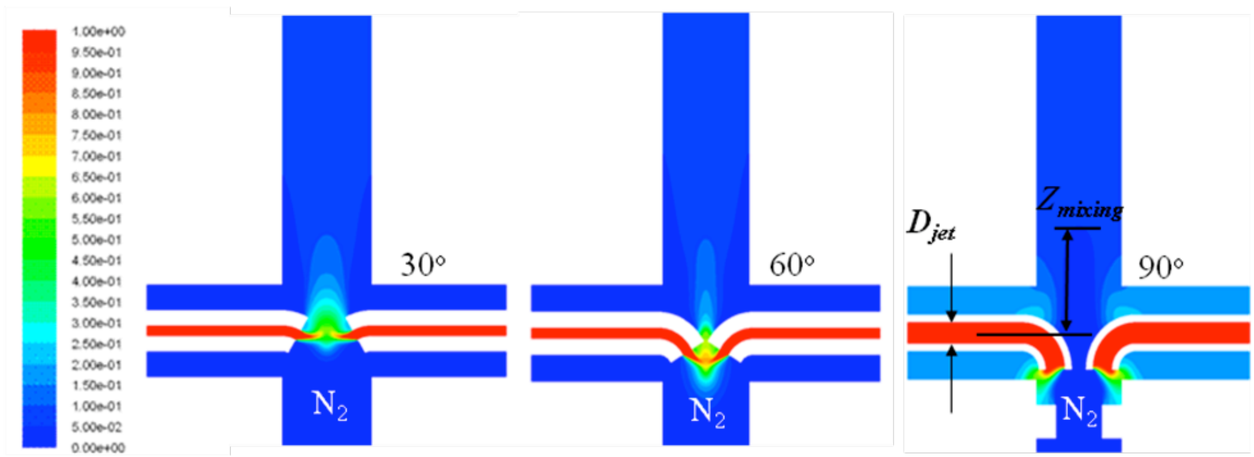

Figure 2. Oxygen mass fraction for different injection angles.

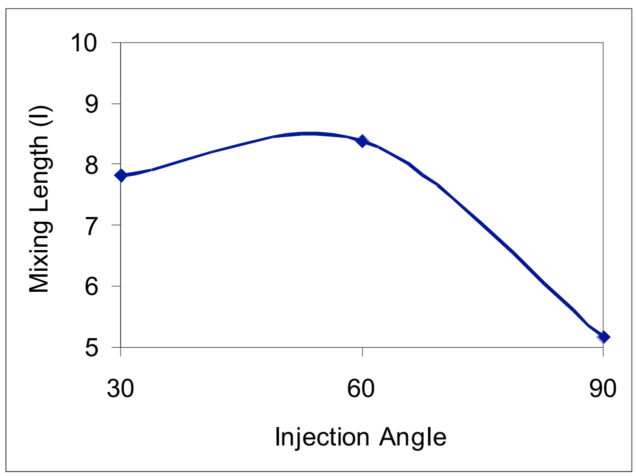

Figure 3. Effect of varied injection angles on the mixing length.

Effect of bluff body configuration with injector orifice

In this investigation 30° injection was used along with different bluff body configurations. Straight and conical bluff bodies were investigated where the conical bluff body has different orientations, as shown in Figure 4. On the other hand, an orifice inside the injectors was used to enhance the generated vortices so that mixing took place in a uniform fashion due to the curly path of the injected stream. Figure 5 shows the proposed design of the injector orifice.

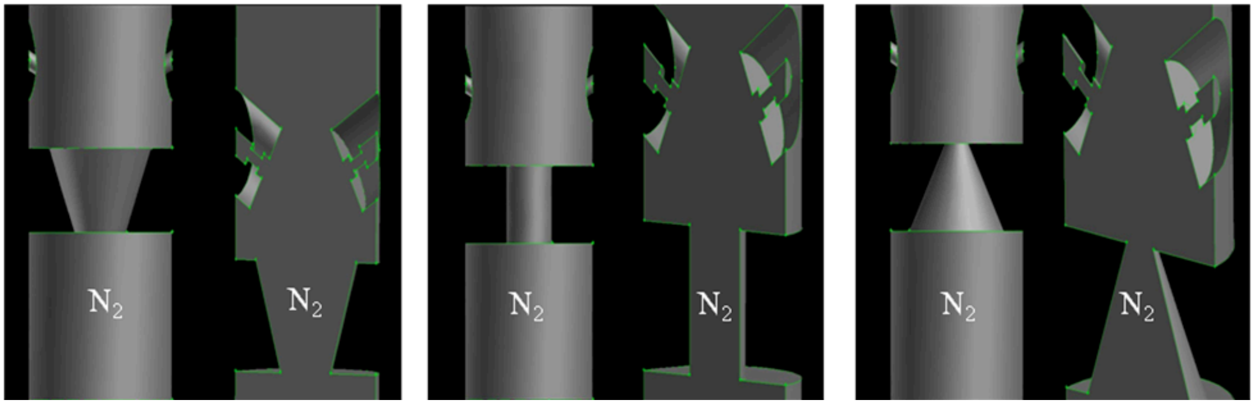

Figure 4. Different examined configurations: configuration 1 (left), configuration 2 (middle), configuration 3 (right).

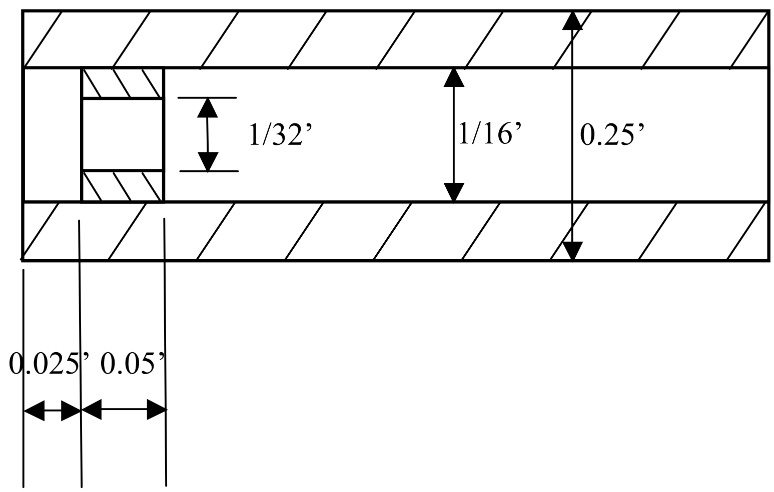

Figure 5. Longitudinal cross section of the injector with orifice.

Figures 6 and 7 show oxygen mass fraction and vorticity magnitude for the different configurations, respectively. The first configuration shows very poor mixing characteristics compared to the others, which is attributed to the weak vorticity generated by the bluff body. In other words, the sudden contraction and gradual expansion of the main stream is not favorable. The second and third configurations depict better mixing characteristics compared to the first configuration. However, the third configuration generated much more vorticity magnitude compared to the second configuration; hence the gradual contraction and sudden expansion of the main stream is favorable. Figure 8 assures that the highest vorticity magnitude obtained from different configurations increases dramatically in the third configuration.

Figure 9 shows the path lines of the group of particles of the injected stream inside each configuration. Note that that the first two configurations have much shorter path lines compared to the third geometry, which translates to shorter residence time inside the reactor in the reactive case. On the other hand, the path line of the third configuration revealed a much more complicated and longer swirling path line along the reactor. This results in better mixing and H_2S/O_2 reaction due to the swirling motion of particles along the reaction zones for a long time.

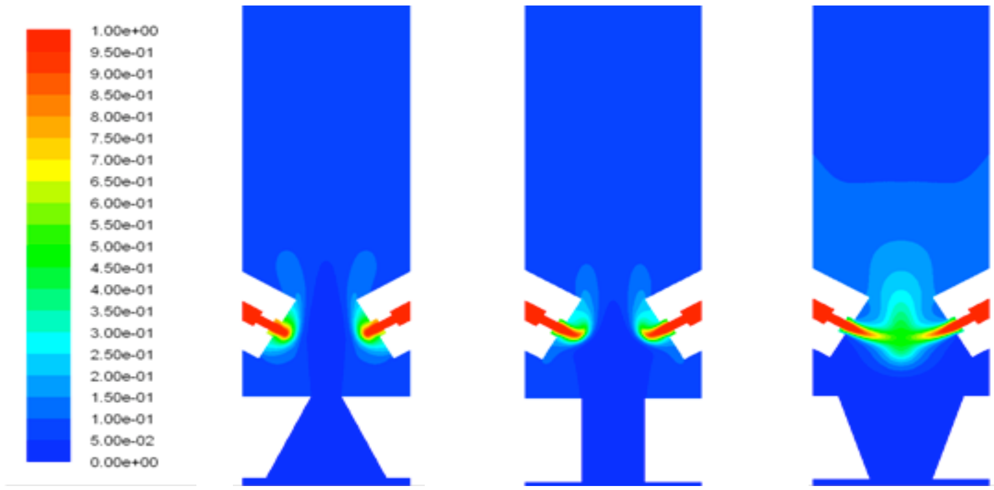

Figure 6. Oxygen mass fraction for different configurations: configuration 1 (left), configuration 2 (middle), and configuration 3 (right).

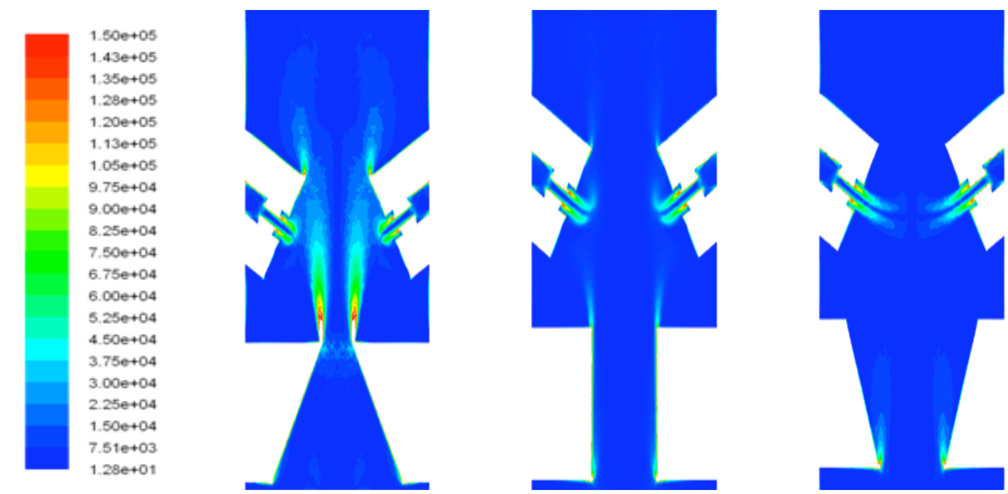

Figure 7. Vorticity magnitude (1/s) for different configurations: configuration 1 (left), configuration 2 (middle), and configuration 3 (right).

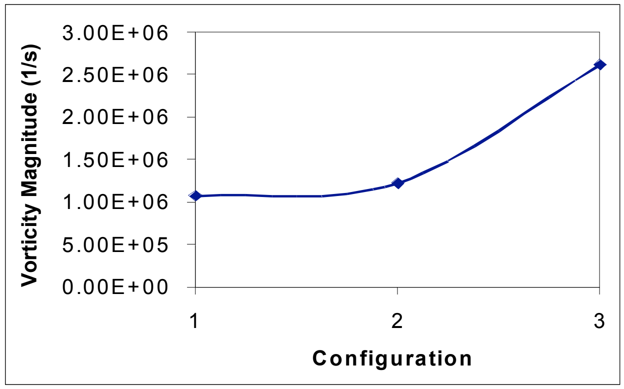

Figure 8. Maximum vorticity obtained in the field for different configurations.

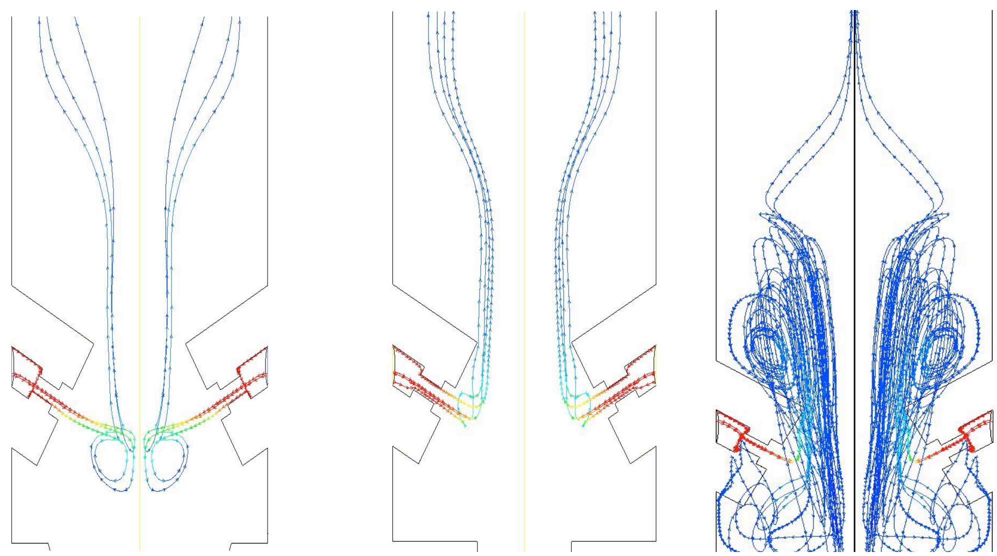

Figure 9. Path line of group of particles of the injected stream inside each configuration: configuration 1 (6 particles), configuration 2 (8 particles), configuration 3 (4 particles).

4.2 DERE analysis for the reduced mechanism

The implementation of the direct relation graph and error propagation methodology enabled us to reduce the detailed mechanism by Leeds university[1] from 111 reactions down to 24 reactions, and from 41 species down to 14 species. A novel equation has been developed by us to calculate the error generated in every main species by removing any elementary reaction. The Direct Elementary Reaction Error (DERE) is the error that appears in every main species due to discarding a specific elementary reaction. The DERE is defined as:

$$DERE_{A,i} = \sum_{\substack{Elementary \\ \mathrm{Re}\,action\ Species}} \left(\sum_{N\ species} \left(\left(\underbrace{\frac{\nu_{i,B}\omega_i}{\sum_{i=1,n_R} \left|\nu_{i,B}\omega_i\right|}}_{P} r_{jB} \right) r_{Aj} \right) \right)$$

where
$DERE_{A,i}$: error appears in main species A if reaction *i* is removed
$\upsilon_{i,B}$: the stoichiometric coefficient of species B in reaction *i*
ω_i: reaction rate of elementary reaction *i*
rA,j: error appears in species A by removing species *j* from the mechanism
$R_{j,B}$*:* error appears in species j by removing species B

Figures 10 and 11 show the DEREs of main species for the elimination of different elementary reactions. The results revealed that the error generated by removing a specific reaction can be compensated for by removing another reaction according to its DERE. The figures show the distribution of the DERE of every main species along the temperature range we are interested in. Negative DERE reflects a decrease in the main species if this elementary reaction is removed, and vice versa. As an example, the results show that the error appearing in the S_2 mole fraction by discarding the reaction H_2S+S = HS_2+H is less than the error appearing by discarding the reaction S+H_2 = SH+H.

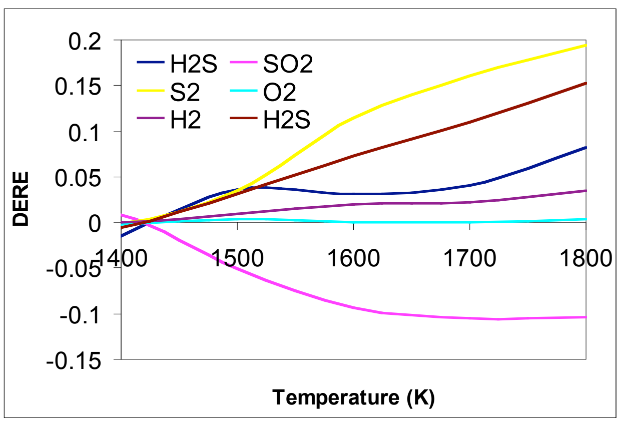

Figure 10. Effect of removing reaction (H_2S+S = HS_2+H) on each main species.

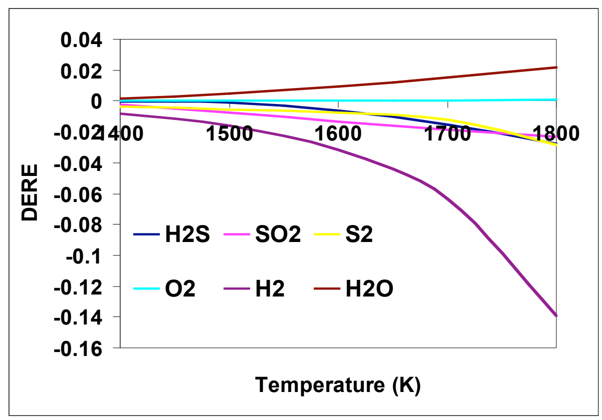

Figure 11. Effect of removing reaction (S+H_2 = SH+H) on each main species.

Figure 12 shows a comparison between the 24-reaction reduced mechanism and the 21-reduced mechanism where three elementary reactions are discarded. The three discarded reactions are:

HSO+H = SH+OH,

HSO+H = S+H_2O,

HSO+H = SO+H_2

These reactions showed very weak effect on the reduced mechanism. However, the reason we were not able to discard them in the previous analysis of the DRGEP is that they give a high error in main species but only after these species finish their role in the reaction. In other words, the maximum error can be in O_2 mole fraction, but this error is after consuming O_2 totally where its mole fraction order of magnitude is 10^{-6}. Therefore, we were able to eliminate the aforementioned reactions. The results showed good agreement between the two mechanisms. However, some discrepancies are found in some of the main species' asymptotic values. This means the 21-reaction mechanism is capable of tracking the kinetics of the reactions as well as the 24-reduced mechanism, which was previously compared with the detailed mechanism and shown to be successful.

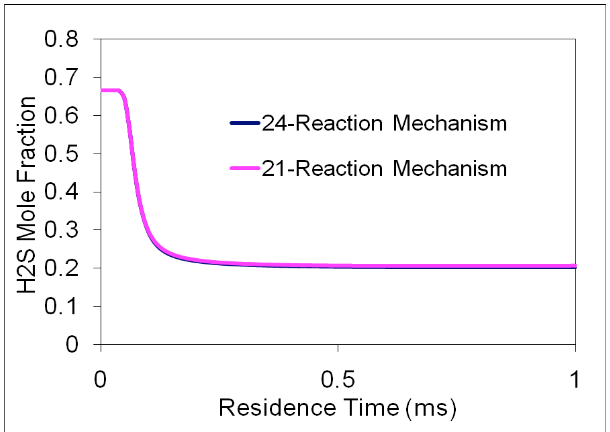

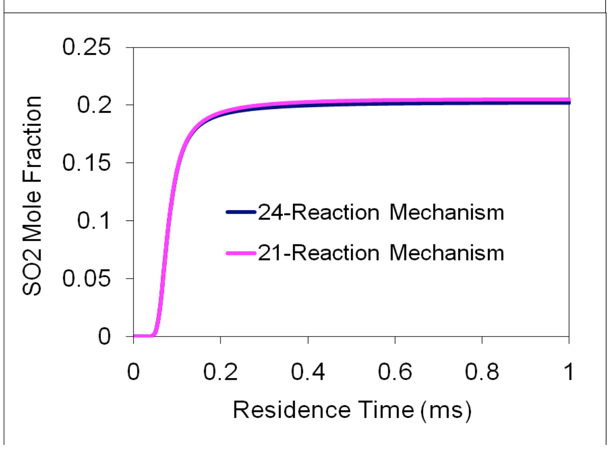

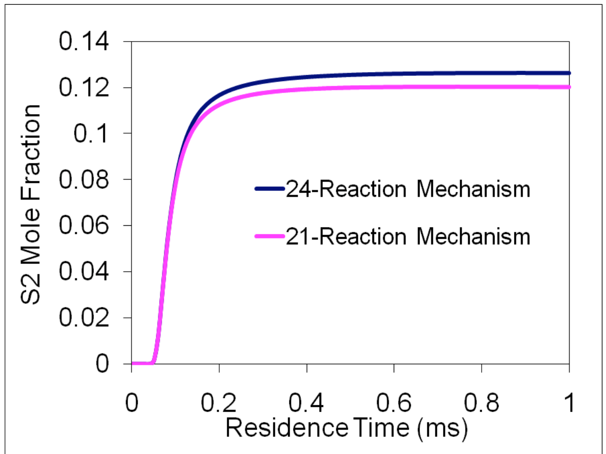

S2 Mole Fraction
0.14
0.12
0.1
0.08
0.06
0.04
0.02
0
0
0.2
0.4
0.6
0.8
1
Residence Time (ms)
24-Reaction Mechanism
21-Reaction Mechanism

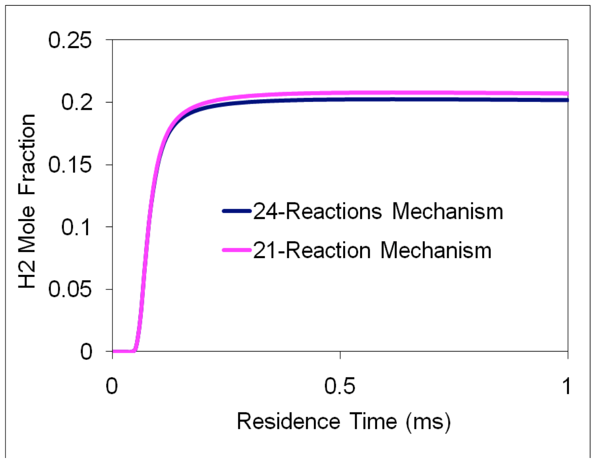

H2 Mole Fraction
0.25
0.2
0.15
0.1
0.05
0
0
0.5
1
Residence Time (ms)
24-Reactions Mechanism
21-Reaction Mechanism

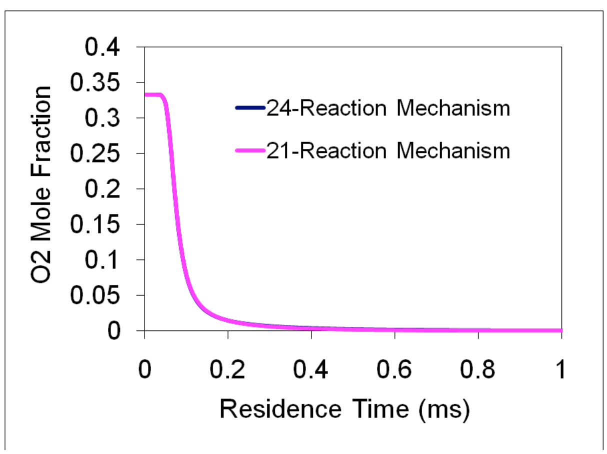

O2 Mole Fraction
0.4
0.35
0.3
0.25
0.2
0.15
0.1
0.05
0
0
0.2
0.4
0.6
0.8
1
Residence Time (ms)
24-Reaction Mechanism
21-Reaction Mechanism

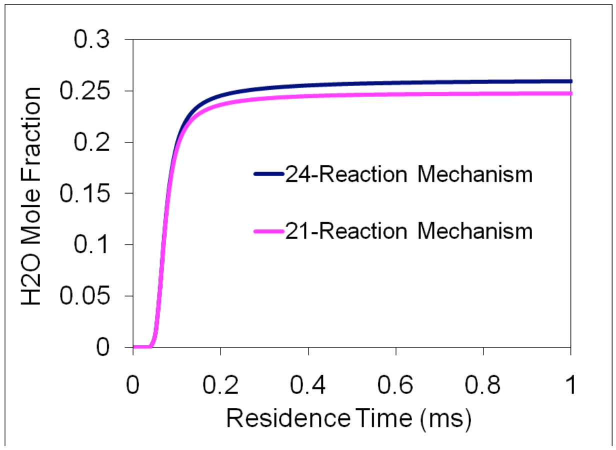

Figure 12. Comparison between main species behavior obtained by the 21-reaction mechanism and the 24-reduced mechanism.

4.3 Equilibrium and kinetic analyses on Claus reactions

Equilibrium Investigation

A parametric study was performed to investigate the effect of the change of acid gas composition on the sulfur conversion efficiency as well as the optimum reactor temperature. Sulfur conversion efficiency is defined as:

$$Conversion\ Efficiency = \frac{Mass\ of\ recovered\ sulfur}{Mass\ of\ sulfur\ in\ inlet\ H_2S}$$

Figure 13 depicts the effect of the change of acid gas feed concentrations of H_2S, CO_2, N_2, and Claus furnace temperatures on the conversion efficiency of S_2 having the H_2O concentration fixed at 9 mol %. At low concentrations of CO_2, maximum conversion efficiencies do not change significantly. However, the corresponding optimum temperature shifts slightly to the left as the concentration of N_2 increases from 10 to 30 mol %. This increase in N_2 concentration reduces the partial pressure of the reactants, as it acts as a diluent, which provides higher affinity for dissociation of available species including recovered S_2 at high temperatures. Therefore, a decrease in Claus furnace temperature is essential to achieve maximum conversion efficiency. On the other hand, at high concentrations of CO_2 the effect on the maximum conversion efficiency becomes more evident. Sulfur conversion efficiency declines by 20% as the CO_2 concentration increases to 60 mol %. At high temperatures, CO_2 dissociates to CO and O radicals, which enhance the oxidizing medium in the Claus reactions. Subsequently, hydrogen sulfide reaction tends to produce SH radicals, which act as an intermediate channel to form SO_2. This dissociation process causes S_2 conversion efficiency to decrease, thus the optimum Claus furnace temperature should be decreased.

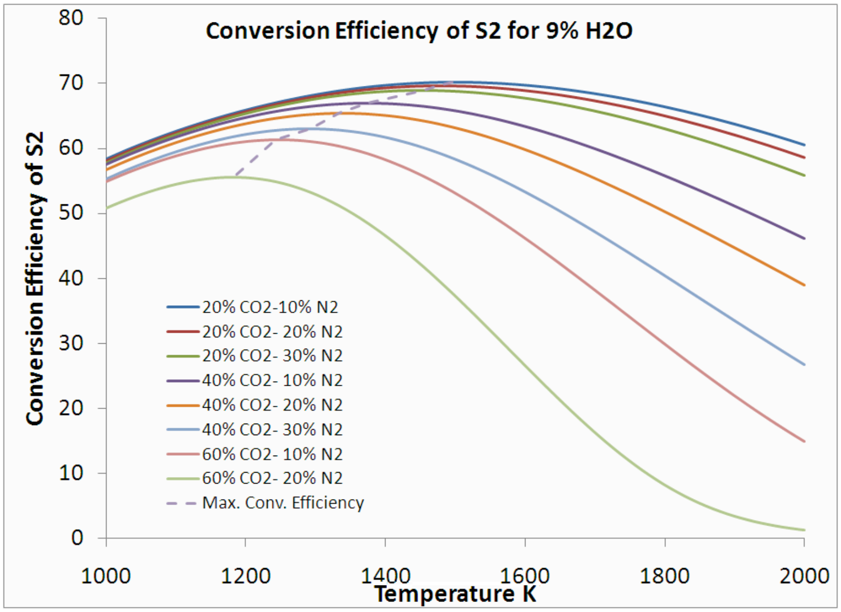

Figure 13. Effect of the change of acid gas feed concentrations and Claus furnace temperature on the sulfur conversion efficiency.

Similar to the CO_2 concentration result, the presence of H_2O contributes to a decrease in S_2 conversion efficiency. Water vapor acts as an oxidizer by supplying OH radicals into the radicals pool, which reacts with S to form SO to subsequently hinder the formation of S_2. The reaction below shows the effect of increase in OH concentration on the formation of SO. Subsequently, SO reacts further to produce SO_2.

$$S + OH \leftrightarrow SO + H$$

The previous investigation was repeated for different concentrations of H_2O in the acid gas, where it was found that the increase of H_2O concentration always deteriorates the conversion efficiency. From the results obtained, a mathematical correlation was generated to find the optimum temperature of maximum conversion efficiency as a function of H_2O, CO_2 and N_2 concentrations in the acid gas stream with a maximum error of 1.24%:

$$T(K) = 1706.4 - 7.0153\,CO_2\% - 3.0629\,N_2\% - 2.0534\,H_2O\%$$

<u>Chemical kinetic investigations:</u>

The goal of these investigations was to determine the Claus reaction behaviors and the change in product concentrations under isothermal as well as adiabatic conditions. Meanwhile, a reactor-type study was performed in order to elucidate the difference in the conversion efficiency obtained by isothermal and adiabatic reactors. The runs performed can be categorized as high oxidizers feed; i.e., the concentration of CO_2/H_2O is high, and low oxidizers feed.

<u>High oxidizers feed</u>

The evolution of the main species mass fraction as a function of residence time for isothermal and adiabatic cases is shown in Figure 14. In the isothermal case, Figure 14 (left), the SO_2 composition increases to a maximum then decreases until it reaches steady state, and the S_2 mass fraction leaving the reactor is greater than that of SO_2. In the adiabatic run, Figure 14 (right), S_2 composition increases to a maximum then decreases until it reaches steady state, resulting in a greater SO_2 composition leaving the reactor. This increase in SO_2 concentration is attributed to the increase in reaction rate of reactions that produce SO. For instance, the reaction rate of reaction SO + H + M ↔ HSO + M increases in the adiabatic cases by a factor of 11 up to 21 compared to the isothermal cases. This increase is attributed mainly to the higher temperatures in the adiabatic reactor. It is to be noted that this reaction progresses in the reverse direction to produce SO. Moreover, the distinct increase in the reaction rate of reactions S + OH↔ SO + H and S + O_2 ↔ SO + O contribute to the production of SO which further reacts to form SO_2.

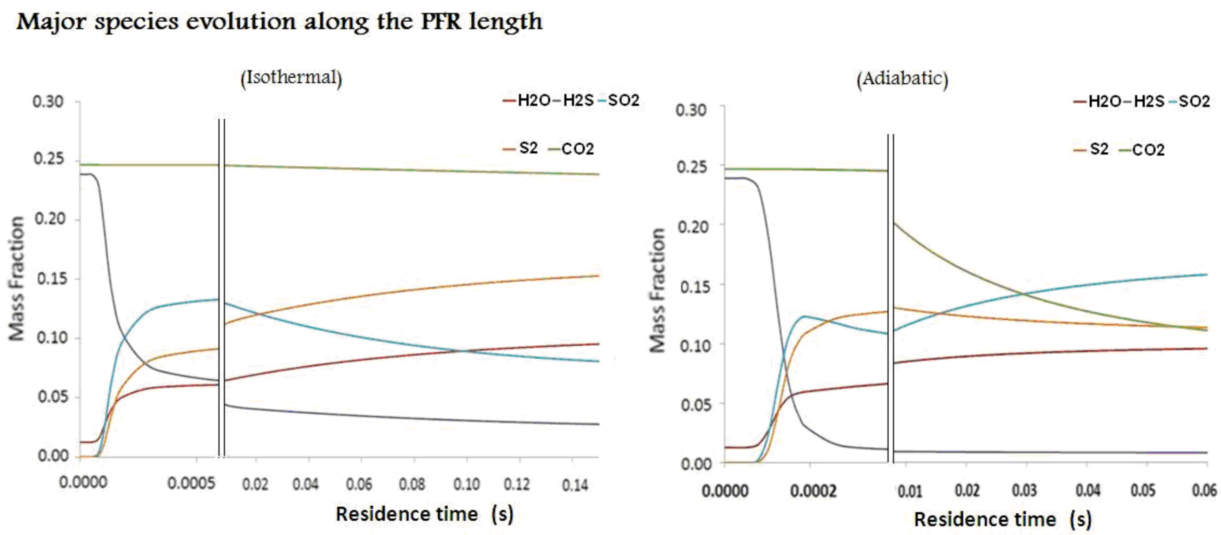

Figure 14. Mass fraction of the major species as a function of residence time for isothermal (left) and adiabatic case (right) of high oxidizers feed in a PFR.

Low oxidizers feed

The results of the isothermal case of low oxidizers feed exhibits the same trend as the high oxidizers feed. However, the behavior of the adiabatic case of the contrasts with that of the latter adiabatic case. For low oxidizers feed, the composition of S_2 in the effluent stream is greater than the composition of SO_2 (see Figure 15). This increase in concentration is attributed to the increase of the reaction rate of reaction S + OH↔ SO + H in the reverse direction.

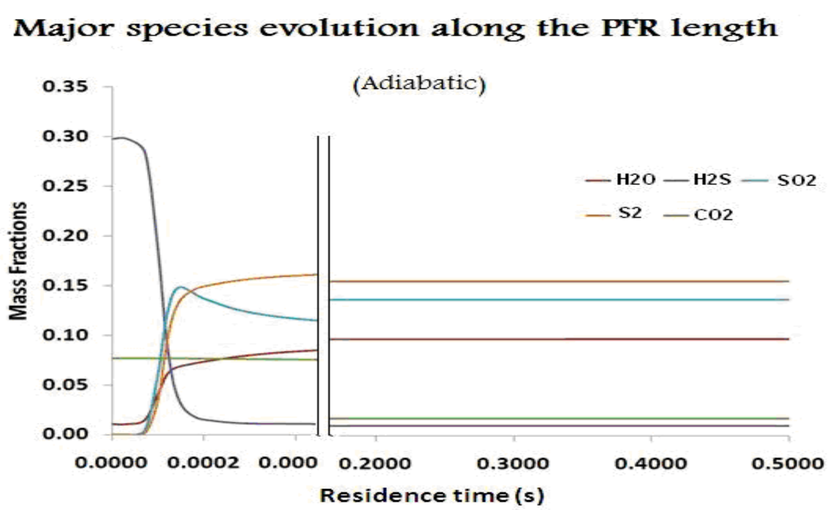

Figure 15. Mass composition of the major species for the adiabatic case of low oxidizers feed.

The effect of temperature and species concentration on the pathway of this reaction was examined to interpret its behavior. The pathway of this reaction in both types of feed proves that it switches its net direction from forward to reverse (backward). However, in high oxidizers feed the reaction reverses direction when its rate magnitude is relatively insignificant to other dominant reactions. To elucidate this observation, the temperature effect on this reaction was examined by simulating the low oxidizer feed isothermally at different temperatures. The results of the simulations prove that the change in temperature does not alter the pathway of this reaction, and thus direct temperature effect can be eliminated. On the other hand, the examination of the switch of this reaction's direction with respect to the change in species concentration reveals that the switch is strongly dependent on OH concentration. In other words, as the OH concentration reaches its minimum, the reaction reverses direction in an attempt to achieve equilibrium. Figure 16 shows the reaction rate of reaction S + OH↔ SO + H and OH mass fraction as a function of PFR residence time in low and high oxidizers feed, respectively. The results shown in the figure reveal distinct synchronization on the behavior of the reaction rate and OH mass fraction with residence time. It can be noticed that in low oxidizers feed, OH concentration decreases at an earlier stage, which forces the reaction to reverse its direction and produce more OH and S radicals. Subsequently, S radical reacts further with SH to produce S_2.

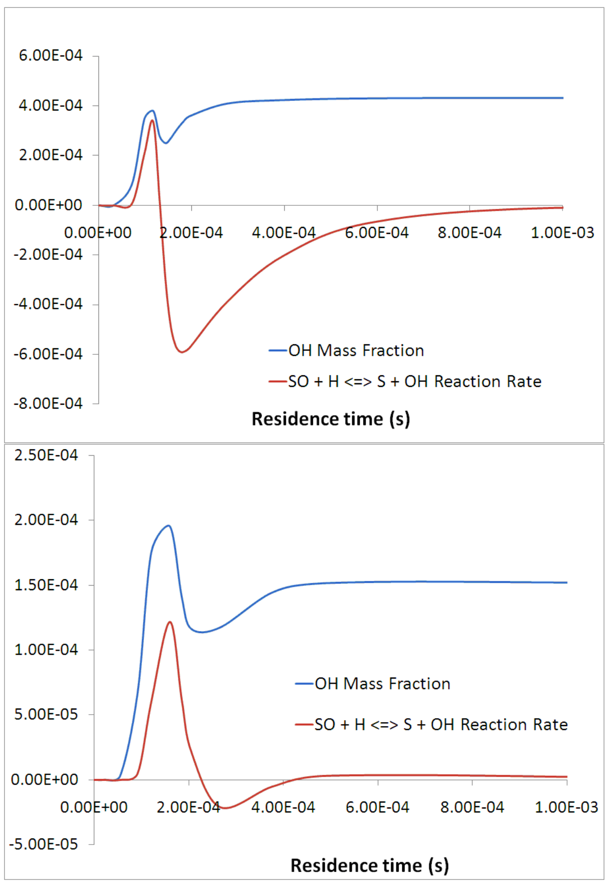

Figure 16. Reaction rate of SO + H ↔ S + OH and OH mass fraction as a function of PFR residence time in low and high oxidizers feed, respectively.

Claus Furnace Reactor type examination

Isothermal and adiabatic reactor comparisons have shown that the isothermal reactor achieves higher conversion efficiency compared to the adiabatic reactor. As evidence for this observation, the adiabatic reactor can be divided into a number of infinitesimal pseudo-reactors where each reactor operates hypothetically at constant temperature, and hence it can be considered as an isothermal reactor. Each pseudo-isothermal reactor functions at constant temperature for the same fraction of time that this temperature exists in the adiabatic reactor during the temperature evolution. The summation of the pseudo-isothermal reactor efficiencies, corrected by a scale factor, will result in the total conversion efficiency obtained by the adiabatic reactor. Figure 17 shows the infinitesimal division for one pseudo-isothermal reactor in an adiabatic Claus reactor.

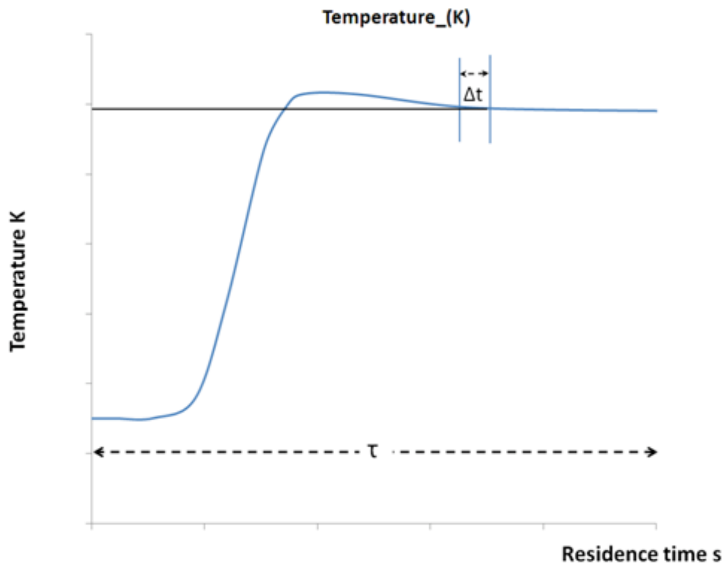

Figure 17. Fraction of time for one pseudo-isothermal reactor in an adiabatic reactor.

The scale factor (χ_i) is defined as the ratio of the infinitesimal fraction of time (Δt_i) where the temperature is almost constant to the time needed for the reactions to complete in the adiabatic reactor (τ) as follows:

$$\chi_i = \frac{\Delta t_i}{\tau}$$

The scale factor ranges from 0 to 1 in value; i.e., for a perfectly isothermal reactor the scale factor is unity. Consequently, the conversion efficiency (η_{ad}^{*}) is calculated based on the assumption that each pseudo-isothermal reactor is operating at equilibrium conditions; thus, η_{ad}^{*} is defined as:

$$\eta_{ad^*} = \sum_{i=1}^{n} \chi_i \eta_i^{eqm}$$

where η_i^{eqm} is the equilibrium conversion efficiency for each pseudo-isothermal reactor at its operating temperature, and n is the number of reactors.

The results obtained by the previous equation were compared to the overall conversion efficiency of the adiabatic reactor. The results are in agreement with a maximum error of 4.12%. Therefore, according to previous equation, in order to achieve higher conversion efficiencies it is desired to run the Claus process for a longer residence time, i.e. a larger χ, at the pseudo-isothermal reactors with higher conversion efficiencies. Therefore, operating the reactor under perfect isothermal conditions, χ=1, for pseudo-isothermal reactors with higher conversion efficiencies will result in an increase in the overall conversion efficiency.

5. Summary

Further non-reactive examination was performed in order to improve the mixing characteristics that reflect better Claus process reactions. The angle of injection was investigated where 30°, 60°, and 90° injectors are used. The 90° injection, which is considered an opposed injection scheme, was examined along with the effect of having a bluff body in the main stream. The results showed that 30° injection geometry achieved better mixing than 60° injection geometry. On the other hand, opposed injection with bluff body geometry showed the least mixing length amongst the three geometries. However, opposed injections had a very poor mixture fraction uniformity, where the injected stream hovers inside the cross legs instead of flowing inside the reactor with the main stream. This reveals that 30° injection geometry had the best performance in terms of small mixing length as well as good mixture fraction uniformity. Therefore, the 30° injection geometry was examined further, along with the effect of having bluff body in the main stream.

Different bluff body geometries and orientations were also examined. In addition, the injector orifice added to the injector in order to improve the generated vorticity magnitude before introducing the injected stream into the main stream. The results showed much better improvement in terms of mixing as well as mixture uniformity. Conversion bluff body provided the best mixing characteristics and the longest path line compared to other configurations. This results in better mixing and H_2S/O_2 reaction due to swirling motion of particles along the reaction zones for a long time.

Moreover, a kinetic study was conducted in order to calculate the error generated by the removal of every elementary reaction. The direct elementary reaction error (DERE) was calculated using the equation provided in the quarterly report of December 2008. The physical meaning of DERE is the error generated in any main species by removing a certain elementary reaction. The analysis showed the error generated by any elementary reaction can be compensated for by removing another elementary reaction. Based on this, three elementary reaction were discarded and a comparison between the new 21-reduced mechanism and the 24-reduced mechanism was performed. The results showed good agreement between both mechanisms. However, some discrepancies in the asymptotic value were found in some main species. This means that the 21-reduced mechanism can track the kinetics of the reaction efficiently.

Moreover, sulfur recovery and optimum operating temperature of Claus furnace that provides maximum sulfur recovery was investigated. The acid gas analyzed contained hydrogen sulfide along with carbon dioxide, nitrogen and water vapor. The scope of the investigation was on equilibrium and chemical kinetic analyses. The results of the equilibrium analysis indicate that the presence of contaminants in the acid gas stream decreases the sulfur recovery and the optimum operating temperature of the Claus furnace. At low temperatures the contaminants decrease the reactants' partial pressure and decrease the required temperature for maximum sulfur recovery. On the other hand, at high temperatures CO_2 and H_2O behave as oxidizers where the conversion efficiency drops significantly.

The use of equilibrium conditions have allowed us to formulate an analytical equation that could be used to predict the optimum reactor temperature to obtain maximum sulfur recovery from the known concentrations of CO_2, H_2O and N_2 in the acid gas stream. On the other hand, the chemical kinetic examination has provided a direct comparison on the behavior of Claus reactor operating under adiabatic and isothermal conditions. The results prove that, at adiabatic operation, low oxidizer concentration forces the main reaction responsible for the production of sulfur dioxide to reverse its net direction, and thus, the production of sulfur is increased.

Finally, a reactor type study was performed in order to elucidate the difference in the conversion efficiency obtained by isothermal and adiabatic reactors. It was found that operating the reactor under perfect isothermal conditions for pseudo-isothermal reactors with higher conversion efficiencies results in an increase in the overall conversion efficiency. This observation is evident from the results obtained in the isothermal chemical kinetic analysis.

6. References

[1] http://www.chem.leeds.ac.uk/combustion/sox.htm

7. Difficulties Encountered/Overcome

Experiments with hydrogen sulfide require strict safety assurance from our safety office prior to conducting any experiments so that we must build new modifications to the facility with an enclosed environment and exhaust decontamination system prior to performing our experiments. This will cause some delays in conducting our planned experiments. This is currently in progress.

8. Deliverables for the Next Quarter

- Further examination for the non-reactive mixing characteristics. Advanced mixing techniques will be examined in order to improve the mixing characteristics as well as the flow mixture fraction uniformity.
- Further reduction for the current reduced mechanism. We will optimize the number of reduced elementary reactions using the DERE approach in order to discard the maximum number of elementary reactions with the least corresponding error. Meanwhile, we will implement the steady state assumptions on the species that behave steadily along the reaction.
- Examination of the effect of the injection techniques on the degree of mixing under non-reacting conditions using experimental and numerical techniques.
- Design and development of safe working facility for use with hydrogen sulfide.

9. Publications

1. Gupta, A. K. and Sassi, M. "Sulfur Recovery from Acid Gas Using the Claus Process and High Temperature Air Combustion Technology," American J. of Environmental Sciences, Vol. 4, No. 5, 2008, pp. 502-511.
2. Selim, H., Gupta, A. K. and Sassi, M. "Variation of Optimum Claus Reactor temperature with Acid Gas Composition," IECEC Conference, Cleveland, OH, July 28-30, 2008, Paper No. AIAA-2008-5797.
3. Selim, H., Gupta, A. K. and Sassi, M. "Reduced Mechanism for Hydrogen Sulfide Oxidation," 47th AIAA Aerospace Sciences Conference, Orlando, FL, January 5-8, 2009, Paper No. AIAA-2009-1392.
4. Selim, H. and Gupta, A. K. "Nonreactive Study for the Reactants Mixing in Claus Reactions," 7th Intl. Energy Conversion Engineering Conference (7th IECEC), Denver, CO, August 2-5, 2009, Paper No. AIAA-2009-4506.
5. Selim, H and Gupta, A. K. and Sassi, M. "Reduction and Validation of Detailed Kinetic Reactions in Thermal Stage of Claus Process," 48th AIAA Aerospace Sciences Conference, Orlando, FL, (accepted for presentation and Publication), January 3-7, 2010, Paper AIAA-2010-1356.
6. Al Amoodi, N., Selim, H., Gupta, A. K., Sassi, M. and Al Shoaibi, A. "Numerical Simulations of the Thermal Stage in Claus Process: Equilibrium and Kinetic

Investigation," 48th AIAA Aerospace Sciences Conference, Orlando, FL, (accepted for presentation and publication), January 3-7, 2010, AIAA-2010-1355.

Appendix

Justification and Background

Hydrogen sulfide is present in numerous gaseous waste streams from natural gas plants, oil refineries, and wastewater treatment plants, among other processes. These streams usually also contain carbon dioxide, water vapor, trace quantities of hydrocarbons, sulfur, and ammonia. Waste gases with ammonia are called sour gases, while those without ammonia are called acid gases. Sulfur must be recovered from these waste streams before flaring them. Sulfur recovery from sour or acid gas typically involves application of the well-known Claus process, using the reaction between hydrogen sulfide and sulfur dioxide (produced at the Claus process furnace from the combustion of H_2S with air and/or oxygen), yielding elemental sulfur and water vapor: $2H_2S(g) + SO_2(g) = (3/n)\ S_n(g) + 2H_2O(g)$ with $\Delta H_r = -108$ kJ/mol. Therefore, higher conversions for this exothermic, equilibrium-limited reaction call for low temperatures, which lead to low reaction rates that dictate the use of a catalyst. The catalytic conversion is usually carried out in a multistage, fixed-bed, adsorptive reactor process, which counteracts the severe equilibrium limitations at high conversions. This technology process can convert about 96% to 97% of the influent sulfur in H_2S to S. However, higher removal requires critical examination of the process and use of a near isothermal reactor, since the conversion is critically dependent upon the exothermic and endothermic conditions of the reactions.

Flameless combustion has been shown to provide uniform thermal field in the reactor so that the reactor temperature is near uniform. Reactor size can also be reduced and combustion-generated pollutants emissions can be reduced by up to 50%. Energy efficiency can be increased by up to 30%. The application of this technology appears to offer great advantages for the processes under consideration. The UAE, which pumps about 2.4 million bpd of crude oil, is also home to the world's fifth biggest gas reserves at about 200 trillion cubic feet. Abu Dhabi Gas Industries (GASCO), an operating company of the Abu Dhabi National Oil Company (ADNOC), is leading a drive to boost gas production in the UAE from five to seven billion cubic feet per day. This calls for sulfur recovery capacity of over 3,000 metric tons per day with the associated SOx and NOx emissions. Therefore, the adoption and further development of flameless combustion technology for sulfur recovery among other commercial and industrial heating processes is expected to be crucial and beneficial, both economically and environmentally.

The conventional sulfur recovery process is based upon the withdrawal of sulfur by in situ condensation within the reactor. The selective removal of water should, however, be a far more effective technique, as its effect on the equilibrium composition in the mass action equation is much greater. The in situ combination of the heterogeneously catalyzed Claus reaction and an adsorptive water separation seems especially promising, as both reaction and adsorption exhibit similar kinetics, and pressure can be adapted to the needs of the adsorptive separation. Such an adsorptive reactor will lead to almost complete conversion as long as the adsorption capacity is not exhausted. There are numerous possibilities for implementing these two functions, ranging from fixed-beds with homogeneous catalyst/adsorbent mixtures to spatially structured distributions or even fluidized beds. Most of the previous studies have concentrated on the Claus catalytic conversion reactors and the TGTU. However, some previous studies have identified the Claus furnace as one of the most important yet least understood parts of the modified Claus process. The furnace is where the combustion reaction and the initial sulfur conversion (through an endothermic gaseous reaction) take place. It is also where the SO_2 required by the downstream catalytic stages is produced and the contaminants (such as ammonia and BTX (benzene, toluene, xylene) are supposedly destroyed. The main two reactions in the Claus furnace are: $H_2S + 3/2\ O_2 = SO_2 + H_2O$, with $\Delta H_r = -518$ kJ/mol, and $2H_2S + SO_2 = 3/2\ S_2 + 2H_2O$, with $\Delta H_r = +47$ kJ/mol. This last endothermic reaction is responsible for up to 67% conversion of the sulfur at about 1200 °C. Moreover, many side reactions take place in the furnace; these side reactions reduce sulfur recovery and/or produce unwanted components that end up as ambient pollutant emissions. Therefore, it would be useful to combine the endothermic and exothermic process using an isothermal reactor offered by flameless oxidation combustion.

Approach

Critical review

We propose to conduct a critical review of the various approaches used for sulfur removal from the sour gas. The emphasis here will be on sulfur chemistry with due consideration to the fate of ammonia. Following the review, an experimental and a CFD numerical study of the flameless oxidation of the fuel will be conducted as follows:

CFD simulation

A numerical simulation study of the flame under normal and flameless oxidation of fuels in the furnace will be conducted using the available codes. Global features of the flow and thermal behavior will be obtained using the Fluent CFD and Chemkin computer codes. These codes provide detailed simulation of the flow, thermal and chemical behaviors (i.e., detailed chemistry) in the reactor flow using gas-phase reactants. The sulfur in the fuel is in gas phase, so we will be able to simulate and monitor the fate of sulfur during various stages of endothermic and exothermic reactions and over a range of temperature regimes, including those covered in the Claus furnace process. The simulation results will also guide the final design of the flameless furnace. The simulations will also help assist in the experimental program for data validation with the eventual goal of implementing the process for sulfur removal.

Experimental study

An experimental study of the flameless vs. normal flame combustion process for the conditions examined in the theoretical study, including that of Claus furnace, will be conducted. We will explore the operating conditions and the exhaust gas analysis under conditions of both flame and flameless modes to determine the extent of sulfur conversion under the two conditions over the temperatures that can simulate endothermic and exothermic conditions in the Claus furnace. The goal is to seek conditions that yield the highest sulfur recovery from a process. To some extent, these conditions will be based on the composition of the acid/sour gas, from sulfur-rich (> 50% H_2S) to lean (< 20% H_2S). It is expected that our fundamental information will contribute to the eventual design guidelines of an advanced sulfur recovery process furnace operating under flameless combustion mode.

Evaluating Solid Oxide Fuel Cell Systems for Operation on Petroleum Off-Gases with Contaminants

UMD Investigators: Greg Jackson, Bryan Eichhorn
UMD GRAs: Siddarth Patel, Lei Wang
PI Investigators: Ali Almansoori, Valerie Eveloy, Ahmed Nafees
Start Date: March 2009

1. Objective/Abstract

In this program, UMD and PI will build on the established collaboration from earlier work – both experimental and modeling – to explore the impact of petroleum off-gas composition including effects of contaminants (H_2S and HCl) on SOFC performance/design. Single-cell SOFC experiments will be used to enhance and validate existing single-cell SOFC models to incorporate the effects of hydrocarbon composition and H_2S on SOFC performance. These single cell models will then be translated to full stack evaluations in higher dimensions, and these models will then be incorporated into process-level plant models to evaluate the effectiveness of SOFCs for capturing energy from petroleum gases and for providing a means for possible CO_2 capture within a plant context. This Phase II testing and development effort will also seek to bring an industrial collaborator to work with the team to explore design and implementation challenges for a future SOFC demonstration operating on relevant petroleum gas streams.

2. Deliverables for the Completed Quarter

Task 1: Establishing experimental facilities for MEA testing with trace contaminants
- UMD is beginning work on automated operation for long-term durability tests.

Task 2: Long-term testing MEAs for selected fuels and syngas with trace H_2S and HCl
- Efforts have begun for joint publication on SOFC experimental studies with syngas and n-butane/H_2O direct feeds

Task 3: Enhancing MEA models to evaluate contaminant-tolerant designs
- MEA models were used to fit experimental data to validate models before integration into system-level models.

Task 4: Performing system level analysis of integrated SOFC / off-gas processing plant
- PI and UMD have identified a system for process model development in Aspen/Hisys at PI with support from UMD.

Task 5: Establishing SOFC-industry partner for future demonstration
- No activities were pursued for this task during this quarter.

3. Summary of UMD Project Activities for the Completed Quarter

The second quarter of this Phase II effort included the following:

- A visit by Prof. Almansoori to UMD in late July to work on this and other projects;
- Identification of a researcher at the PI (Mr. Ahmed Nafees) to work on the system level simulations (Task 4) in collaboration with UMD;
- Beginning of a new graduate research assistant (Mr. Lei Wang) working on the project at UMD to address the issues of long-term durability testing (Task 2) and enhanced SOFC and system modeling (Tasks 3 and 4);

- Validation of SOFC MEA models against experimental database from spring testing;
- Beginning of advances in SOFC test rig at UMD to permit long-term testing in an automated fashion.

The project was in a transition period, as both PI and UMD were waiting for new participants on the project (Mr. Nafees at PI and Mr. Wang at UMD) to join the project. They have both come aboard in September and the group has started a bi-weekly conference call to ensure that collaboration on the project is strengthened going forward.

Task1: Establishing experimental facilities for MEA testing with trace contaminants
During this past quarter, the UMD team has begun to work on software and instrumentation aspects of the SOFC membrane electrode assembly (MEA) test rig in order to update it for long-term testing of MEA's with carbonaceous fuels and with trace contaminants. This has included updates to hardware such as improved humidifier and controls as well as upgrading of data acquisition software for improved rig operation both for safety and for automated electrochemical testing during durability studies. These upgrades, which are still ongoing, will allow for the experimental set-up to perform voltammetry and electrochemical impedance spectroscopy studies at regular intervals over a long period of operation. This will facilitate direct comparison of the degradation of performance of different MEA designs while running for long periods of time on a range of fuels of interest including syngas (i.e., reformate, with and without trace contaminants) and also direct hydrocarbon (n-butane)/steam feeds. To improve the steadiness of humidification for these streams, a higher-end temperature controller was purchased, which now permits humidifier operation to temperatures as high as 90 °C. The improved humidifier control has reduced temperature oscillations to < 1 °C, and MEA test results over this past quarter have shown significant reductions in oscillations of voltammetry measurements.

The updated data acquisition system, currently in progress, will be based on National Instruments LabView (version 8.7i). The UMD team is working on a state-machine control algorithm, which allows for the rig to operate automatically by programming transitions between states during a long-term durability test.

Task 2: Long-term testing MEAs for selected fuels and syngas with trace H_2S and HCl
Due to visa issues, the new research assistant (Mr. Wang) did not arrive as originally scheduled and only arrived at the end of this quarter. As he plans to be the key person working on this task, UMD did not accomplish significant work on this task and is behind here. However, the group has begun to update the rig for these tests as described in Task 1. In addition, some existing equipment has been acquired at no cost to this project in order to facilitate trace-contaminant injection and to provide emissions measurements of MEA tests. A portable gas chromatograph with appropriate columns has been acquired, and the project team is being trained to use this instrument in conjunction with long-term durability tests. In addition, the existing magnetic sector mass spectrometer has been calibrated for H_2S measurements during durability tests as well.

Task 3: Enhancing MEA models to evaluate contaminant-tolerant designs
UMD has extended the MEA models over the past quarter in two ways to improve their amenability for integration with larger-stack models. Firstly, the energy equation solver has been improved and made more robust and has been used to explore how internal reforming influences through-the-MEA temperatures during operation on direct hydrocarbon feeds. For this study, only the modified C1 surface chemistry for Ni/YSZ anodes has been developed as in previous reports. As such, the non-isothermal through-the-MEA model was tested with CH_4/H_2O feeds in Ni/YSZ anodes rather than the C_4H_{10}/H_2O feeds that have been the focus of the experimental tests. Results from the non-isothermal MEA model were found for an MEA operating for a Ni/YSZ anode operating with a feed of CH_4/H_2O at a high steam-to-carbon ratio (*S/C*) of 5.3 (15% CH_4/balance H_2O). Figure 1 shows the temperature profile through the MEA with the improved non-isothermal MEA model. In general, it can be seen that the temperature variations are quite small in the 1-D model.

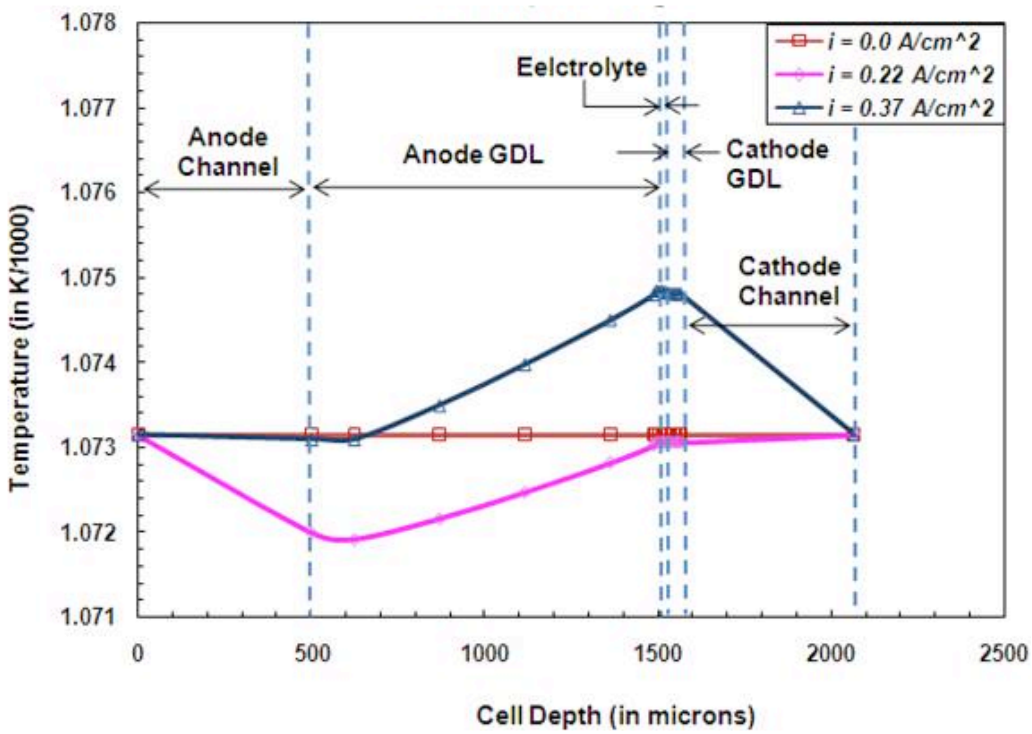

Figure 1. Temperature distributions for three different current densities for a through-the-MEA model of an SOFC button cell with a Ni/YSZ anode – YSZ electrolyte – LSM/YSZ cathode. Anode feed is 15% CH_4 and 85% H_2O, and cathode feed is dray air.

Figure 1 shows the minor effect of steam reforming and exothermic oxidation on the temperature distribution through the MEA. Temperature in the anode support layer drops at lower current densities (0.22 A/cm^2) as CH_4 reforming is more significant than oxidation. At higher current densities (0.37 A/cm^2), the temperature in the anode starts to rise as oxidation rates overtake reforming. The low-temperature variation for these simulations suggests that for through-the-MEA model, isothermal operation is a good assumption. This is important for looking at MEA design studies where the much longer simulation times of the non-isothermal model are problematic. For the non-isothermal operation, one sweep of 25 steady-state simulations (with the maximum current density of 0.97 A/cm^2) takes almost 10 hours on a 3.0 GHz dual core processor.

Although the above temperature profiles may not be significant enough to affect performance (~ 1-2 K temperature difference due to reforming) through the MEA of a button cell, the importance of the non-isothermal model is highlighted when analyzed in two-dimensional and stack models as discussed before. The almost non-significant temperature profile in a 1-D model is expected as the cell geometries are such that a thickness of a mere millimeter through the depth of the MEA renders the conditions almost isothermal. Similar observation has been recorded by Zhu & Kee (1), who report temperature differences through the MEA of the order of 1-2 K as well. However, as shown in a study by Janardhanan et al. (2), non-isothermal behavior is important for capturing large temperature gradients along the channel axis of SOFCs operating with internal reforming. Thus, when system models are built in Task 4, the improved robust thermal model developed here is critical for down-the-channel simulations of an SOFC stack.

In addition to the non-isothermal model, the UMD team used the through-the-MEA model to assess micro-architecture parameters to fit the measured *V-i* curves for button cells with Ni/YSZ anodes. By incorporating an electrolyte pinhole leakage model, the micro-architecture parameters agreed well with what was expected from cell fabrication.

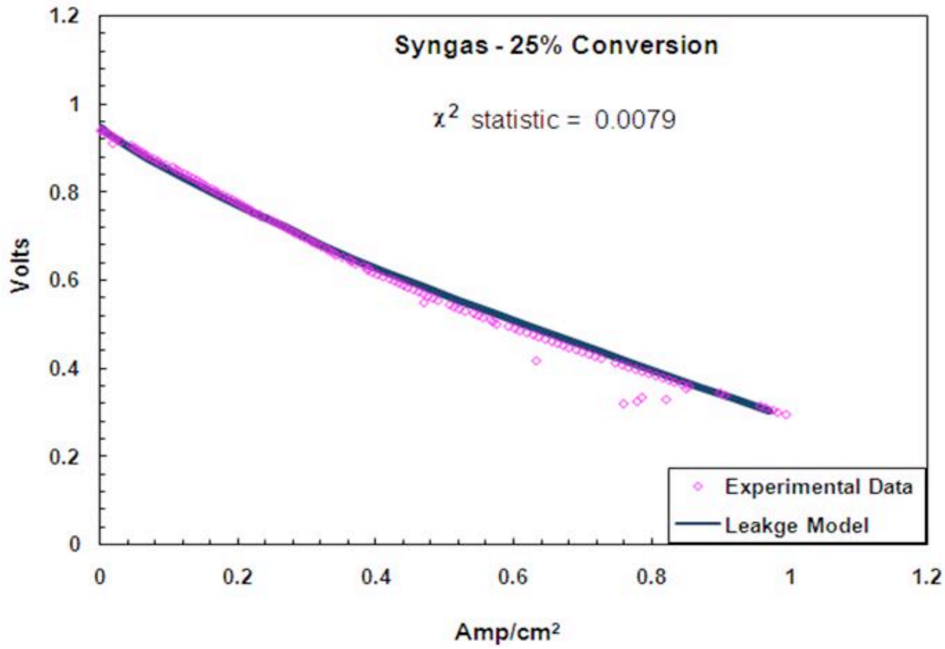

Figure 2. Example comparison of measured and model calculated voltage vs. current density curves for Ni/YSZ anode-supported MEAs, with properties provided in Table 1 below, operating at 800 °C on syngas with X_{H2} = 0.50, X_{H2O} = 0.23, X_{CO} = 0.15, X_{CO2} = 0.12.

Table 1. MEA micro-architecture parameters used to fit measurements of button cells with Ni/YSZ anodes and LSM/YSZ cathodes

	Anode	Cathode
TPB length, l_{TPB} [m^{-2}]	3e13	6e12
Average pore radius, r_p [μm]	0.5	0.5
Average particle diameter, d_p [μm]	2.5	2.5
Utilization thickness, δ_{util} [μm]	5	5
Support layer thickness [μm]	1000	50
Support layer porosity, φ_g	0.60	0.26
Support layer tortuosity, τ_g	3.5	2.9
Functional layer thickness [μm]	20	-
Functional layer porosity, $\varphi_{g,int}$	0.23	-
Functional layer tortuosity, $\tau_{g,int}$	4.5	-
Catalyst fraction of solid phase	0.6	0.47
Catalyst surface site density, Γ_{cat} [mol/cm^2]	1.66e-9	1.66e-9
Catalyst surface area a_{cat} [m^{-1}]	1e7	1e7
Electrolyte surface site density, Γ_{elec} [mol/cm^2]	1e-9	1e-9
Electrolyte surface area, a_{elec} [m^{-1}]	1e7	1e7
Double layer capacitance, C_{dl} [F/m^3]	0.003	0.2

Figure 2 shows the quality of the model fits to the data using realistic micro-architecture parameters as listed in Table 2. This model is modified from a previous model presented in Moeller et al. (3) The high quality of the fits show that the MEA model can readily capture performance of SOFCs. Furthermore, the model has shown that it can work well over a range of fuel compositions, and thus it is expected to work well in down-the-channel simulations that will be integrated into the system model in Task 4.

Task 4: Performing system-level analysis of integrated SOFC/off-gas processing plant
Neither PI nor UMD have begun working together to establish the system-level models for an SOFC power plant using Aspen/Hisys. It is expected that the MEA models in Task 3 will be implemented as a basis for a full-stack model that will be integrated with an Aspen/Hisys model. UMD and PI have discussed an initial SOFC power plant process shown in Figure 3. The initial system incorporates a small gas-turbine and natural-gas pre-reformer but is without CO_2 capture and not yet put in the context. Over the next quarter, the system in Figure 3, with perhaps slight modifications, will be modeled in Aspen/Hisys by the UMD/PI team.

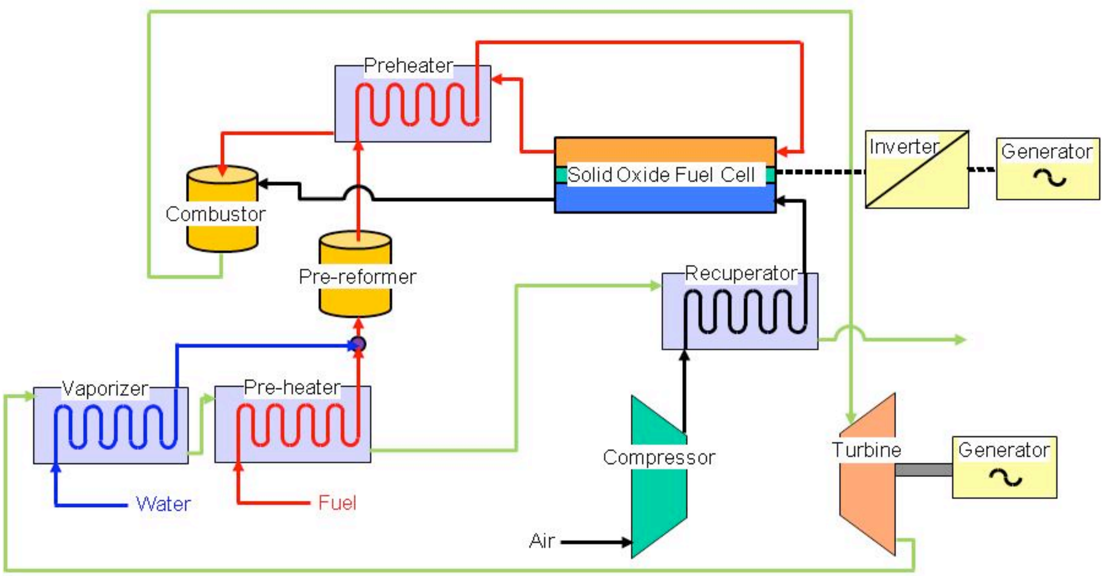

Figure 3. Proposed SOFC power plant operating on light hydrocarbon with gas-turbine cycle for modeling in Aspen/Hisys.

Task 5: Establishing SOFC-industry partner for future demonstration
At the moment, nothing is being pursued for this task. This task will likely be pursued more fully in the second year of this program.

4. Difficulties Encountered/Overcome

The difficulties in upgrading the rig for durability testing were encountered due to the delay in the arrival of Mr. Wang at UMD. The team has begun implementing knowledge gained from other control program developments to have a plan for the control software development for the durability tests. These rig upgrades will be completed in the next quarter.

Difficulties in moving the system-level studies forward have been resolved now that Mr. Nafees at PI has come on board. Bi-weekly conference calls have now been established to help develop the system model, and the system in Figure 3 has been identified as a system to target for the system modeling effort over next quarter.

5. Planned Project Activities for the Next Quarter

The following activities are planned for this quarter and will be facilitated by the joining of Mr. Wang at UMD and Mr. Nafees (part-time on the project) at PI.

- Complete the upgrade of the system for automated durability testing for carbonaceous fuel feeds with and without the inclusion of trace H_2S.
- Develop improved chemistry for light hydrocarbons in through-the-MEA models and incorporating the through-the-MEA models in down-the-channel SOFC models for stack-level design studies and thermal management.
- ASPEN-Hisys modeling of SOFC power plant as indicated in Figure 3.

Appendix

Justification and Background

There has been a movement for petroleum processing facilities to move to zero-flaring of off gases. These gases, derived from the petroleum extraction as well as downstream processing, can contain various hydrocarbons, some H2S, and depending on the process, HCl (derived from processes for well stimulation). These gases can be returned to an oil well to maintain well pressure. However, it is also possible to extract useful power from these gases employing SOFCs, which can provide high energy conversion efficiencies (> 50% based on fuel heating value) while maintaining separation of fuel oxidation products from N2 dilution that comes with conventional combustion processes. If SOFC architectures can be designed to operate effectively on such off-gases, then they can produce not only useful power but also concentrated CO2 and H2O streams which can be readily pumped to high pressure for oil-well re-injection. This provides a potential carbon footprint reduction of the petroleum processing both by producing power from waste streams and by providing an efficient means for re-injection of C-containing gases back into the well for sequestration. System level modeling in this program will show that such potential can be realized if stable SOFC systems are successfully developed.

Approach

This effort will extend earlier single membrane electrode assembly (MEA) testing and modeling at UMD and PI by looking at new gas compositions and the impact of trace H_2S and HCl contaminants on SOFC with potentially contaminant-tolerant materials and micro-architectures. UMD will employ additional MEA experiments with Raman spectroscopy to evaluate surface chemistry on selected SOFC materials (4). Functionally graded anode micro-architectures and material systems will be investigated for high power density and sulfur tolerance. These efforts will build on the earlier work exploring ceria/metal composite anodes and on recent work of others (5) showing the effectiveness of ceria nanoparticles for high-sulfur-tolerant SOFC anodes. The benefits of integrating an SOFC with an external steam or autothermal reformer will be explored by comparing SOFC performance with syngas vs. light hydrocarbon streams, where both are impacted by trace H_2S.

This work will rely on the progress made from integrating ceria (doped and/or un-doped_ with appropriate metal electrocatalysts for MEA designs tolerant of hydrocarbons. The testing will be done on selected fuels (CH_4, C_3H_8, C_4H_{10}) and on syngas contaminated with trace amounts of H_2S and separately trace amounts of HCl. Durability tests will be explored for preferred MEA designs. Modeling efforts will be expanded on both the micro-scale MEA level and on the large process scale to assess how contaminants handling will influence both SOFC design as well as overall process feasibility.

The simultaneous modeling effort in this program will also extend ongoing modeling efforts, which will have explored both MEA models for micro-architecture design as well as higher level process models for assessing the potential for integrating SOFC systems into oil well operations. The micro-architecture MEA modeling will expand on Phase I efforts by developing the semi-empirical kinetic models for internal reforming of hydrocarbons and of H_2S decomposition. The engineering viability of an SOFC integrated into a petroleum facility for energy recovery and possible CO_2 capture (3) will be investigated via system modeling within the context of petroleum processes by combining the SOFC models with process simulation in ASPEN/Hisys available at PI and UMD. The process models will rely on full stack SOFC models derived from the MEA models to explore overall balance of plant, adequacy of fuel supplies, and power requirements for CO_2 capture. If possible, process simulation will be done in consultation with ADNOC experts to explore how SOFCs might be integrated into petroleum processing facilities.

Specific tasks for the program are summarized in the proposed schedule below. The testing and model development effort will also seek to bring an industrial collaborator to work with the team to explore the possibility of a future demonstration SOFC system operating on petroleum processing offgases.

Task list: The overall approach can be summarized into 5 overarching tasks.

1) Establishing experimental facilities for MEA testing with trace contaminants
2) Long-term testing MEAs for selected fuels and syngas with trace H_2S and HCl
3) Enhancing MEA models to evaluate contaminant-tolerant designs
4) System level analysis of integrated SOFC / off-gas processing plant
5) Establishing industrial partner

Anticipated Deliverables: The following deliverables will be provided on this project:

1) Summary of MEA test results for preferred SOFC material and micro-architectures for high power density operation with syngas and hydrocarbons laden with selected contaminants,
2) MEA modeling results illustrating preferred micro-architectures with metal/ceria systems for contaminant-tolerant operation
3) System-level modeling tool with process evaluation for integration of SOFC into petroleum off-gas processing

Two-Year Schedule

Year 1:

- Upgrade SOFC MEA-testing facilities at UMD for handling trace contaminants
- Further development of SOFC experimental facilities at PI
- Perform post-testing material characterization for evaluation of long-term exposure to carbonaceous fuels
- Testing MEAs for selected fuels and syngas with trace H_2S and HCl
- Adopt SOFC models at UMD for hydrocarbon studies.
- Develop system level analysis of integrated SOFC / off-gas processing plant with analysis of contaminant flow

Year 2:

- Perform experiments with preferred material systems for typical off-gas compositions (with varying team loadings) for long-term durability with trace contaminants
- Enhance MEA models to evaluate micro-architectures for contaminant-tolerant operation
- Establish industrial partner in SOFC industry and ADNOC companies for development of demonstration project

7. References

[1] H.Y. Zhu and R.J. Kee, *Journal Of The Electrochemical Society*, **155**(7), B715 (2008).

[2] V.M. Janardhanan, V. Heuveline, and O. Deutschmann, *Journal Of Power Sources*, **172**(1), 296 (2007).

[3] B.F. Moeller, J. Arriagada, M. Assadi, and I. Potts, *Journal of Power Sources*, **131**(1-2), 320 (2004).

[4] M.B. Pomfret, J. Marda, G.S. Jackson, B.W. Eichhorn, A.M. Dean, and R.A. Walker, *Journal Of Physical Chemistry C*, **112**(13), 5232 (2008).

[5] H. Kurokawa, T.Z. Sholklapper, C.P. Jacobson, L.C. De Jonghe, and S.J. Visco, *Electrochemical And Solid State Letters*, **10**(9), B135 (2007).

Separate Sensible and Latent Cooling with Solar Energy

UMD Investigators: Reinhard Radermacher, Yunho Hwang
GRA: Ali Al-Alili
PI Investigator: Isoroku Kubo
Start Date: August 2007

1. Objective/Abstract

The main objective of this project is to design, fabricate and test a solar cooling system with the highest possible cooling COP measured to date. The approach involves combining a very efficient concentrating PV-T collector with a separate sensible and latent cooling approach developed at CEEE. This solar cooling system is expected to operate under the UAE's harsh climate conditions.

2. Deliverables for the Completed Quarter

The following tasks were accomplished:

- Investigate the performance of sensible vapor compression cycle using the EES
- Investigate the hybrid solar system performance under Abu Dhabi's climate conditions
- Explore the optimization capability of MATLAB
- Couple the TRNSYS with MATLAB

3. Summary of Project Activities for the Completed Quarter

The performance of the sensible vapor compression system was modeled using the EES in order to obtain better understanding of its operation. A performance map of the sensible VCC was created and implemented into the TRNSYS model. The complete hybrid solar system performance was investigated under Abu Dhabi's weather conditions. Its performance was compared to a standalone VCC during the heating and cooling seasons.

The optimization capability of TRNSYS was expanded by creating an interface that enables the coupling of TRNSYS with MATLAB. MATLAB has a powerful optimization toolbox that deals with single and multi-objective problems, whereas the current TRNSYS optimization component deals only with single objective problems. The link between MATLAB and TRNSYS was established. An example problem was used to test various optimization algorithms in MATLAB.

3.1 Investigation of the Sensible Vapor Compression Cycle

The Vapor Compression Cycle (VCC) is a key component in the cooling sub-system. Its performance under normal conditions, when taking the latent and sensible loads, is well understood. However, its performance when accommodating only sensible load needs to be investigated. Therefore, an EES code has been created to investigate its performance using ASHRAE 1% design conditions for Abu Dhabi (T_{amb} = 42.5°C and RH_{amb} = 19%) with conditioned space T_{space} = 25°C and RH_{space} = 50%. A performance map was created and implemented into the TRNSYS model. Figure 1 and Figure 2 show that the sensible VCC is operating at higher evaporating temperature and pressure. Operating at higher evaporating pressure reduces the compressor's pressure ratio, and hence increases its efficiency. This is expected since the VCC does not have to lower the evaporator temperature below the dew point of the incoming air stream in order to dehumidify. The dehumidification of the outside air is accomplished in the desiccant wheel before being sent to the VCC.

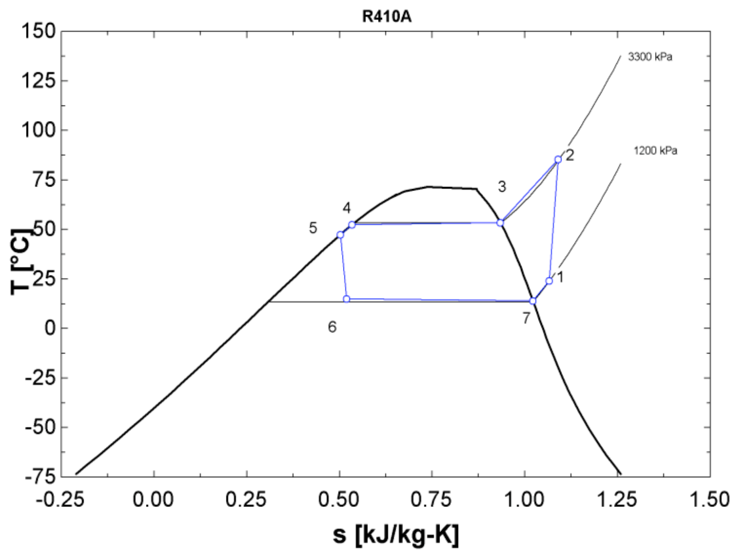

Figure 1. T-S diagram of the sensible VCC.

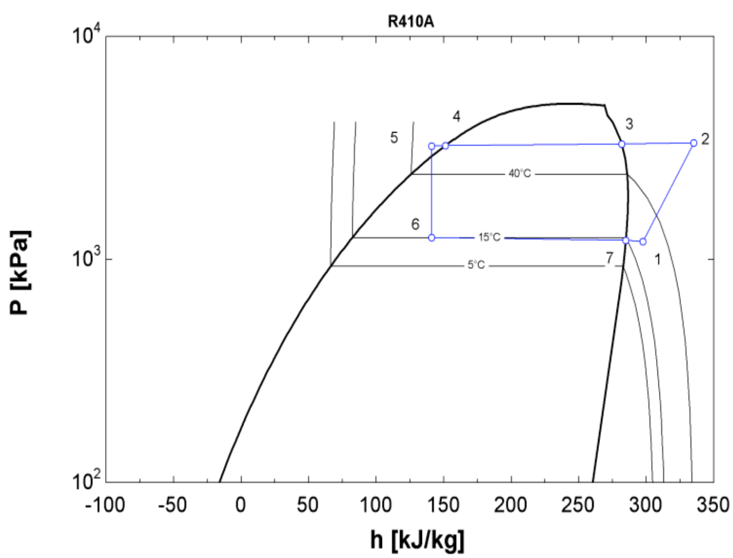

Figure 2. P-h diagram of the sensible VCC.

Figure 3 shows the air conditions across the sensible VCC's evaporator. It can be seen that the air is sensibly cooled and there is no latent load on the VCC.

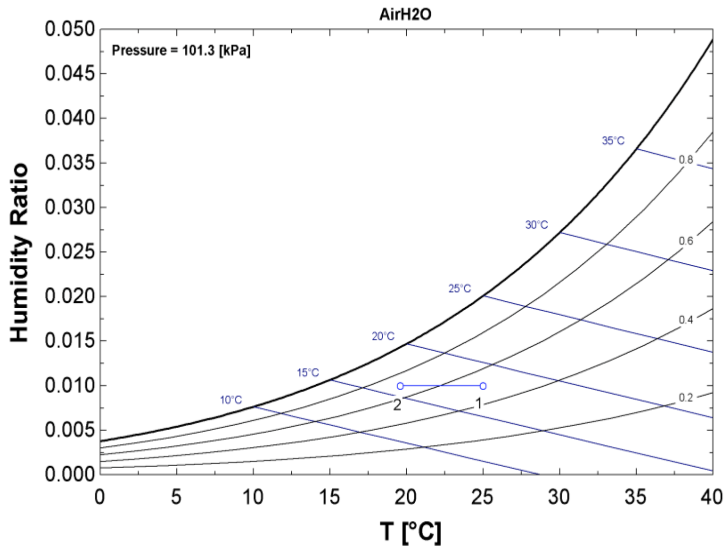

Figure 3. The conditions of the air across the sensible VCC's evaporator.

3.2 Complete System Performance

A Typical Meteorological Year 2 (TMY2) data file is used to obtain the solar irradiance and various weather conditions. The cooling and heating seasons for Abu Dhabi are set as shown in Figure 4. The comfort zone for each season is defined based on ASHRAE comfort zones for heating and cooling.

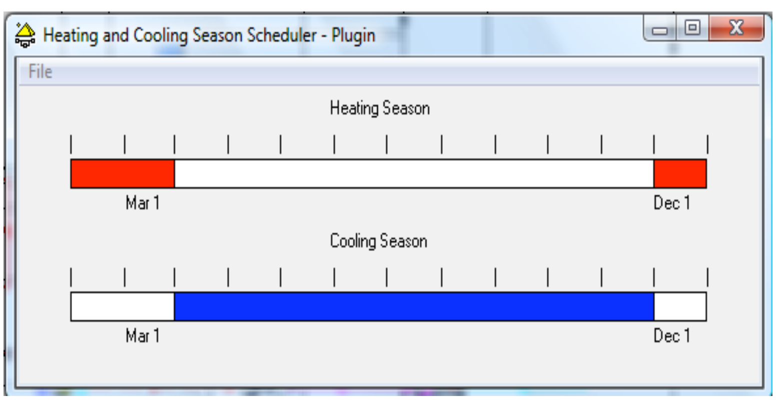

Figure 4. Heating and cooling seasons.

The hourly conditioned space (green points) and ambient temperatures (purple points) for the heating season are plotted in the psychrometric chart as shown in Figure 5. The performance of the hybrid solar system was compared to a standalone VCC, Figure 6. It can be seen that hybrid solar system is more efficient in maintaining the humidity ratio around 6 g_w/kg_a while the standalone VCC is not able to keep the humidity ratio in the comfort levels.

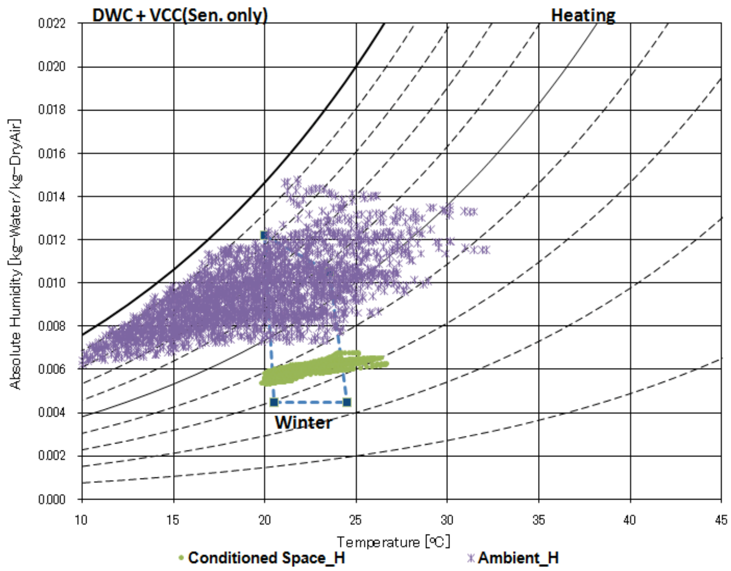

Figure 5. Heating hourly conditions (hybrid solar system).

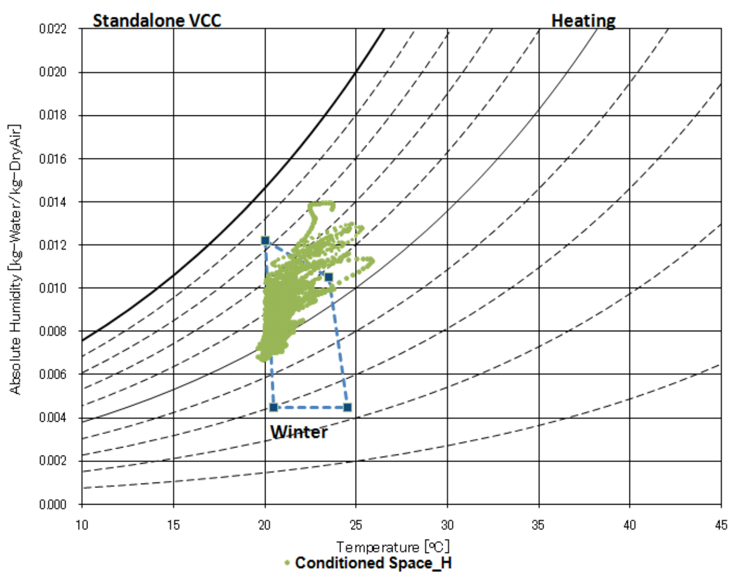

Figure 6. Heating hourly conditioned space conditions (standalone VCC).

The performance of the hybrid solar system was also compared to the standalone VCC during the cooling seasons. Figure 7 shows the performance of the hybrid solar system, which maintains the conditioned space temperature above the heating set point of 18°C and below the set humidity ratio of 8 g_w/kg_a.

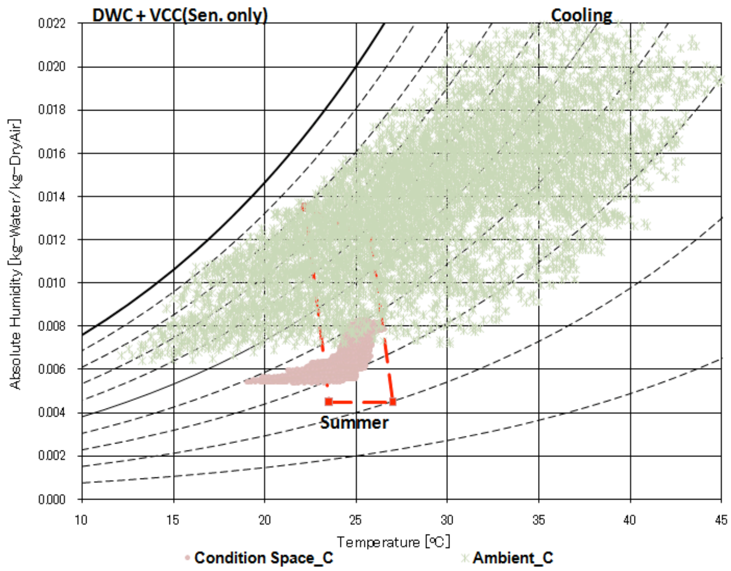

Figure 7. Cooling hourly conditions (Hybrid solar system).

Figure 8 shows that the standalone VCC is less effective in maintaining comfort conditions inside the conditioned space.

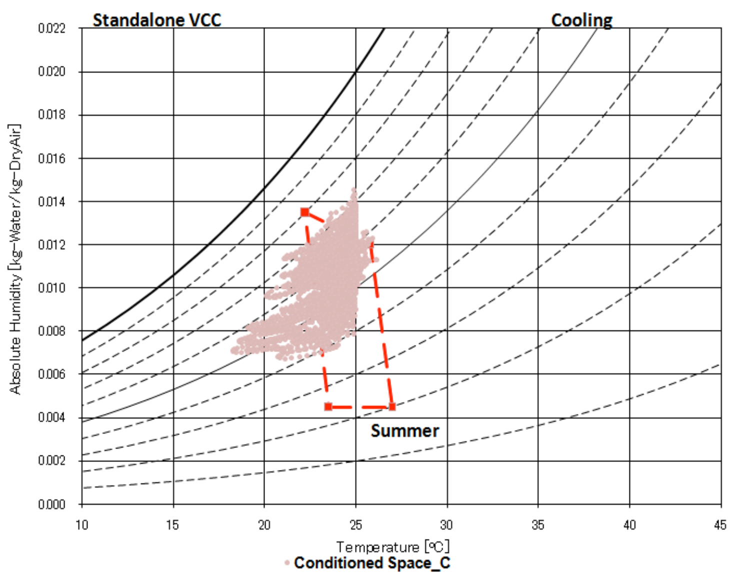

Figure 8. Cooling hourly conditioned space conditions (standalone VCC).

It can be concluded that the VCC alone is not as effective as the hybrid solar system in keeping the space conditions inside the desired comfort zone. Throughout the year, the hybrid solar system shows less scatter among the indoor conditions. This result indicates that it is very suitable for buildings requiring specific indoor temperatures and humidity ratios, such as hospitals and manufacturers.

3.3 Optimization

There are various ways in which optimization studies can be carried out for the hybrid solar system, as illustrated in Figure 9. A component is available in TRNSYS, TYPE 583, which launches the TRNOPT optimization program. TRNOPT acts as an interface between TRNSYS and the GENOPT Optimizer. GENOPT is a generic optimization algorithm developed by Lawrence Berkeley National Laboratory (LBNL). It is designed to interface with black-box simulation programs such as TRNSYS. Therefore, the objective function that is iteratively called by GENOPT is evaluated by TRNSYS. Another method is coupling the TRNSYS with MATLAB. Based on a user-defined interface, MATLAB is used to open the TNRSYS's input file and change the design parameters' values. Then, MATLAB calls the TRNSYS engine to run the modified input file and reads the output file to find the value of the objective function. In addition, the MATLAB has an optimization toolbox which can deal with single or multi-objective, single or multi-variables, unconstrained or constrained optimization problems. It also has a Genetic Algorithm (GA) optimization toolbox for global optimization. Therefore, the second approach allows more robustness and flexibility in formation of the optimization problem.

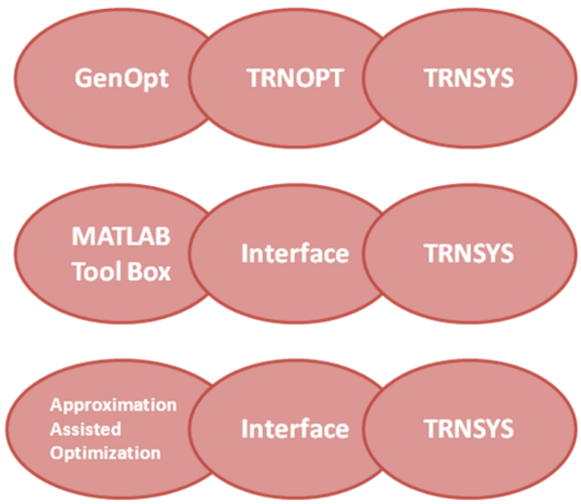

Figure 9. Different optimization approaches.

The link between the TRNSYS and the GenOpt has already been established. The interface between the TRNSYS and the MATLAB toolbox has also been created. By using an example problem, it has been found that the second approach sometimes consumes more time, especially when the global optimization algorithms are used. Therefore, the approximation-assisted optimization approach is under investigation. The goal of the third approach is to represent the optimization problem by a meta-model, which in turn is used in the MATLAB tool box optimization algorithms. This approach is not only expected to be the least time-consuming approach, but also the most flexible.

4. Difficulties Encountered/Overcome

- Creating the interface between MATLAB and TRNSYS
- Finding the most appropriate optimization algorithms from the MATLAB tool box to be used with TRNSYS

5. Planned Project Activities for the Next Quarter

The following activities are to be conducted in the next quarter:

- Present results which demonstrate the difference between the various optimization approaches used
- Finalize the design of experiment (schematics, list of components and instrumentation)

Appendix

References

[1] Stine, W.B., Geyer, W.B., 2001, Power from the sun, www.powerfromthesun.net.

[2] Threlkeld,.J, Kuehn, T., Ramsy, J.,1998, Thermal Environmental Engineering, Prentice-Hall, Inc, USA

[3] http://www.nrel.gov/rredc/solar_data.html

[4] http://rredc.nrel.gov/solar/old_data/nsrdb/tmy2/State.html

[5] Notton , G. , Poggi, P. , Cristofari, C., 2006, Predicting hourly solar irradiations on inclined surfaces based on the horizontal measurements: Performances of the association of well-known mathematical models, *Energy Conversion and Management*, 47 1816–1829

[6] http://rredc.nrel.gov/solar/old_data/nsrdb/1991-2005/siteonthefly.cgi?id=724060

[7] ASHRAE, 1999, Applications Handbook, CH.32

[8] Kreith, F. and Kreider, J.F., 1978, Principles of solar engineering, *Hemisphere publishing corporation* Washington USA

[9] Kalogirou, S., 2004, Solar thermal collectors and applications, *Progress in Energy and Combustion Science* 30 pp. 231–295

[10] Goswami, Y., Kreith, F. and Kreider, J.F., 2000, Principles of solar engineering, *Taylor and Francis,* PA, USA,

[11] Duffie, J.A., Beckman, W.A., 1991, *Solar engineering of thermal processes*, Second edition, John Wiley & Sons, Inc., New York, ISBN: 0-471-51056-4.

[12] Pasupathy, A., Velraj, R., Seeniraj, R.V., 2008, Phase change material-based building architecture for thermal management in residential and commercial establishments, *Renewable and Sustainable Energy Reviews*, pp.39–64

[13] Dieng, A., Wang, R. , 2001 Literature Review on Solar Adsorption Technologies of Ice-making and Air Conditioning Purposes and Recent Developments in Solar Technology, *Renewable and Sustainable Energy Reviews* 5 pp.313–342

[14] Sumathy, K., Yeug, K, Yong, L., 2003, Technology Development in the Solar Adsorption Refrigeration Systems, *Progress in Energy and Combustion Science* 29 pp 301–327

[15] Roger, A. Messenger, J. V., 2005, Photovoltaic Systems Engineering, 2nd ed. Taylor & Francis

[16] http://www.nfpa.org/

[17] http://ieeexplore.ieee.org/iel5/7946/21930/01019771.pdf?arnumber=1019771

[18] TRANE, "Product Data: 4DCZ6036A through 4DCZ6060A" (2008), 22-1815-03

[19] METEONORM, "Global Meteorological Database for Engineers, Planners and Education,"(2007)

Waste Heat Utilization in the Petroleum Industry

UMD Investigators: Reinhard Radermacher, Yunho Hwang
GRAs: Amir Mortazavi, Abdullah Alabdulkarem
PI Investigators: Saleh Al Hashimi, Peter Rodgers
GRAs: Sahil Popli, Alyas Ali Alshehhi
Start Date: January 2009

1. Objective/Abstract

The main objective of this project is to minimize overall energy consumption of gas or oil processing plants by utilizing waste heat and/or improving cycle design. Consideration will include use of absorption chillers and steam cycles, among other options.

2. Deliverables for the Completed Quarter

The following were modeled in HYSYS:
- APCI base cycle
- APCI enhanced with absorption chillers
- Gas turbine
- Different gas turbine combined cycle configurations (double pressure, triple pressure with and without reheat)

3. Summary of UM Project Activities for the Completed Quarter

ASPEN plus models were also modeled in HYSYS as per the sponsor's request. The results are compared in the following sections. Different gas turbine combined cycles were also modeled in order to investigate the best configurations of the driver cycles and waste utilization units for APCI LNG plants.

3.1 APCI base cycle modeling with HYSYS

The HYSYS model of the APCI base cycle is shown in Figure 1. The ASPEN model is shown in Figure 2. In Table 1, some of the HYSYS model results are compared with the ASPEN model. As shown in Table 1 the discrepancy between the two models is less than 0.2%.

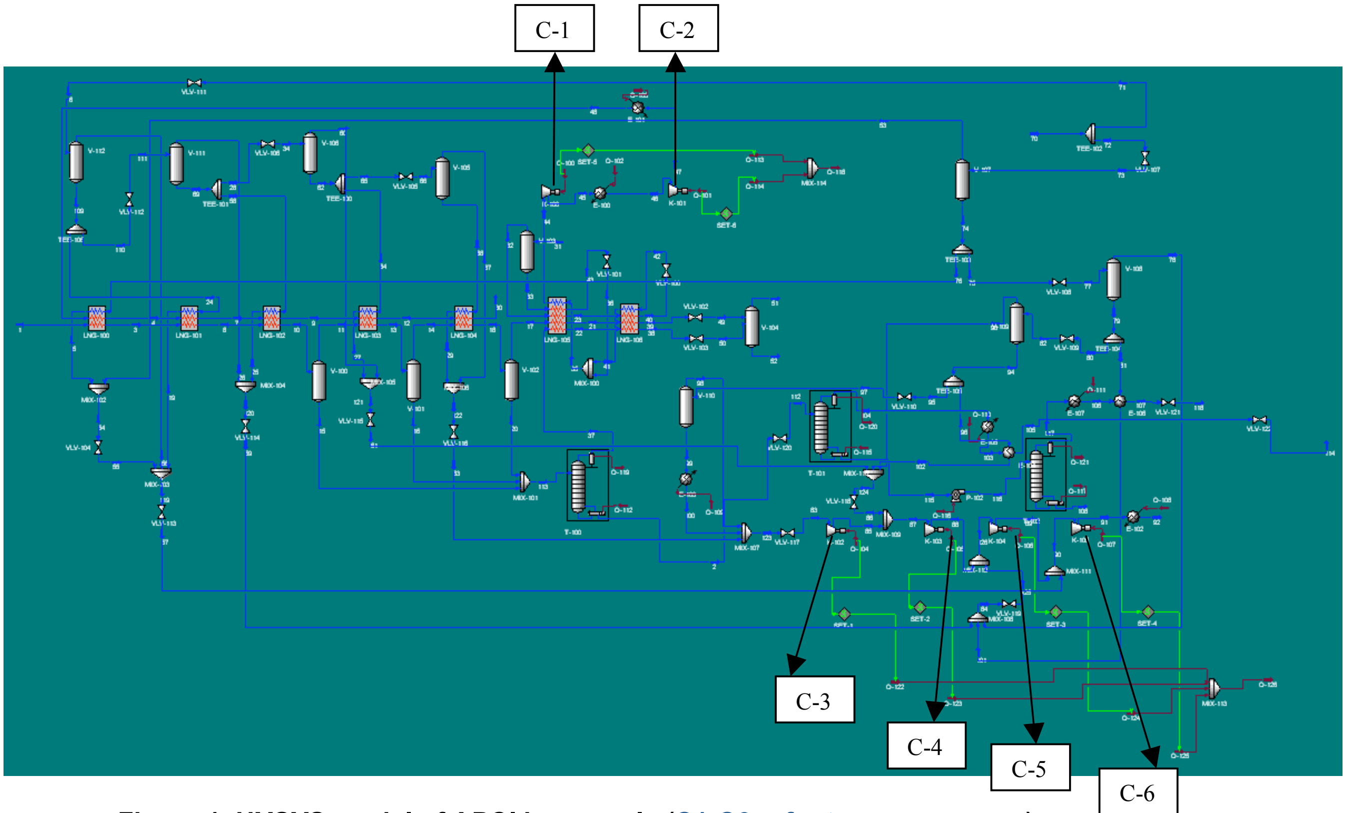

Figure 1. HYSYS model of APCI base cycle (C1-C6 refer to compressors).

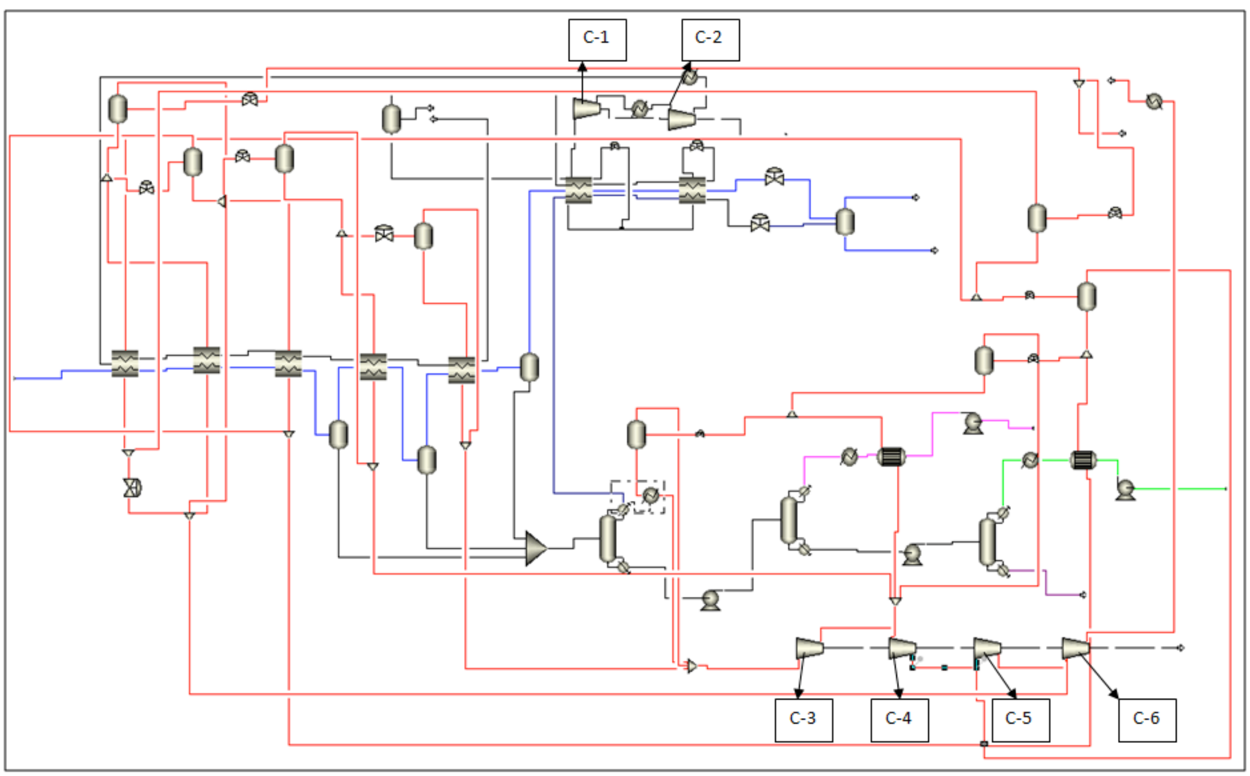

Figure 2. ASPEN model of APCI base cycle (C1-C6 refer to compressors).

Table 1. Comparison of HYSYS model with ASPEN PLUS model

Component	Property	ASPEN PLUS Value	ASPEN HYSYS Value	Percentage Difference (%)
Compressor [C-1]	Temperature (°C)	79.50	78.77	---
	Pressure (Bar)	23.00	23.00	0.00
	Duty (kW)	49686.41	49628.02	-0.12
Compressor [C-2]	Temperature (°C)	40.00	40.00	0.00
	Pressure (Bar)	80.50	80.41	-0.11
	Duty (kW)	16848.85	16847.84	-0.01
Compressor [C-3]	Temperature (°C)	-1.60	-0.42	---
	Pressure (Bar)	2.00	2.00	0.00
	Duty (kW)	2488.09	2488.56	0.02
Compressor [C-4]	Temperature (°C)	13.90	14.67	---
	Pressure (Bar)	3.40	3.40	0.00
	Duty (kW)	5738.89	5738.66	-0.00
Compressor [C-5]	Temperature (°C)	32.40	32.82	---
	Pressure (Bar)	5.80	5.80	0.00
	Duty (kW)	8642.86	8639.82	-0.04
Compressor [C-6]	Temperature (°C)	70.10	70.50	---
	Pressure (Bar)	15.40	15.40	0.00
	Duty (kW)	26810.96	26834.45	0.09

3.2 Modeling different configurations of gas turbine combined cycle:

The HYSYS software was used to model gas turbine combined cycles with:

1. Single pressure steam generator
2. Double pressure steam generator
3. Triple pressure steam generator without reheater
4. Triple pressure steam generator with reheater

These cycles will be used as drivers for APCI liquefaction cycle compressors in modeling, and their combination with absorption chillers will also be considered.

4. Summary of PI Project Activities for the Completed Quarter

A master's student, Mr. Sahil Popli, has commenced graduate studies on this project. His first task has been to undertake a comprehensive review of studies published over the past three decades on waste heat recovery and its utilization in the oil and gas industries. This review has so far analyzed oil refineries having waste heat recovery facilities that utilize: i) energy from stack gases, both boiler and turbine exhaust flue gases, and flared gases, for preheating process streams, and ii) steam generation through a combined cycle or cogeneration. The review has also highlighted that the oil and gas industry has an isolated rather than systematic industry-wide application of waste heat utilization.

A mechanical engineering student, Mr. Alyas Ali Alshehhi, has commenced an energy audit of the GASCO ASAB LNG plant as part of his engineering project thesis. This analysis included identification of potential waste heat sources at two ASAB facilities (ASAB0 and ASAB1), for both gas turbine exhaust gases and flared gases from the gas plant which could be used to provide enhanced process cooling capacity to the natural gas liquid (NGL) plant through absorption cooling.

5. Difficulties Encountered/Overcome

None to report.

6. Planned Project Activities for the Next Quarter

The following activities are to be conducted in the next quarter:

- The UM team will focus on optimization of the combined cycle.
- The PI team will focus on the literature review and GASCO energy audit.
- The waste heat literature survey will be continued and documented for future publication.
- The GASCO energy audit will evaluate waste heat source process data in terms of temperature, quantity and quality. This analysis will aid identification of technologies that could utilize potential waste heat sources at ASAB and be applied to an appropriate end-use, such as absorption cooling.

Appendix

Justification and Background

Waste heat utilization opportunities are abundant in the oil and gas industry. Proper use of waste heat could result in improved cycle efficiency, reduced energy usage, reduction in CO_2 emissions, and increased production capacity.

CEEE at the University of Maryland has extensive experience in the design and implementation of integrated combined cooling, heating, and power (CCHP) projects. The faculty at PI has experience in the design and operation of petroleum processing plants. Jointly, the team is well equipped to address the challenge posed by this project.

References

[1] Alefeld, G., Radermacher, R., 1994, "Heat conversion systems," CRC Press, Boca Raton.

[2] Al-Hamdan, Q.Z., Ebaid, M.S.Y., 2006, "Modeling and simulation of a gas turbine engine for power generation," ASME Journal of Engineering for Gas Turbines and Power, Vol. 128, pp. 302-311.

[3] LNG technology selection, http://www.fwc.com/publications/tech_papers/files/TariqLNG.pdf, Last access, June, 2008

[4] Haring, H., 2008, " Industrial Gas Processing," Wiley-VCH, Weinheim

[5] ASHRAE, 2002, "ASHRAE Refrigeration Handbook," American Society of Heating, Refrigeration and Air-Conditioning Engineers, Atlanta, GA, USA.

[6] ASHRAE, 2005, "ASHRAE Fundamentals Handbook," American Society of Heating, Refrigeration and Air-Conditioning Engineers, Atlanta, GA, USA.

[7] Brant, B., Brueske, S., Erickson, D.C., Papar, R., 1998, "New waste-heat refrigeration unit cuts flaring, reduces pollution," Oil & Gas Journal, May 18, pp.61-64.

[8] Brooks, F.,J., 2000 "GE gas turbine performance characteristics," GE Power Systems Schenectady, NY, GER-3567H.

[9] Cohen, H., Rogers, G.F.C., Saravanamuttoo, H.I.H., 1996, "Gas turbine theory," 4th edition, Longman Scientific & Technical, Singapore.

[10] Erickson, D.C., 2000 "LPG recovery from reformer treat gas," US Patent 6,158,241.

[11] Erickson, D.C., Anand, G., Papar, R.A., Tang, J., 1998, "Refinery waste heat powered absorption refrigeration – cycle specification and design," Proceeding of the ASME Advanced Energy System Division, AES-Vol. 38, pp.391-402.

[12] Erickson, D.C., Kelly, F., 1998, "LPG recovery from refinery by waste heat powered absorption refrigeration," IECEC-98-079, 33rd Intersociety Engineering Conference on Energy Conversion, Colorado Springs, CO.

[13] Giampaolo, T., 2003, "The gas turbine handbook: principles and practices," 2nd edition, The Fairmont Press, Lilburn, GA.

[14] Herold, K.E.; Radermacher, R., Klein, S, 1996, "Absorption chillers and heat pumps," CRC Press, Boca Raton.

[15] Kim, T.S., Hwang, S.H., 2006, "Part load performance analysis of recuperated gas turbine considering engine configuration and operation strategy," Energy, Vol. 31, pp., 260-277.

[16] Klein, S.A., 2005, "Engineering Equation Solver" F-Chart Software.

[17] Kurz, R., 2005, "Gas turbine performance," 44th Turbomachinery Symposium, pp.131-146.

[18] Kurzke, J., 2003, "Model based gas turbine parameter corrections," GT2003-38234, Proceedings of 2003 ASME TURBO EXPO: Power for Land, Sea, & Air, Atlanta, GA, USA.

[19] Li, Y.G., Pilidis, P., Newby, M.A., 2006, "An adaptation approach for gas turbine design-point performance simulation," Journal of Engineering for Gas Turbines and Power, Vol. 128, pp. 789-795.

[20] Orlando, J.,A., 1996, "Cogeneration design guide," American Society of Heating, Refrigeration and Air-Conditioning Engineers, Atlanta, GA.
[21] Pande, M., 1996, "Tools for fractionator design in ammonia-water absorption machines," Master Thesis, University of Maryland, College Park.
[22] Walsh, P.P., Fletcher, P., 1998, "Gas turbine performance," Blackwell Science, Oxford.

Thrust 2
Energy-Efficient Transport Process Projects

Multidisciplinary Design and Characterization of Polymer Composite Seawater Heat Exchanger Module

PI Investigator: Peter Rodgers
UMD Investigators: Avram Bar-Cohen, Satyandra K. Gupta, David Bigio
GRAs: Juan Cevallos, F. Robinson, T. Hall, W. Pappas, M. Chowdhury
Start Date: January 2009

1. Introduction

Heat exchangers are extensively used in all oil and gas processing operations with seawater as the preferred coolant in near-shore operations. The performance and cost effectiveness of conventional metallic heat exchangers in such environments are severely constrained by corrosion and scale deposits. Polymer heat exchangers, currently under investigation by the EERC team, offer a promising alternative to metallic heat exchangers for the fossil fuel industry. Recent advances in carbon-fiber polymer composites, yielding polymer materials with thermal conductivities equal to or higher than titanium, can be applied to the development of low-cost and low-weight compact heat exchangers for corrosive fluids. These attributes, combined with the low energy investment in the formation and fabrication of these polymer heat exchangers and their ease of manufacturing, appear to make near-term applications of seawater polymer heat exchangers viable. Numerical simulations and laboratory experiments, performed by the UMD/PI EERC team in the first phase of this research, strongly support these conclusions.

2. Deliverables for the Completed Quarter

1. Continue investigation on the mechanical and surface effects of immersing polymer composites in fresh and saltwater (A5)
2. Utilize Moldflow® to predict how varying injection molding and material conditions affect fiber orientation (B2)
3. Characterize the suitability of injection molding for creating thermally-enhanced polymer heat exchangers (B1)
4. Validate Moldflow® predictions experimentally (B1)
5. Integrate the mold-fill meta-model in the design process of a modular heat exchanger (update from last quarter) (B1)
6. Investigate parametrically the use of an effective isotropic thermal conductivity for fins with local anisotropy (A3)
7. Design a polymer heat exchanger prototype at The Petroleum Institute (A1)
8. Two journal articles have been drafted and are currently being revised [2][3].
9. A draft of a polymer heat exchanger survey paper is being circulated among members of the PHX team [4].
10. A literature review on thermally enhanced polymer materials and polymer heat exchangers has been undertaken at The Petroleum Institute to supplement previous literature surveys.
11. Mr. Mohammad Chowdhury has commenced PhD studies at PI.

3. Summary of Project Activities for the Completed Quarter

I. Continue investigation on the mechanical and surface effects of immersing polymer composites in fresh and salt-water

a. Experimental Setup

- Tensile specimens were injection molded in accordance with American Society for Testing and Materials (ASTM) standards for testing for the tensile properties of plastics. Two commercially available materials were used: unreinforced PA12 from EMS-Grivory and short carbon fiber reinforced PA12 (33 vol. %, 51 wt. % carbon fiber) from PolyOne.
- All specimens were molded then dried at 80°C over calcium sulfate until additional drying time did not result in additional moisture removal. Each specimen was then weighed on a scale with a precision of 0.1 milligrams.
- Twelve specimens of each material were placed into six different water baths. The water baths were maintained at three temperatures (40, 50, and 60 °C) and two salinity levels (freshwater, 45g/kg).
- A temperature controller and relay regulated the power to the heater to maintain constant temperature in each water bath. LabVIEW, a thermocouple input device, and a thermocouple in each water bath recorded temperature in each water bath.
- A pump circulated the water in the tank to prevent temperature and salinity stratification. The experimental setup is shown in Figure 1.

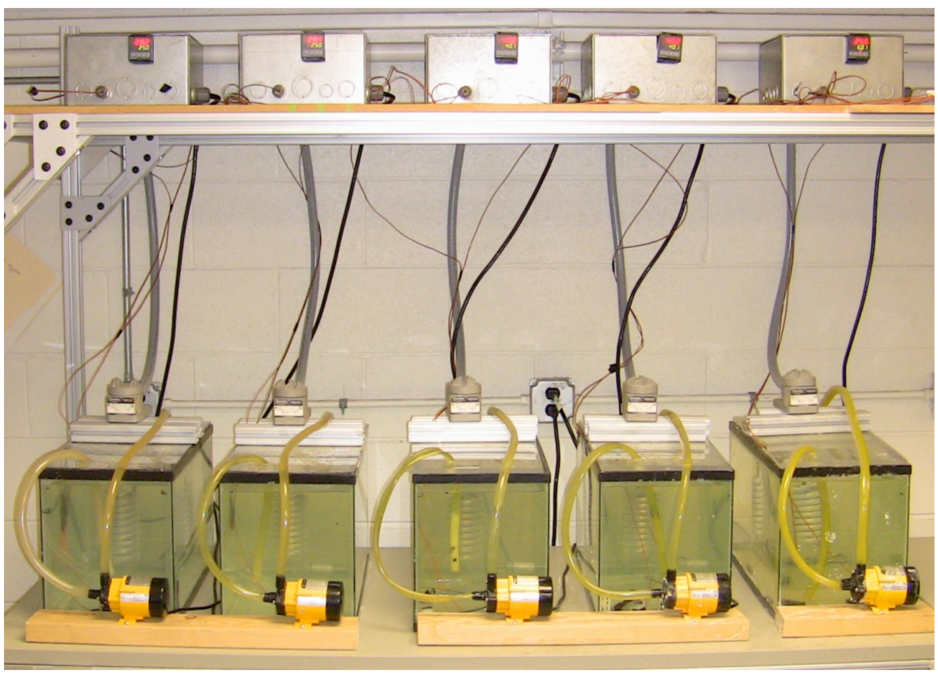

Figure 1. Experimental setup for hygrothermal aging experiment.

b.Equilibrium Moisture Content Results

Immersion time was based on diffusion times from previous study and confirmed by repeating weight measurements until additional immersion time no longer increased moisture content. Upon removal from the water baths, all specimens were weighed, and the equilibrium moisture content of each specimen was calculated.

- *Unreinforced PA12 Results:* Equilibrium moisture content results for unreinforced PA12 are shown in Figure 2.

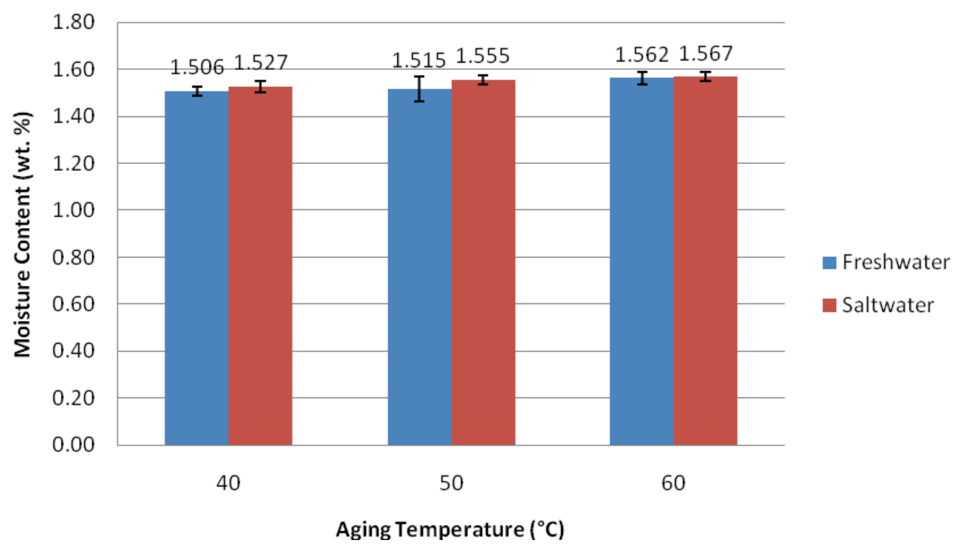

Figure 2. Equilibrium moisture content (wt. %) of unreinforced PA12.

Unreinforced PA12 results show a trend of increasing moisture content with increasing temperature and increasing salinity. However, differences between the values are statistically insignificant. Accordingly, within the error of this experiment, neither temperature nor salinity significantly affects the equilibrium moisture content of unreinforced PA12.

- *Reinforced PA12 Results:* Equilibrium moisture content results for reinforced PA12 are shown in Figure 3.

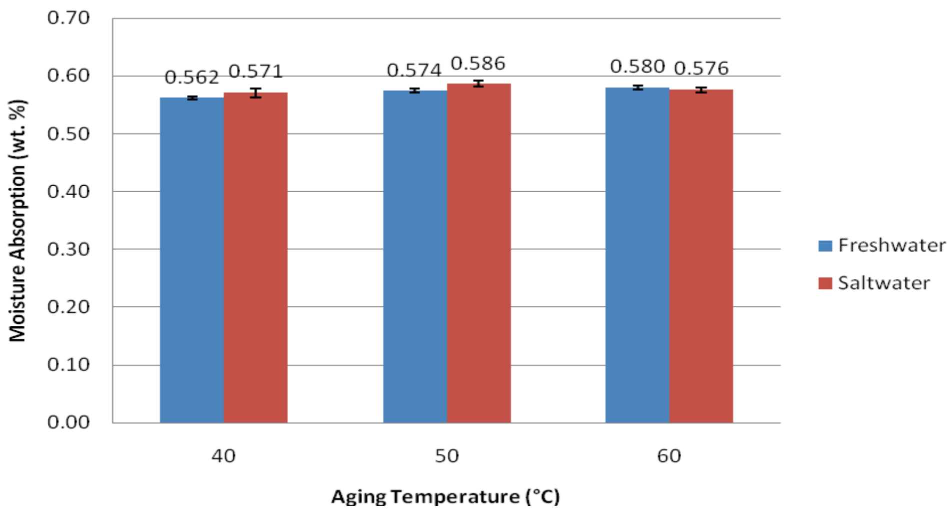

Figure 3. Equilibrium moisture content (wt. %) of unreinforced PA12.

Reinforced PA12 results show a trend of increasing moisture content with increasing freshwater temperature. The same trend is not seen in saltwater. No trend is seen between freshwater and saltwater moisture content. Any disparities in the data are not statistically significant. Accordingly, within the error of this experiment, neither temperature nor salinity significantly affects the equilibrium moisture content of reinforced PA12.

- ***Comparison of Unreinforced PA12 and Reinforced PA12 Results:*** Equilibrium moisture content disparity between unreinforced PA12 and reinforced PA12 is significant. Among unreinforced PA12 samples, average equilibrium moisture content was 1.539 percent. Among reinforced PA12 samples, average equilibrium moisture content was 0.575 percent. The disparity in equilibrium moisture content is partly the result of the addition of the carbon fibers, which do not absorb any water. Also, the carbon may reduce the free volume by constraining the molecular structure between particles. Further, the additives required to functionalize the carbon in the composite mixture could fill the free volume of the composite specimens, reducing equilibrium moisture content.

c. Re-dried Weight Results

- After weighing the saturated specimens, six of the 12 specimens from each aging condition were re-dried at 80°C over calcium sulfate until additional drying time did not result in additional moisture removal. Re-dried weights of specimens were compared to the weights recorded prior to immersion in the water baths.
- No statistically significant difference exists between unaged and re-dried weights of unreinforced PA12 or reinforced PA12. For reinforced PA12 this conclusion verifies that, for the water temperatures of this experiment, there is no leaching effect of the carbon fibers.
- Ishai studied environmental effects on the deformation, strength, and degradation of glass-fiber reinforced plastics (GRP). He found that all GRP (47 vol. %) exposed to hot water (80°C) were characterized by irrecoverable weight loss. Weight loss was attributed to "temperature-controlled attack on the glass-fiber surface and the interfacial coupling agent phase by the water, with consequent leaching and removal of glass constituent molecules" [1]. No such behavior was seen in our unfilled specimens.

d. *Mechanical Property Results*

- ***Baseline mechanical properties for both the unreinforced PA12 and reinforced PA12*** are shown in Table 1.

Table 1. Baseline mechanical properties of unreinforced PA12 and reinforced PA12

Material	Elastic Modulus (GPa)	Yield Strength (MPa)	Elongation at Yield (%)	Ultimate Strength (MPa)	Elongation at Failure (%)
Unreinforced PA12	1.44	39.8	2.9	41.7	> 100
Reinforced PA12	21.1	80.6	0.59	103	1.46

Addition of carbon fibers makes the specimens approximately 15 times as stiff, twice as strong at yield, one-fifth as ductile at yield, 2.5 times as strong at fracture, and less than one-seventieth as ductile at fracture.

- ***The effect of water temperature on degradation of mechanical properties of hygrothermally-aged, unreinforced PA12*** is shown Table 2. Combined values for freshwater and saltwater at each temperature are shown because the effect of the saltwater was not statistically significant. Percent retention values are aged values divided by baseline values times 100 percent.

Table 2. Effect of water temperature on mechanical properties of hygrothermally-aged unreinforced PA12

Temperature (°C)	Elastic Modulus (GPa)	Yield Strength (MPa)	Elongation at Yield (%)	Ultimate Strength (MPa)
40	0.73	19.9	3.0	43.6
% Retention	50.7%	50.0%	100%	105%
50	0.69	18.7	2.9	42.3
% Retention	49.3%	46.9%	99.3%	101%
60	0.69	17.9	2.8	38.3
% Retention	49.3%	45.0%	96.6%	91.7%

At any temperature, both elastic modulus and yield strength are roughly reduced to half their original values. Elongation at yield remains roughly constant at all three temperatures. Ultimate strength increases relative to baseline at 40 and 50 °C. This may be the result of the moisture content allowing the polymer chains to slip past each other more readily, which prolongs time before fracture. Reduction in ultimate strength at 60 °C may be the result of damage done to the matrix, which overwhelms any increase in yield strength that was a result of the polymer chains slipping more readily.

- ***The effect of water temperature on the degradation of mechanical properties of hygrothermally-aged, reinforced PA12*** is shown Table 3. Combined values for freshwater and saltwater at each temperature are shown because the effect of the saltwater was not statistically significant. Percent retention values are aged values divided by baseline values times 100 percent.

Table 3. Effect of water temperature on mechanical properties of hygrothermally-aged reinforced PA12

Temperature (°C)	Elastic Modulus (GPa)	Yield Strength (MPa)	Elongation at Yield (%)	Ultimate Strength (MPa)	Elongation at Failure (%)

40	14.0	55.6	0.62	84.5	2.8
% Retention	66.4%	69.0%	105%	82.0%	192%
50	16.0	53.2	0.56	84.9	3.0
% Retention	75.8%	66.0%	94.9%	82.3%	205%
60	11.6	54.4	0.70	84.8	3.1
% Retention	54.9%	67.5%	119%	82.3%	212%

Hygrothermal aging reduced the elastic modulus, yield strength, and ultimate strength of reinforced PA12. Greater retention, relative to unreinforced PA12, is seen in elastic modulus and yield strength. Lower retention, relative to unreinforced PA12, is seen in ultimate strength. Elongation at yield and elongation at failure tends to increase with increasing temperature.

- ***The effect of water temperature on the degradation of mechanical properties of re-dried, unreinforced PA12*** is shown in Table 4. Combined values for freshwater and saltwater at each temperature are shown because the effect of the saltwater was not statistically significant. Percent recovery values are re-dried values divided by baseline values times 100 percent.

Table 4. Effect of water temperature on mechanical properties of re-dried unreinforced PA12

Temperature (°C)	Elastic Modulus (GPa)	Yield Strength (MPa)	Elongation at Yield (%)	Ultimate Strength (MPa)
40	1.29	36.4	3.0	43.0
% Recovery	89.6%	91.5%	103%	103%
50	1.26	38.4	3.3	44.8
% Recovery	87.5%	96.5%	114%	107%
60	1.21	32.3	2.9	39.7
% Recovery	84.0%	81.2%	100%	95.2%

Elastic modulus and yield strength are not fully recovered at any of the water temperatures, indicating the aging process causes permanent damage to unreinforced PA12. Elongation at yield and ultimate strength increase slightly at 40 and 50 °C, while staying constant and decreasing slightly at 60 °C, respectively.

- ***The effect of water temperature on the degradation of mechanical properties of re-dried, reinforced PA12*** is shown in Table 5. Combined values for freshwater and saltwater at each temperature are shown because the effect of the saltwater was not statistically significant. Percent recovery values are re-dried values divided by baseline values times 100 percent.

Table 5. Effect of water temperature on mechanical properties of re-dried reinforced PA12.

Temperature (°C)	Elastic Modulus (GPa)	Yield Strength (MPa)	Elongation at Yield (%)	Ultimate Strength (MPa)	Elongation at Failure (%)
40	22.5	78.5	0.58	106	1.62
% Recovery	107%	97.4%	98.3%	103%	111%
50	18.1	74.3	0.62	100	1.68
% Recovery	85.8%	92.2%	105%	97.1%	115%
60	16.6	76.3	0.67	96.0	1.39
% Recovery	78.7%	94.7%	114%	93.2%	95.2%

Mechanical properties of re-dried, reinforced PA12 at 40 °C are nearly fully recovered. At 50 and 60 °C, elastic modulus and yield strength are reduced and elongation at yield increased.

e. *Summary of Findings*

- Hygrothermally aging unreinforced PA12 and reinforced PA12 significantly reduces elastic modulus, yield strength, and ultimate strength and significantly increases ductility at yield and failure.
- Hygrothermally aged PA12 has significantly improved mechanical properties relative to aged and unaged unreinforced PA12.
- Increasing salinity from freshwater to 45 g/kg does not significantly affect equilibrium moisture content or tensile properties of unreinforced PA12 or reinforced PA12.
- Increasing temperature from 40 to 60°C does not change equilibrium moisture content but does tend to reduce yield strength, ultimate strength, and elastic modulus and increase ductility at yield and failure.
- Re-dried samples recover 80 percent or better of their tensile strength properties.
- Greater retention and recovery of yield strength in reinforced PA12 relative to the unreinforced PA12 suggests the aging process damages the polymer matrix more significantly than the carbon fibers or the interfacial bonding between the polymer matrix and carbon fibers.

II. *Utilize Moldflow® to predict how varying injection molding and material conditions affect fiber orientation*

a. *Approach:* *Four controllable input conditions were varied to study their effects on fiber orientation in steady-state conditions and sharp geometry changes (Figure 4).*

- Fiber concentration, by volume - 10-90%
- Viscosity of the base polymer - PolyOne, PA12, PA6, and PA66
- Injection pressure - 180-500 MPa
- Injection flow rate - 1-5 cm^3/s

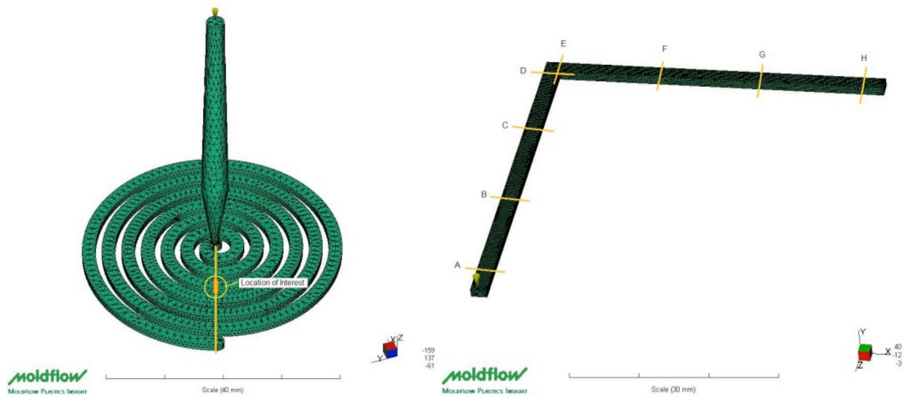

Figure 4. Preliminary Moldflow® models used to analyze varying injection and material conditions for steady-state conditions and sharp geometry changes, respectively.

b. *Preliminary Findings:*

- Steady-state conditions:
  - Fewer fibers will be aligned along the direction of fluid flow as fiber concentration increases, as shown in Figure 5.
  - More fibers will be aligned along the direction of fluid flow as the viscosity of the material increases
  - Material fills more of the mold as the viscosity decreases.
- Sharp geometry changes
  - Fewer fibers will be aligned along the direction of fluid flow as fiber concentration increases
  - Slightly more fibers will be aligned along the direction of fluid flow as injection pressure increases
  - Fewer fibers will be aligned along the direction of fluid flow as injection flow rate increases

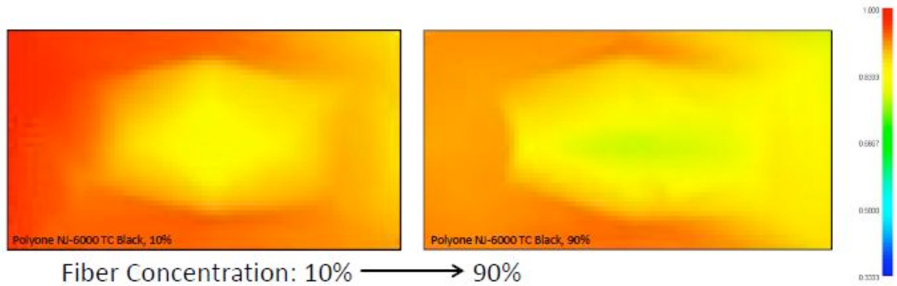

Figure 5. Cross-sections from Moldflow® simulation representing the effects of varying fiber concentration under steady-state conditions on fiber orientation (Material: PolyOne NJ-6000 TC Black; Scale: The probability that fibers are aligned with fluid flow, Red = 100% - Blue = 33%).

III. *Characterizing the suitability of injection molding for creating thermally-enhanced polymer heat exchangers*

a. Approach: *Reviewed materials from the following books to establish a set of guidelines for designing injection molded heat exchanger components*

- Injection Mold Design Engineering - David Kazmer
- Design Formulas for Plastics Engineers - Natti S. Rao and Günter Schumacher
- Injection-Mold Design Fundamentals - A. B. Glanvill and E. N. Denton

b. Preliminary Findings:

- Traditional design rules and guidelines apply only to thermally insulating polymers with moderate to no fillers. Thermally enhanced polymers are generally highly filled and have significantly higher conductivity values than standard polymers. These unique properties conflict with the foundation for many of the conventional injection molding design rules.
- The high conductivity of thermally-enhanced polymers can lead to the material freezing relatively earlier in the mold as the material sheds heat much more quickly than a traditional polymer, leading to an increased number of short shots. Additionally, the high conductivity may also lead to different shrinkage behavior due to reduction of the internal temperature gradient. Mold filling and shrinkage are both very important aspects of injection mold design, and a new set of standards must be created to account for the differences in thermally enhanced polymers.
- The high filler concentration in thermally enhanced polymers can also have significant effects on injection molding performance, specifically on the orientation distribution of fibers. Orientation within the part has a dramatic effect on the local thermal conductivity and strength of the part, and these properties are of the utmost importance for polymer heat exchangers. Traditional design rules account for moderately filled polymers, but an updated set of guidelines must be developed to account for highly filled polymers.

IV. *Validate Moldflow® predictions experimentally*

a. Approach: *Began training on how to use the following equipment for creating and using injection molds to validate results from Moldflow® analyses.*

- Pro/E - CAD software used to design parts and injection molds and prepare them for machining
- CNC Milling Machine - Used to create injection molds
- Injection Molding Machine - Used to injection mold parts over a range of input conditions to verify similar Moldflow® analyses

b. Preliminary Findings:

- Equipment and material limitations determine the types and sizes of geometries that can be studied. The particular injection-molding machine that will be used for testing has a maximum shot size of 6.5 cm^3, which limits the size of parts that can be tested to fairly small geometries.
- The limited shrinkage and relatively small size of the parts molded can lead to significant part ejection problems and necessitates a draft angle of at least 1-3° to prevent mold or part damage when ejecting the part.
- There are five parameters of the injection-molding machine and material structure that have a significant impact on the molded part: fiber concentration, viscosity of the base polymer, injection pressure, injection flow rate, and melt temperature. These properties will be the subject of a future investigation to determine how they affect the injection molding of thermally enhanced polymer composites.

V. *Integrate the mold-filling meta-model in the design process of a modular heat exchanger*

- As shown in the previous quarterly report, a plate-fin design that yields a minimum cost can be found using hierarchical search algorithms within the design space. Figure 6 below shows plots of the different cost components as functions of the design variables.

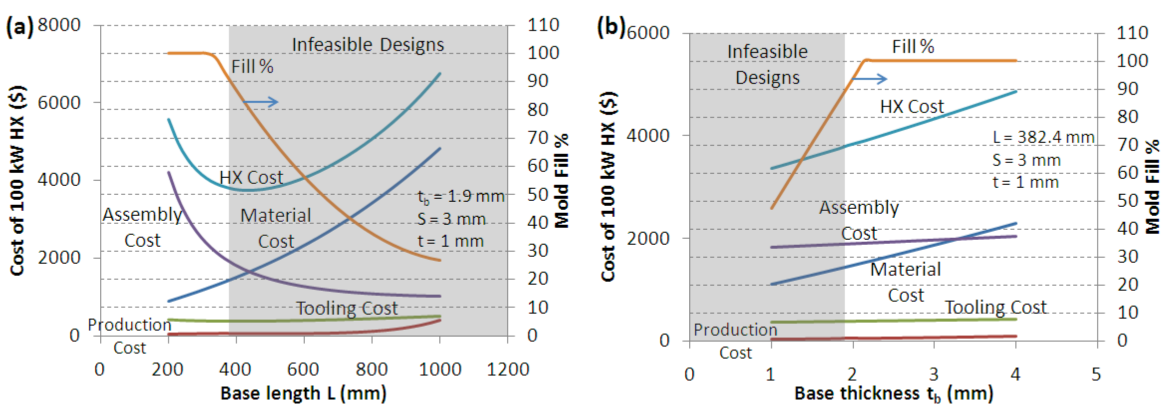

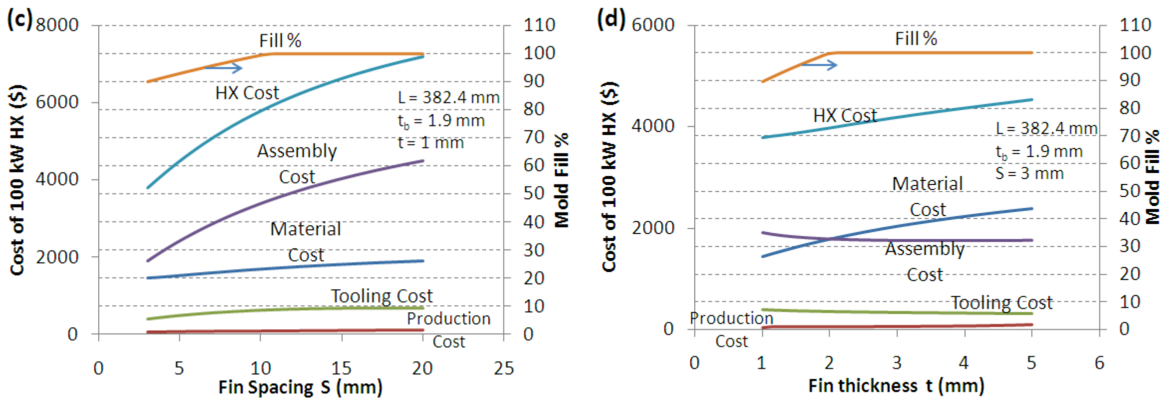

Figure 6. HX Cost (Eq. 1) and its components as functions of the design variables: (a) base length, (b) base thickness, (c) fin spacing, (d) fin thickness.

- As Figures 6(a) and (b) show, a minimum cost solution often lies in the boundary of infeasible/feasible designs (Fill = 90 %). The geometry that yields minimum cost can be refined using Moldflow® simulation results to discard the error associated with using the mold-fill meta-model. Figure 7 shows a plot of the mold-fill percent as a function of L and t_b. The data in this plot was calculated using interpolation of simulation results at selected points in the region around the initial solution.

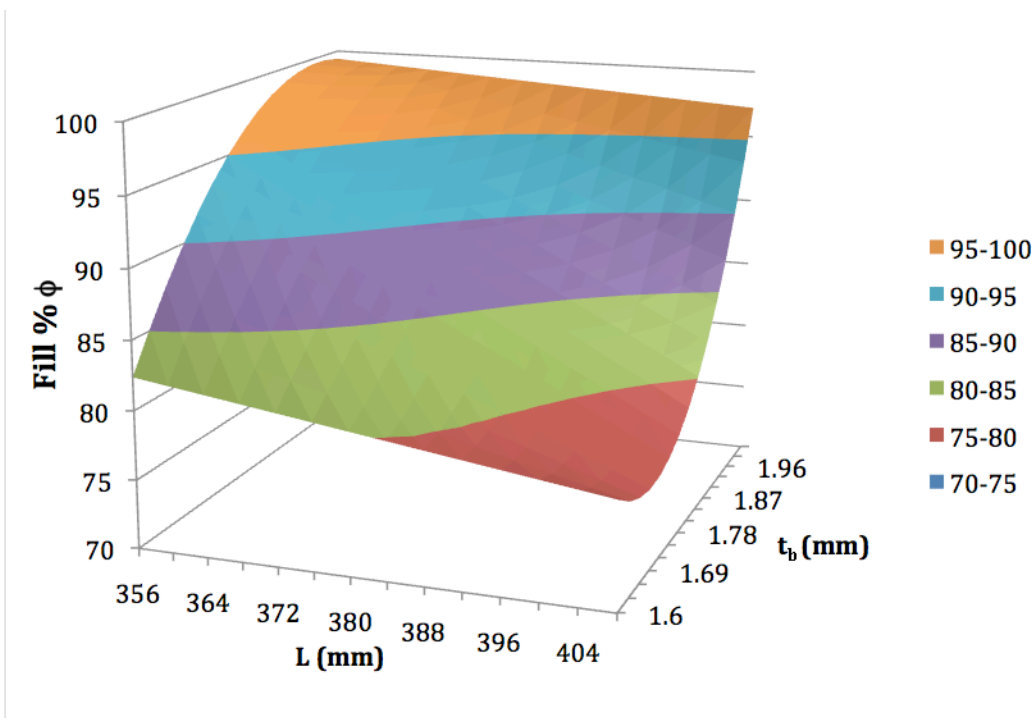

Figure 7. Fill % as a function of plate length L and plate thickness t_b using Moldflow® simulations at the corners (S = 3 mm, t = 1 mm).

- Using the new interpolated data to replace the meta-model in the range of the initial solution, the HX cost can be re-calculated to find a new minimum.

VI. *Investigate parametrically the use of an effective isotropic thermal conductivity for fins with local anisotropy*

- A large parametric space was studied to investigate the errors incurred by using an effective isotropic thermal conductivity for fins with local anisotropy.
- Figure 8 below shows the percent error in the heat transfer rate through the fin base as a function of the heat transfer coefficient. If the heat transfer coefficient is low, the percent error is small for any "effective" thermal conductivity. However, as the heat transfer coefficient increases, the errors can be as high as 27% for the RMS effective conductivity. The harmonic mean stays consistently below every other "average" and is followed by the geometric mean, arithmetic mean, and finally RMS.

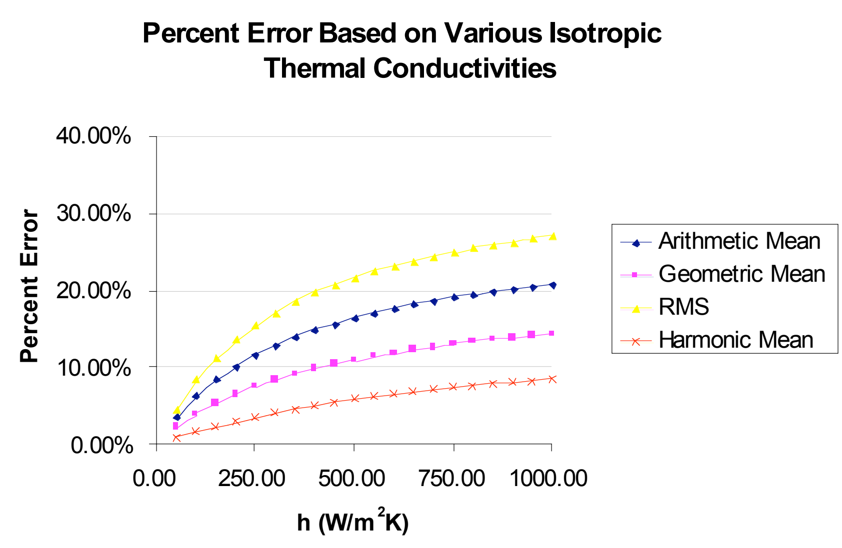

Figure 8. Percent error of q relative to anisotropic value as a function of h (t_f=2.5mm, H=5mm, θ_b=55K, t_{amb}=298K).

VII. *Design of a polymer heat exchanger prototype at the Petroleum Institute*

- The ENGEL Victory Tech 200/70 injection molding machine has been commissioned at PI, including three days of user training.
- The design of an injection mold for the manufacture of the PI polymer heat exchanger prototype has commenced.

4. Difficulties Encountered/Overcome

None to report.

5. Planned Project Activities for the Next Quarter

- Hygrothermally age specimens in 25°C freshwater and saltwater to determine if mechanical property degradation is a result of moisture diffusion or aging temperature.
- Develop ANSYS model using hygrothermally aged mechanical properties to determine feasibility of replacing metallic heat exchangers at the Das Island liquefied natural gas facility with polymer composite heat exchangers.
- Create new Moldflow® models for analyzing how fiber orientation and mold filling are affected by varying input conditions (fiber concentration, viscosity, injection pressure, injection flow rate, and melt temperature) over a range of common heat exchanger geometries.
- Compile a list of common heat exchanger geometries that are suitable for injection molding based on injection molding design rules and guidelines.
- Design and machine molds to begin experimental validation of Moldflow® simulation results.
- Continue development of predictive models for anisotropic heat exchanger modules.
- Manufacture and commissioning of the injection mold for the production of the prototype polymer heat exchanger. The prototype will be injection molded using polyethylene, while we await delivery of thermally enhanced polymer materials.
- Mr. Ahmed Khalil's UMD internship work relating to Moldflow simulations will be continued at PI.

Appendix

Goals

The goal of the proposed 3-year EERC II polymer composite heat exchanger (PCHX) project is to develop the science and technology needed to underpin the systematic design of polymer-fiber composite heat exchanger modules that address the needs of the fossil fuel industry. The project team, lead by A. Bar-Cohen, brings together expertise in thermal science and technology (Bar-Cohen, Rodgers) with polymer composite molding and manufacturing (Gupta, Bigio). Design studies and molding simulations, as well as fabrication and testing of laboratory-scale polymer composite heat exchangers, during the first phase of this project, have provided the foundation for aggressive pursuit of such polymer composite heat exchangers.

Successful development of cost-effective, high-performance PCHX's will require a detailed understanding of the limitations imposed on the thermal performance, mechanical integrity, and cost of such heat exchange devices by the candidate polymer material; carbon fiber geometry, orientation, and concentration; thermal and mechanical anisotropy of the polymer-fiber composite; molding processes; thermal and structural failure mechanisms in the molded heat exchanger; and the energy investment in the fabrication and formation of the heat exchangers. The development and experimental as well as numerical validation of a multi-disciplinary computerized design methodology, along with the fabrication and testing of scaled polymer heat exchanger modules, would provide a unique knowledge-base from which low-life-cycle-cost heat exchange systems for the petroleum and gas industries could be developed.

Project Tasks

A. Thermal Design and Characterization of Polymer Composite Heat Exchanger Module (Prof. Avram Bar-Cohen - UMD, Prof. Peter Rodgers - PI)

1. ***Design and thermofluid evaluation of PHX concepts for LNG applications***, including sensitivity of thermal performance to key parameters, quantification of primary thermal and exergy figures-of-merit (metrics), comparison to conventional heat exchangers, and identification of least-mass/least-energy designs;

2. ***Detailed design, fabrication, and thermal characterization of least-energy PCHX module***, including mold fabrication for most promising design, assembly and instrumentation of laboratory prototype, analysis of thermal and structural performance under simulated LNG processing conditions;

3. ***Development of predictive models for anisotropic heat exchanger modules***, including use of molding CFD software for prediction of fiber orientation and effective thermal/ structural properties, numerical and analytical models for molded anisotropic fins, derivation of least-material anisotropic fin equations, determination of heat flow sensitivity to fiber geometry/concentration/orientation;

4. ***Evaluation of convective enhancement features in molded channels***, including identification of "best practices" in conventional heat exchangers, manufacturability analysis of candidate features with attention to mold complexity, part ejection, and warpage, polymer composite molding of 3-5 candidate enhanced channels; thermofluid characterization of candidate enhanced channels under simulated LNG processing conditions; and

5. ***Determination of seawater effects on polymer composite finned plates***, including design and molding of test samples, immersion in saltwater tanks at different temperatures and concentrations for pre-determined periods, surface/bulk imaging and mechanical characterization before and after immersion, analysis and correlation of effects.

B. Manufacturability Analysis and Mold Design for Polymer Composite Heat Exchanger Module (Prof. SK Gupta – UMD):

1. ***Development of an improved meta-model for mold filling predictions***: We plan to develop an improved meta-model for predicting mold filling for typical heat exchanger geometries. This meta-model will account for multiple gates with adjustable spacing. The data for developing this meta-model will be generated using mold flow simulations. We plan to utilize radial basis function based meta-models to provide the right balance of accuracy and computational speed.

2 ***Creation of a computational framework for gate placement to optimize fiber orientation****:* We plan to develop a computational framework for placing gates to optimize the fiber orientation, utilizing simulated fiber orientations to select the gates. The sensitivity of the gate locations on fiber orientation will be developed. Gradient-based optimization techniques will be used to optimize the fiber orientation. The optimization problem will incorporate the constraint satisfaction formulation of the weld-line locations to ensure that the fiber orientation formulation produces acceptable weld-lines.

3. ***Generation of insert molding process models to incorporate connectors at the weld-lines*****:** In order to ensure that the weld lines do not compromise the structural integrity, we plan to embed metal connectors at the expected weld-lines locations. In order to accurately place these metal connectors in the structures, we plan to develop process models of the insert molding process and mold design templates for performing insert molding.

C. Polymer-Fiber Interactions in Polymer Composite Heat Exchanger Modules (Prof. David Bigio):

1. ***Develop key relationships for the dependence of fiber orientation on the flow geometry of the finned-plate PCHX module,*** in commercially available polymer composites, including the effect of carbon fiber length and diameter, for high and low fiber concentrations, for both base plate and fin passages in the mold, and the effect of fiber orientation/distribution on thermo-mechanical properties, verify relationships with suitable small scale experiments;

2. ***Determine achievable thermo-mechanical property enhancement*** through control of carbon fiber orientation, in the commercially available polymer composites, with attention to flow regimes, mixing processes in the flow of the melt, and heat exchanger module design, and verify experimentally;

3. ***Explore optimization of PCHX polymer composite properties through the creation of novel polymer composite compositions***, including multi-scale filler geometries, develop the molding methods for the desired geometries, create the novel composites and experimentally verify improved thermo-mechanical polymer composite properties.

References

[1] Ishai, O, *Environmental Effects on Deformation, Strength, and Degradation of Unidirectional Glass-Fiber Reinforced Plastics.* Journal of Polymer Engineering and Science, 1975. **15**(7): p.491-499.

[2] Luckow, P., Cevallos, J.G., Bar-Cohen, A., *Thermal Anisotropy in Injection Molded Heat Exchanger Plates,* 2009 (in progress)

[3] Cevallos, J.G., Gupta, S.K., Bar-Cohen, A., *Incorporating Moldability Considerations during the Design of Thermally Enhanced Polymer Heat Exchangers,* 2009 (in progress)

[4] Cevallos, J.G., Bar-Cohen, A., Bergles, A.E., Gupta, S.K., Rodgers, P., *Polymer Heat Exchangers – History, Opportunities, and Challenges*

Study on Microchannel-Based Absorber/Stripper and Electrostatic Precipitators for CO_2 Separation from Flue Gas

UMD Investigators: Serguei Dessiatoun, Amir Shooshtari
GRAs: Mohamed Alshehhi
PI Investigators: Michael Ohadi, Afshin Goharzadeh
Start Date: April 2009

1. Objective/Abstract

This project is focused on the development of a high-efficiency CO_2 separation process from flue gas flow. The project addresses three stages of the separation process: cooling down the flue gas, separating the solid particles and condensed water droplets, and separating the CO_2 using the absorption process. A microchannel CO_2 separator developed in this project will significantly increase the efficiency of the separation process while decreasing the energy consumption involved. Moreover, using such technology will lead to a reduction of equipment size and, therefore, minimize the footprint and cost of the equipment.

Flue gas also usually contains many contaminants in solid and liquid forms. The bulk of them are separated in gravity and inertia-driven feed gas separators. However, fine particles are carried on with the flow and can damage compressors, contaminate the gas absorption process, and reduce the quality of gas products. Currently, electrostatic separation is the most effective technique for separation of those particles and will be used in this project. The current stage of this study intends to address separation of droplets and particles using a EHD gas-liquid separation technique to remove conductive and nonconductive liquid particles suspended in a moving gaseous medium.

2. Deliverables

- Finished building the test setup
- Water droplet generation
- Tested the separator performance

3. Summary of Project Activities for the Completed Quarter

Introduction
The literature review and results of early experimental work conducted during the EERC first phase showed a good potential for EHD separation of CO_2 from flue gas. The EHD mechanism will be combined with microchannel adsorption technology for more effective enhancement. First, the EHD separation will be used to remove ashes, smoke and particles of matter from flue gas. Then the flue gas will undergo a second-stage separation process of separating CO_2 from flue gas.

The following report will focus on the completion of the test setup and rationale for some of its modifications. Then some results showing the separator performance will be shown. The first testing will focus on water removal from air to test the performance of the separator.

Test Setup Design
The test setup was modified and redesigned as follows:

1. **Switching from the refrigeration unit to a chiller**

The operating temperature of the test loop was set to be close to the Aerodynamic Particle Sizer (APS) temperature to limit the evaporation of water droplets. If the operational temperature of the test setup is lower than the APS, then water droplets will evaporate as they travel to the APS for measurement. If this happens, then it will be hard to verify the separator performance. Figure 1 shows how the temperature difference affects the APS measurements. The plot shows that once the temperature values of APS and test section are close, the highest concentration is attained. Also, Figure 2 shows water evaporation as water droplets travel from the separator to the APS. It shows another scenario where their temperature is close to each other and evaporation is eliminated.

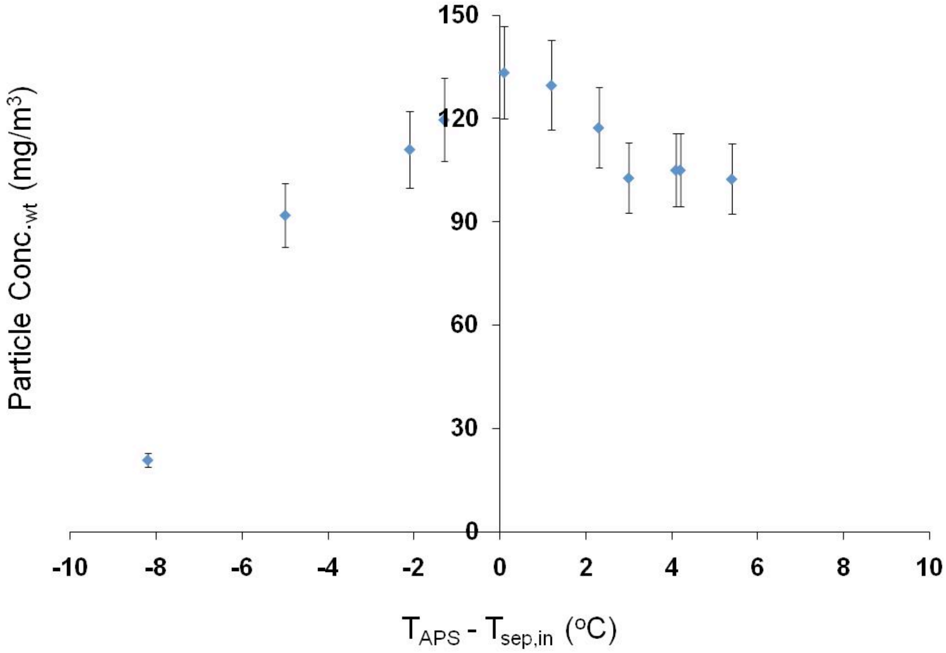

Figure 1. Temperature difference effect on APS measurements.

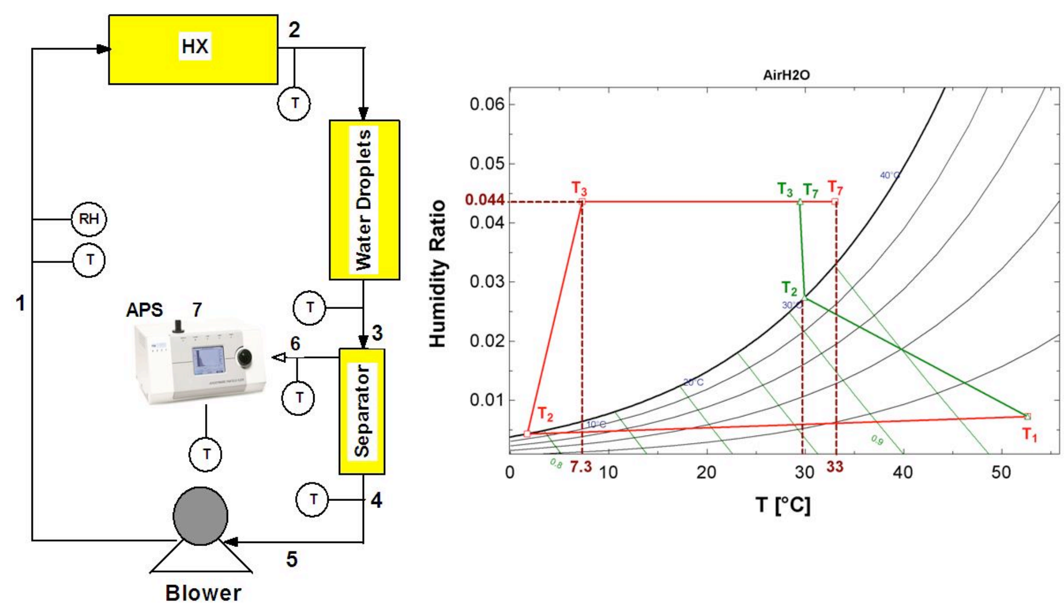

Figure 2. Water evaporation on the Psychometric chart showing two cases; T_3 = 7.3 °C, and T_3 = 30 °C while T_7 = 33 °C.

Based on the results of our study, we chose to set the operating temperature of test setup close to the APS. A chiller is used instead of the refrigeration unit because it is easier to control, and the cooling capacity needed is not a lot and can be supplied by a chiller, shown in Figure 3.

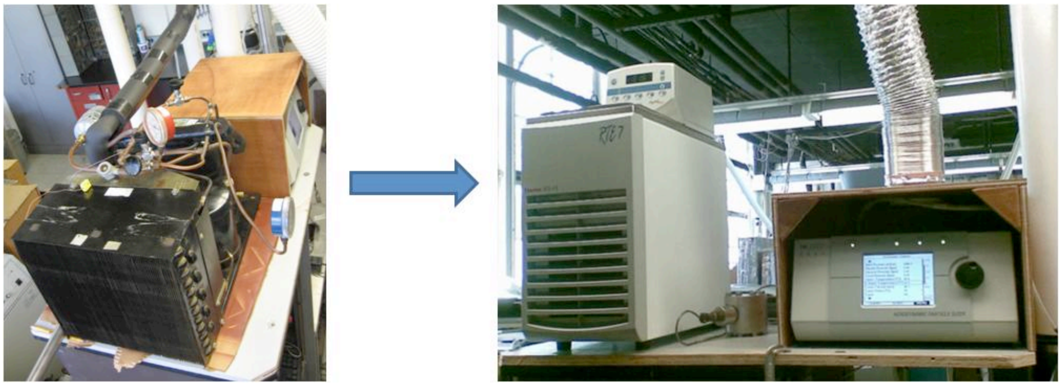

Figure 3. A chiller is used instead of the refrigeration unit.

2. **Changing the flow direction inside the separator**

To investigate the effect of the airflow direction, the direction was changed during testing, as shown in Figure 3.

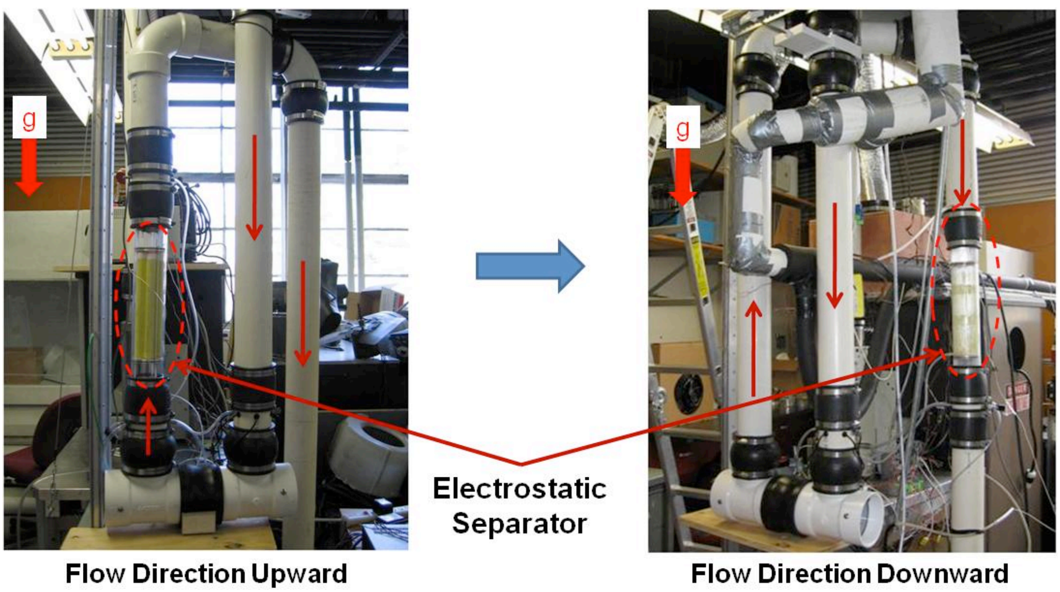

Figure 4. Changing the flow direction inside the separator.

The schematic of the test loop and test setup are shown in Figures 5 and 6, respectively.

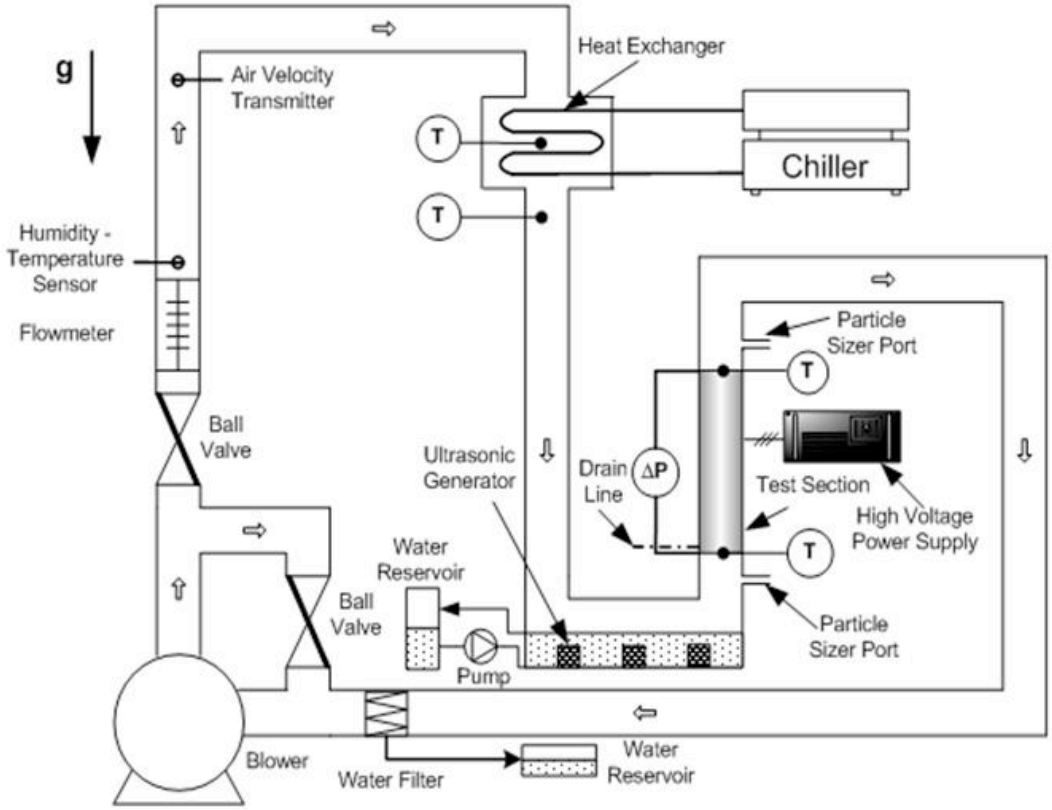

Figure 5. Schematic of test setup.

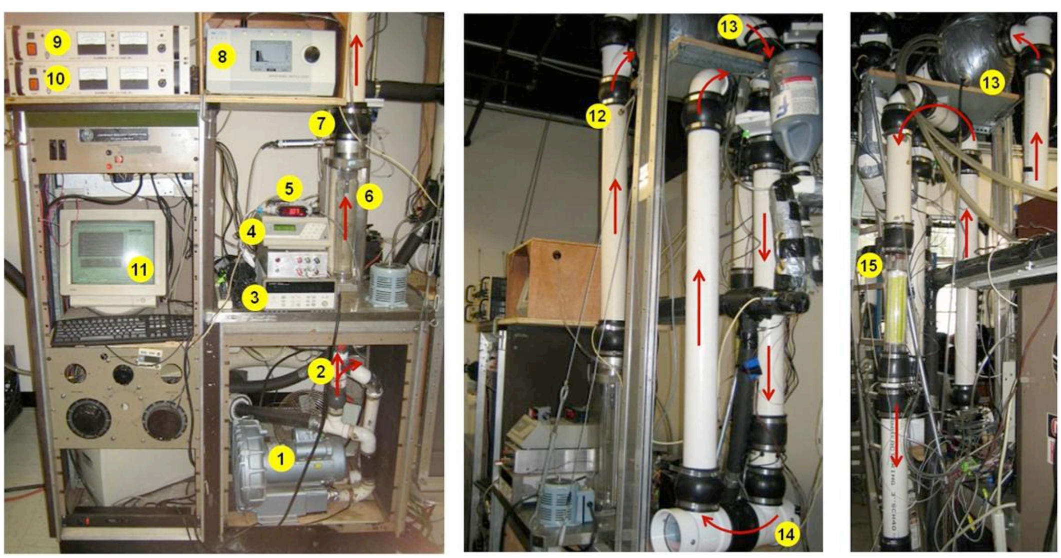

Figure 6. Air-water droplet separation test setup, where:

1. Blower	2. Ball Valves	3. DAS Unit
4. Humidity Sensor Reader	5. AVT Reader	6. Flowmeter
7. Humidity Sensor Probe	8. APS Unit	9. HV Power Supply (-)

10. HV Power Supply (+) 11. Computer 12. AVT Probe

13. HX Vessel 14. Water Pool 15. EHD Separator

Water Droplet Generation

Different sets of tests were conducted to verify the water droplet output in terms of size and concentration from the three different methods used: ultrasonic generators, a six-jet atomizer and a nozzle. There are two concentration outputs that the APS can measure: concentration based on the total number of particles ($Conc._{No}$) and concentration based on the weight of particles ($Conc._{Wt}$). Since it is unfeasible to generate monodisperse water droplets based on the methods used, it makes more sense to evaluate the performance of the separator based on particle weight concentration than number concentration. Therefore, the total efficiency (η), Equation (01), will be used:

$$\eta = 1 - \frac{\text{Wt. of Escaped Particles}}{\text{Wt. of Injected Particles}} \qquad \textbf{(01)}$$

The results for the measured water droplet concentration were conducted at the separator inlet. Figure 7 presents the droplets concentration generated by the ultrasonic generators. The water injection rate measured by scaling the water reservoir showed 4.5 ml/min of water consumption. The water concentration measured by the APS for one of the cases was 282 mg/m^3. This difference was due to large water droplets that were out of the APS range. The mean diameter of the droplets was 3.6 μm.

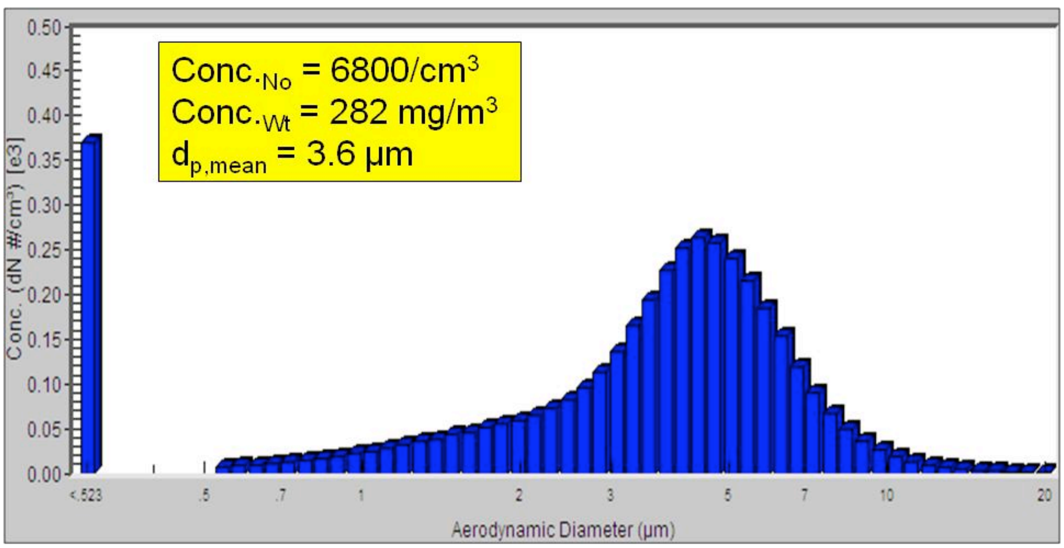

Figure 7. Water droplet concentration generated by ultrasonic generators (5 units, Q_{air} = 0.01 m^3/s).

The second method used was the six-jet atomizer. A dry nitrogen tank was used as the high-pressure source for the atomizer. The weight concentration was 170 mg/m^3, which was smaller than the one obtained with the ultrasonic generator. The droplet mean diameter was 3.2 µm, as shown in Figure 8.

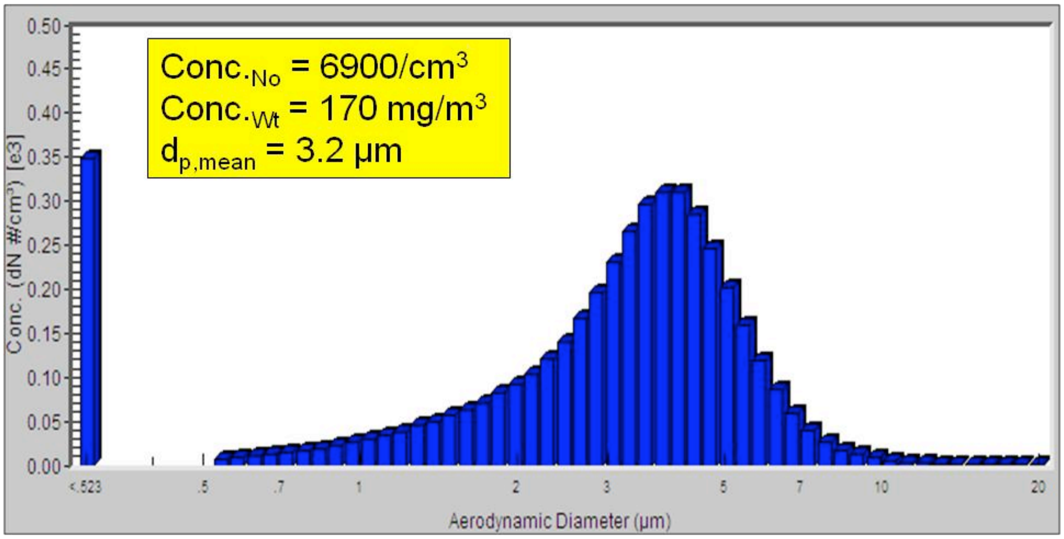

Figure 8. Water droplet concentration generated by the six-jet atomizer (inlet pressure = 310 kPa, 3 jets, ,,□.-□□□.= 0.01 m^3/s).

The nozzle testing produced larger particles than the APS could measure. The water injection rate with the nozzle was 20 ml/min.

Separator Performance Results

Figure 9 shows the effect of EHD on separation efficiency. The ultrasonic generators were used in this study, which showed that particle weight concentration at the separator outlet dropped from 282 mg/m^3 to 0.044 mg/m^3 when the applied voltage was increased from 0 kV to 7 kV. This performance reflects an efficiency of 0.9998%.

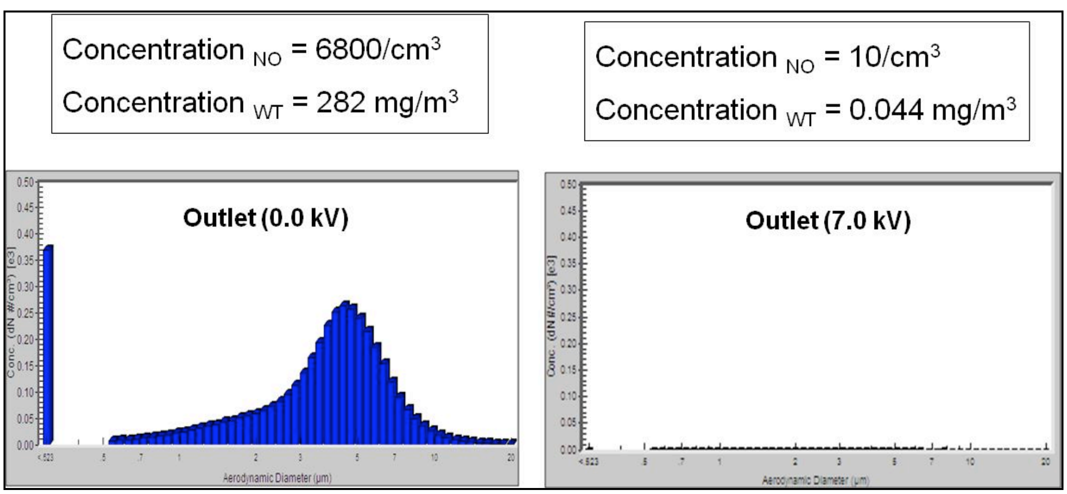

Figure 9. Separator performance for low water concentration.

Figure (10) shows the same performance of the separator under high water concentration testing. In this study both ultrasonic generators and the nozzle were used to provide small droplets of micron size and high water concentration. The study showed that the particle concentration dropped from 48.1 mg/m^3 to 0.327 mg/m^3 when the applied voltage was increased from 0 kV to 7.0 kV. This reflects an efficiency of 0.993%.

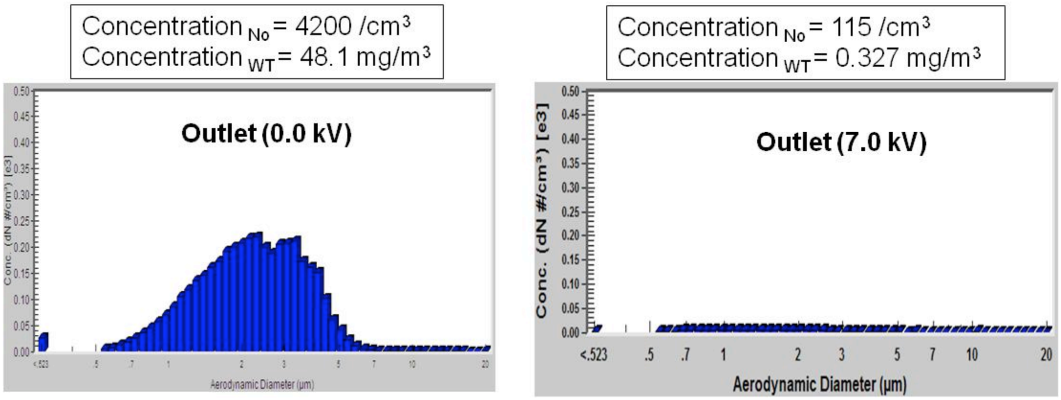

Figure 10. Separator performance for high water concentration condition.

4. Difficulties Encountered/Overcome

Some challenges in the design of gas-and-conductive liquid separator can be identified as:

- Prevention of charge leakages and/or shortages due to the conductive nature of fluid
- Power supply design and control mechanisms

5. Planned Project Activities for the Next Quarter

- Enhance removal of collected water to avoid re-entrainment and breakdown voltage
- Redesign setup to be independent of gravity and flow direction
- Use materials that are corrosion-resistant and independent of temperature and wet environment
- Conduct a parametric study based on the high performance EHD separator
- Study the environmental effects:
  - Ozone production
  - EMI

6. Exploratory Work at the Petroleum Institute:

Two new experimental setups are under construction at the Petroleum Institute. The objective is to validate the numerical results obtained from the UMD models. The velocity distribution of oil particles under the influence of an EHD field will be compared with numerical data. Extensive experimental results will be given in next quarterly report.

The high power supply has been purchased and is operational. The velocity field will be measured using Particle Image Velocimetry (PIV) and/or Laser Doppler Velocimetry (LDV).

During Dr. Dessiatoun’s visit at PI (Figure 11), the first experiment was set up (Figure 12) and the second experiment will be ready the next weeks. Schematics of flow and laser measurement arrangements of both experiments are shown in Figures 13 and 14.

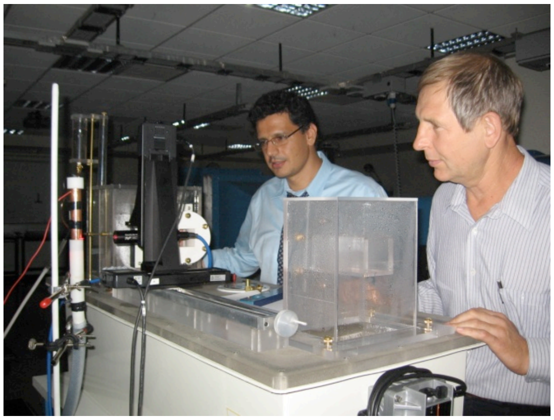

Figure 11. ME Laboratory at PI (11.10.2009).

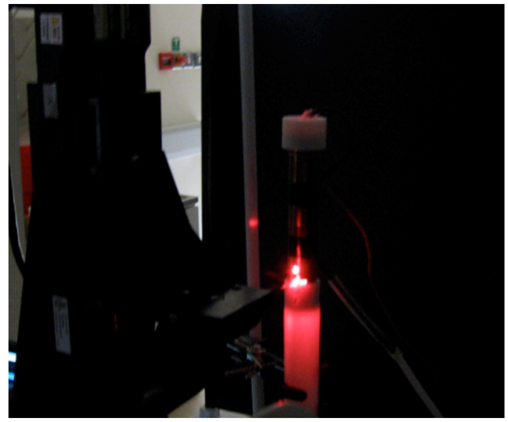

Figure 12. Mini-LDV system.

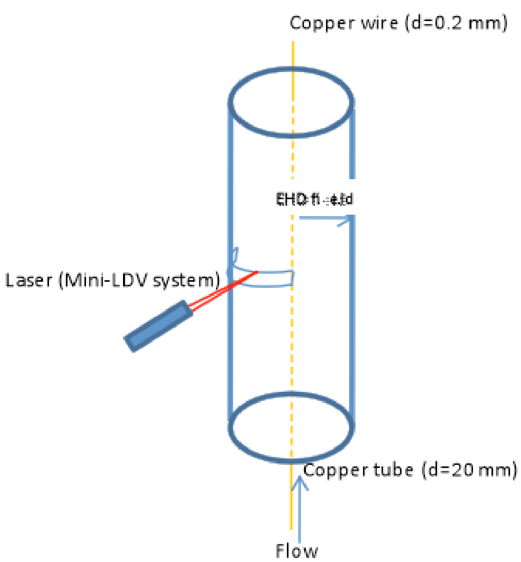

Figure 13. Experiment 1 - Cylindrical geometry (Local Velocity Measurements using Mini-LDV).

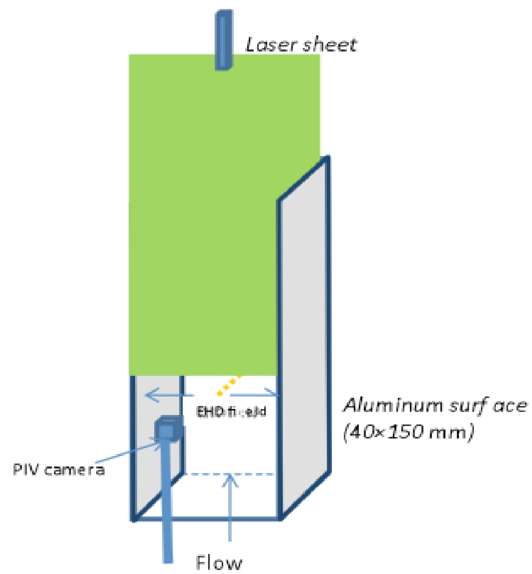

Figure 14. Experiment 2 - Square geometry (2D Velocity Distribution using PIV).

Appendix

Justification and Background

Separation comprises a significant part of the oil and natural gas production process. In many stages of this process, electrostatic separation significantly increases the efficiency and often decreases the cost of production. Most of the oil producers, including ADNOC, operate where the climate is hot and therefore use refrigeration and air-conditioning equipment. The efficiency and reliability of this equipment appreciably suffers due to mal-distribution of lubricant oil in the system. Electrostatic separation can correct this mal-distribution and improve the efficiency of this refrigeration and air-conditioning equipment. Similarly, vapor compression equipment with lubricant circulation is also used in oil refinery processes. This circulation can be significantly improved using EHD separators to increase heat-pumping efficiency. UMD has already developed a working prototype for gas-and-non-conductive droplet separation. However, the fundamentals of this separation mechanism must be better understood to enable optimization of the working design. There is also a need to explore the feasibility of separation of gas-and-conductive liquid mixtures, which poses additional challenges.

Conventional gas/liquid separators are based on inertial and gravitational forces. They have poor efficiency when separating micron-size particles in the flow due to low gravitational and inertial forces acting on small particles. In contrast, electro-hydrodynamic (EHD) forces strongly affect particles of such size. The combination of a conventional separator with EHD allows us to create the most effective and lowest pressure-drop particle separator, with potential applications to separation of electrically conductive and non-conductive liquid particles. The separation of electrically conductive particles like water-air mixtures (fog) imposes significant design constraints on separator electrode design and high-voltage power supply selection.

Approach

Detailed analysis and identification of the phenomena and the design challenges involved in effective implementation of the mechanism. Parametric study of existing and improved separators. Design iterations, including numerical flow and field simulations, fabrication, and testing. Creation of database and engineering design correlations.

Two-Year Schedule

Year 1:

- Conduct literature review to study current technologies for separation of solid or liquid particles from gas flows by electrostatic and electro-hydrodynamic (EHD) forces.
- Evaluate existing technologies and assess their applicability to flow separation of gas-and-liquid-droplet mixtures.
- Evaluate and optimize current designs of UMD EHD separators for non-conductive liquid particles in gas flow.
- Design and fabricate a two-phase gas-liquid droplet separator capable of operating with conductive fluids. Conduct a parametric study of separators for different conductive fluids, concentrations, and gas flow rates.

Year 2:

- Continue optimization and numerical study of hybrid gas-and-non-conductive liquid droplet separator. Continue parametric experimental study of gas-and conductive separator.
- Design iterations and implementation.
- Experiment on different designs.
- Present the best design to ADNOC group of companies.
- Develop design correlation.
- Prepare report.

Key References

[1] Mo, B., Ohadi, M.M., and Dessiatoun, S.V., "Liquid vapor separation and thermal management in an EHD-enhanced capillary pumped loop," Heat Transfer 1998, Proceeding of 11th International Heat Transfer Conference, Vol. 2, Taylor & Francis Inc., Levittown, PA, pp.63-68.

[2] Ohadi, M. M., Ivenkenko, I., and Dessiatoun, S., "Electrohydrodynamic Liquid-Vapor Separator," USA Pat.# 6,582,500

[3] Schrage, D.S., Shoemaker, J.M., and McQuillen, J., 1998, "Passive two-phase fluid separation," AIAA 36th Aerospace Sciences Meeting & Exhibit, Reno, NV, Jan. 1998, AIAA-98-0731

[4] Balachandran, W., Machowski, W., Ahmad, C.N. "Electrostatic atomization of conducting liquids using AC superimposed on DC fields," Industry Applications, IEEE Transactions on Volume 30, Issue 4, July-Aug. 1994 Page(s):850 - 855 Digital Object Identifier 10.1109/28.297899

Microreactors for Oil and Gas Processes Using Microchannel Technologies

UMD Investigators: Serguei Dessiatoun, Amir Shooshtari
GRA: Pradeep Kumar Singh
PI Investigators: Michael Ohadi, Afshin Goharzadeh, Ebrahim Al-Hajri (Returning ADNOC Scholar)
Start Date: April 2009

1. Objective/Abstract

Microfabrication techniques are increasingly used in gas and petrochemical engineering to realize structures with capabilities exceeding those of conventional macroscopic systems. In addition to already-demonstrated chemical analysis applications, microfabricated chemical systems are expected to have a number of advantages for chemical synthesis, chemical kinetics studies, and process development. Chemical processing advantages from increased heat and mass transfer in small dimensions are demonstrated with model gas, liquid and multiphase reaction systems.

A microchannel mixing visualization study was stipulated for the last quarter. An experiment was performed to study microchannel mixing. The scope of this experimental study was to analyze the performance of the microchannels used for the mixing and separation of the lithium bromide and water in the absorption-desorbtion cycle. A single stage absorption and desorbtion system was designed and machined. The main parameter that was used for examining the efficiency was the mass flow rate of the working fluids. The mass flow rates can be used in two approaches:

- Constant flow rates ratio ($\dot{m}_{LiBr}/\dot{m}_{water\ vapor}$= Constant)
- Variable flow rates ratio

Additionally, the difference between the water inlet and outlet percentage ratio was examined.

An extensive literature survey was performed to help us choose an appropriate reaction that is widely used in the petrochemical industry.

2. Milestones/Deliverables Scheduled for the Completed Quarter

- Literature survey.
- Identifying target reaction.

3. Summary of Project Activities for the Completed Quarter

Literature Survey

- **Microchannel mixing visualization**

<u>Absorbers:</u>
The micromixers are divided into two groups: passive and active micromixers. The active mixers, such as electro-osmotic and ultrasonic micromixers, use external forces for mixing. On the other hand, passive micromixers depend on the variation of the geometries of the microchannels in order to force the channels to diffuse. The following is a literature survey on passive and active examples of the micromixers that can be used for absorption.

-Micro fluidic mixers [6]:

1. Fluid properties become increasingly controlled by viscous forces rather than inertia due to the tangible effect of this small dimension.
2. These mixers have a large surface-to-volume ratio, which increases heat and mass transfer efficiencies.
3. The small dimensions allow rapid diffusive mixing to occur in as little as 100 μs.

Types of micromixers:
Figures 1-6 show different examples of passive and active micromixing.

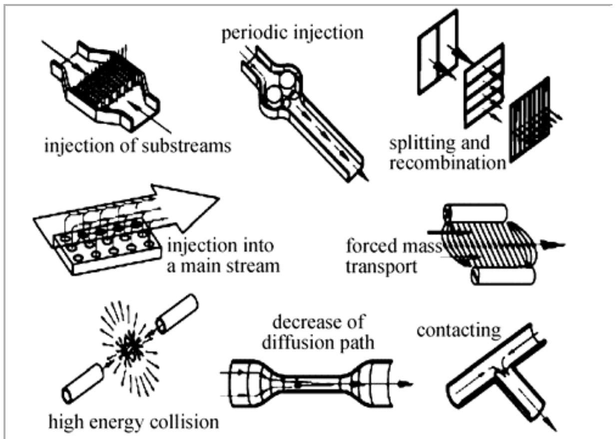

Figure 1. Schematic drawing of selected passive and active mixing techniques.

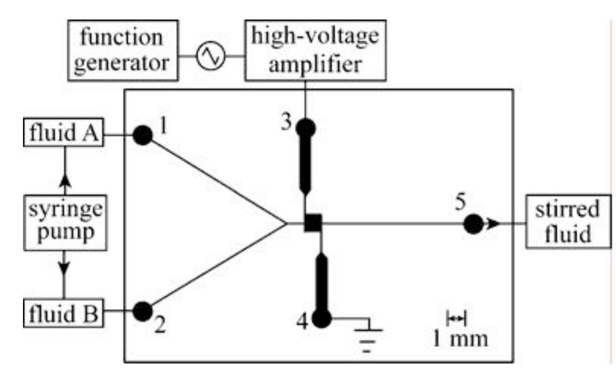

Figure 2. Schematic drawing of selected active mixing process.

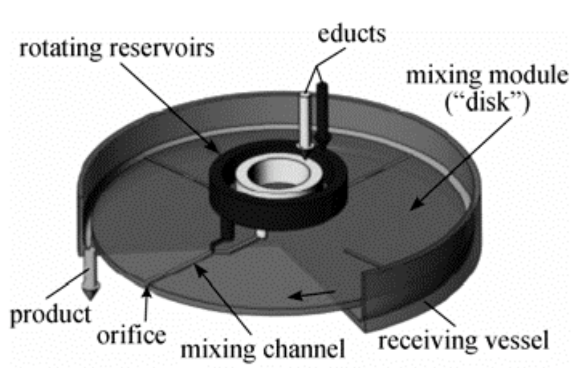

Figure 3. Centrifugal micromixer.

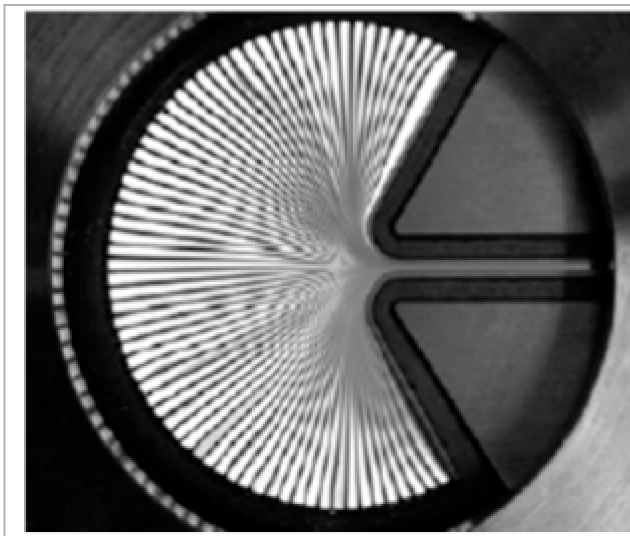

Figure 4. SuperFocus mixer.

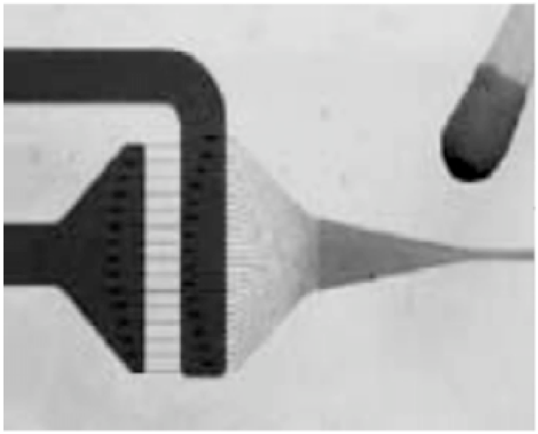

Figure 5. Triangular interdigital micromixer.

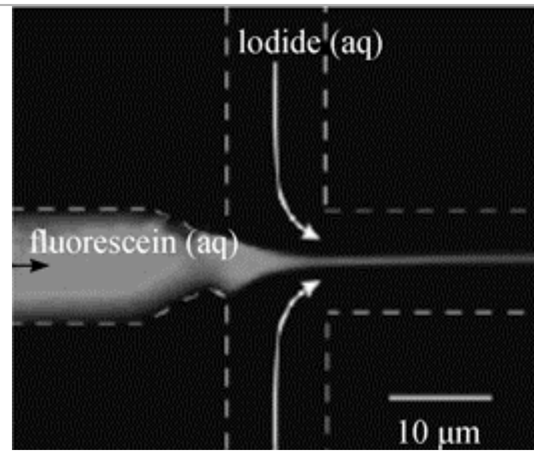

Figure 6. Hydrodynamic focusing mixer.

Variables and parameters:

Dimensions, forces, pressure and temperature must be considered in designing the microchannel. The micro-dimensions raise the significance of the viscosity of the fluid passing through the microchannel. Moreover, the high velocity gradient will increase the viscosity dissipation. Since the fluid viscosity is a function of temperature, and the temperature changes along the tube, the fluid viscosity varies along the channels, and consequently, the viscous shear force changes. Additionally, the pressure distribution in the tube and the Re varies along the flow direction. The friction factor is also used for characterizing the flow in the microchannel.

The temperature variation through the inlet and the outlet of the microchannel is due to the energy of the viscous dissipation. The channel aspect ratio (γ=W/H) and the hydraulic diameter are parameters that affect the viscous heat dissipation through the microchannel. The viscous heating increases as the aspect ratio decreases. The following figure shows the effect of hydraulic length on the temperature distribution along the microchannel obtained by [7].

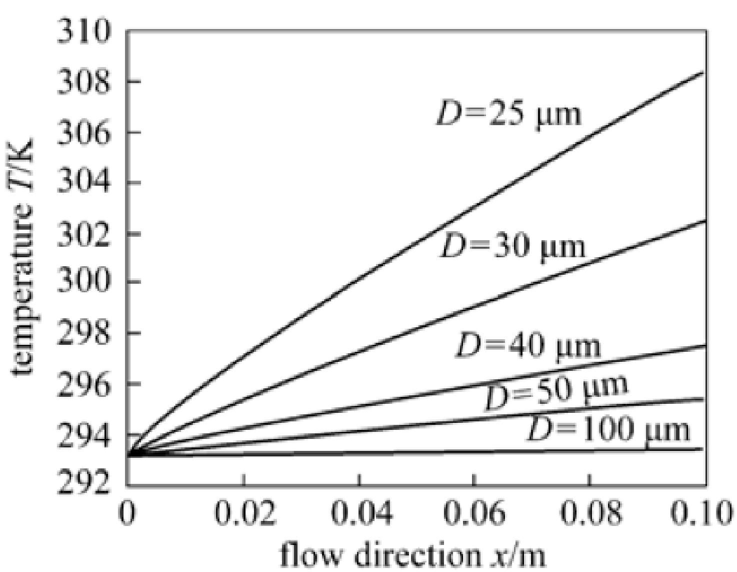

Figure 7. Average temperatures along the flow direction considering the viscous sipation effect (Re=800).

According to Judy et al. [8], a temperature increase of 6.2 °C has been reported experimentally for microchannels with a hydraulic diameter of 74.1 µm and length of 11.4 cm when isopropanol was employed as working fluid with Re=300. They also studied the values for the product of friction factor and Reynolds number. The following figure shows the product of Reynolds and friction factor (f*Re) as a function of dimensionless tube length (L/D).

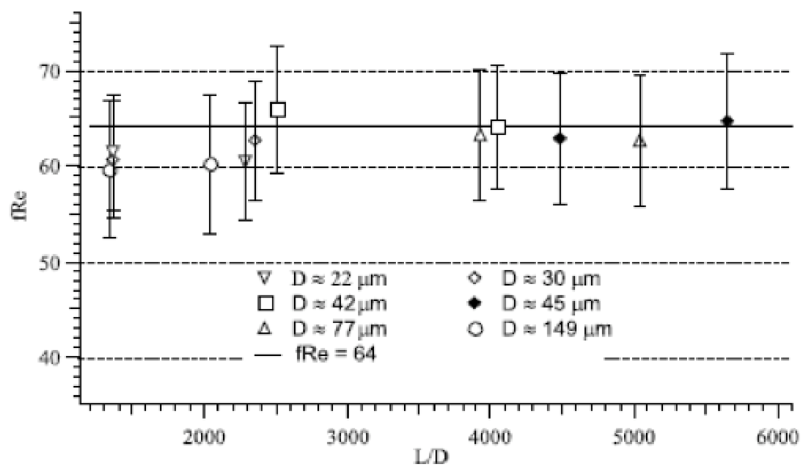

Figure 8. **(f*Re) as a function of dimensionless tube length (L/D).**

Judy et al. conducted the experiment using three different fluids: distilled water, methanol and isopropanol. Moreover, fused silica and stainless steel tubes were used with different cross sectional profiles and dimensions.

The flow velocity affects the mixing efficiency in micro fluidic mixers. It was stated by [9][10][11][12][13] that, with increasing flow velocity, the laminar flow starts to form symmetrical vortices, which enhances the mixing quality. The following figure shows the different stationary flow regimes that result from the flow velocity variation in the microchannel:

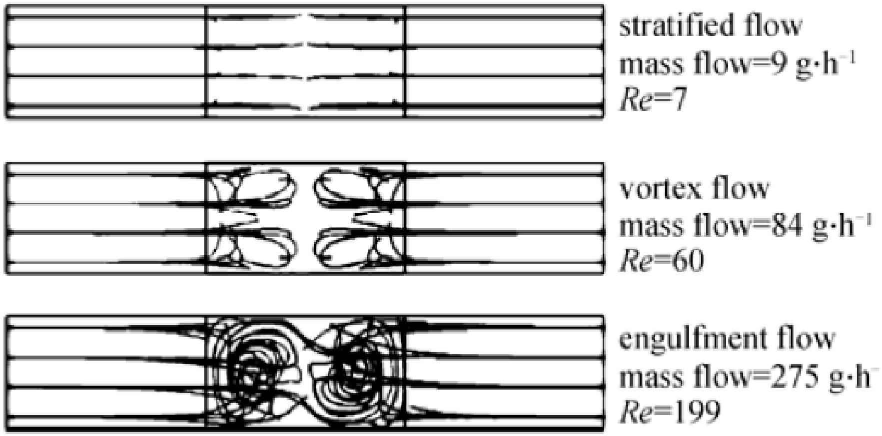

Figure 9. Different stationary flow regimes.

The figure below shows the variation in the mixing quality for three different flow regimes versus the different Re.

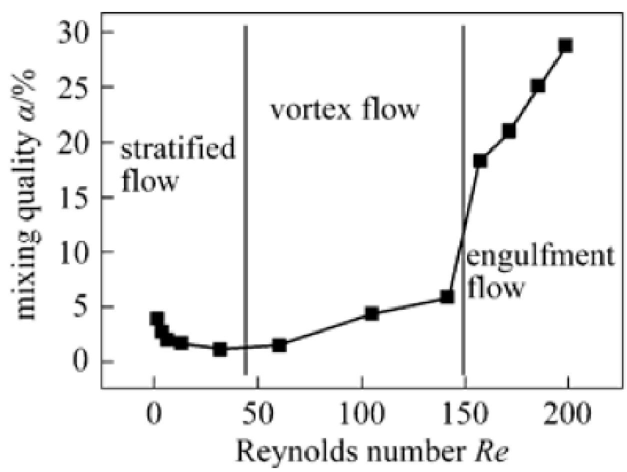

Figure 10. Mixing quality for different flow regimes versus Reynolds number Re.

Geometrical setup of the microchannel plays an important role in improving the mixing percentage in the microchannels. According to several experiments [14] and [15] on T-shaped microchannels, at a mixing length of 443 μm and velocity of 0.81 cm.s^{-1} the mixing efficiency achieved was 80%. On the other hand, channels of 2300 μm were used to achieve the same mixing efficiency in the absence of the slanted walls.

Another experiment [16] showed that using the split and recomine (SAR) method increases the mixing efficiency. Two sets of fluids were mixed:

1. Phenolphthalein and NaOH
2. Blue dye and water

These two sets of solutions provide good visualization of the mixing because of their colors. The mixing occurs at a number of units that make up the whole microchannel. Numerical analysis based on CFD was used to verify the performance of the SAR micromixer. The results of the experiment showed an exponential behavior of the interfaces in the SAR micromixing. Most of the mixing (90%) was achieved after the 7th unit at Re = 0.6099. The investigators also concluded that the number of required units of mixing increases from 7 to 9 as the flow rate increases from Re 0.6099 to 6.099. This corresponding small change in the number of units means that the SAR micromixers can be used for a wide range of fluids flow rates. The following figure shows a schematic view of the SAR micromixer.

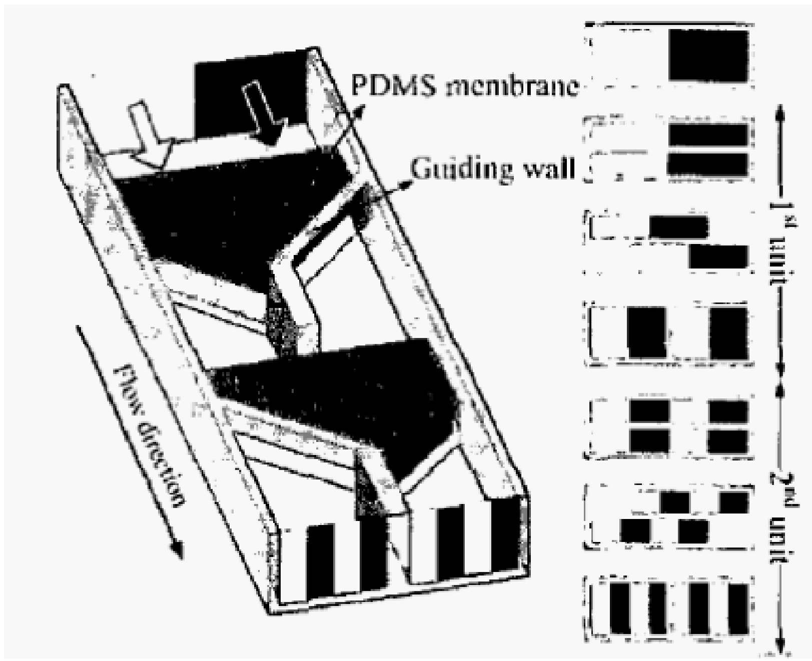

Figure 11. Schematic for a SAR micromixer.

<u>Test facility design</u>

Experimental Set-up

A. Experimental apparatus:

The schematics and photographs of the test facility are included in this part of the report.

Absorber:

The absorber is the component of the heat pump that is used for mixing the working fluids (LiBr/Water).

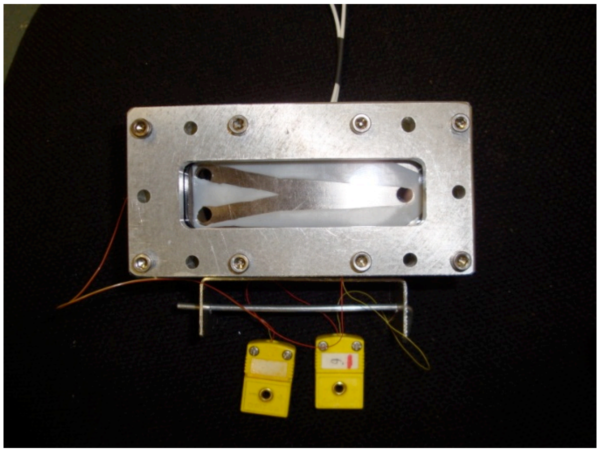

Figure 12. Top view of the absorber.

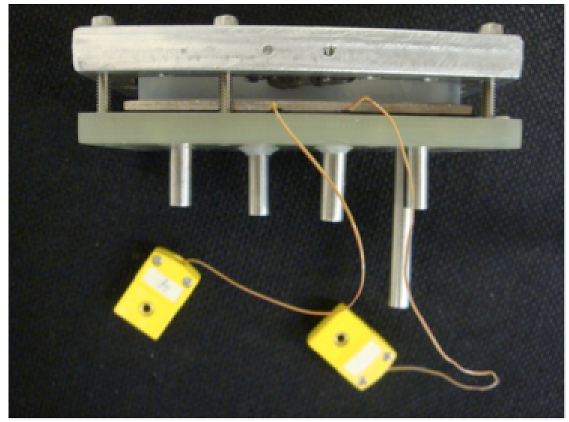

Figure 13. Side view of the absorber.

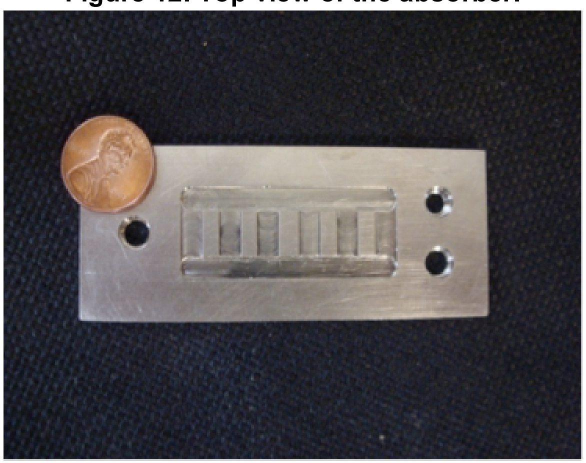

Figure 14. Microchannels for cooling system of the absorber at the lower surface of the brass plate.

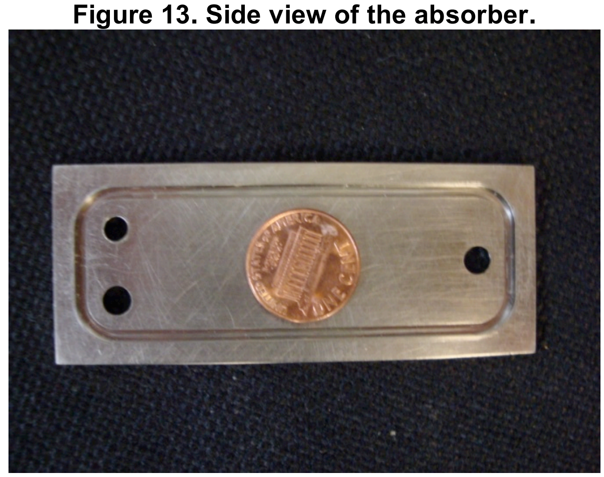

Figure 15. Upper surface of the brass plate used in the absorber.

Figure 15 shows the lower surface of the brass plate that was used for cooling the absorber. Brass has a thermal conductivity of 109 (W/m*K) [17], which is good for exchanging heat between the exothermic mixing of LiBr and water and the cooling water in the lower surface of the plate. A milling machine was used for machining the channels for the cooling water. As shown in Figure 14, a CNC machine was used for grooving the plate. The groove is used for placing the rubber sealing gasket. The same configuration of the upper surface of the absorber applies to the upper surface of the desorber.

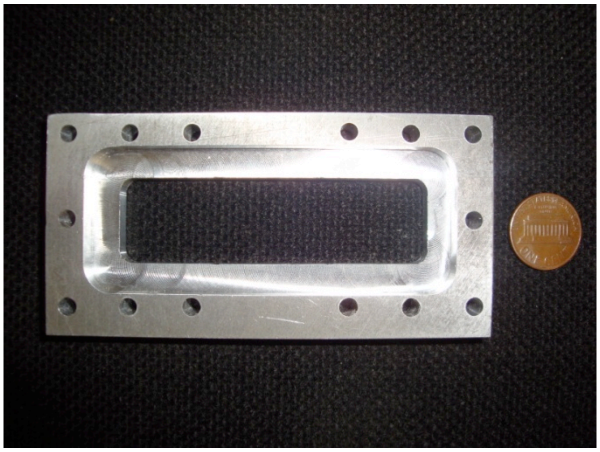

Figure 16. Upper part of the absorber and desorber.

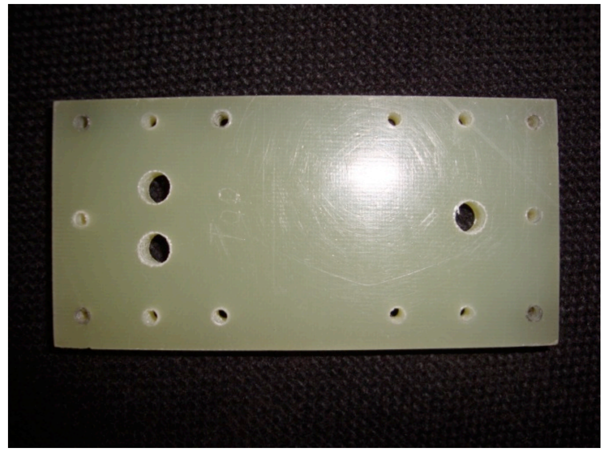

Figure 17. Lower part of the absorber and desorber.

Figure 16 shows the upper part of the absorber and desorber, which is made of aluminum. The milling machine was used for milling the surface of the plate so that it holds the piece of glass that allows visualization. Drilling and tapping were used for machining the holes for the screws in order to attach the different parts of the absorber and desorber together. Figure 17 shows the lower part of both the absorber and desorber, which is made of Gitane. This material has a high thermal resistivity, which eliminates the undesirable heat losses or gains to the system. Certain considerations were taken to machine the Gitane plate, as it is made of fiberglass, which can cause damage to the machining tools.

Desorber:

The desorber is the component of the heat pump at which the separation of the working fluids (LiBr/water) takes place.

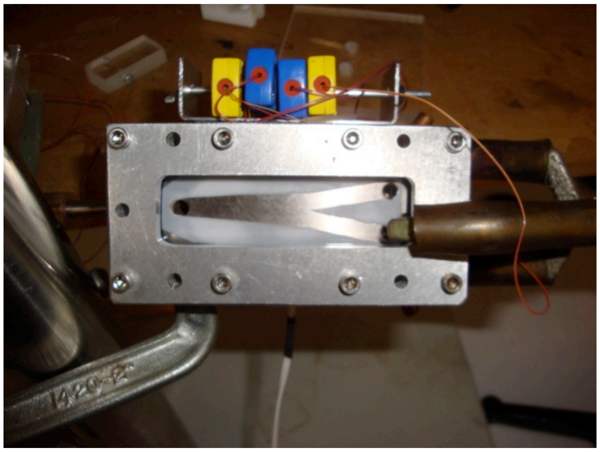

Figure 18. Top view of the desorber.

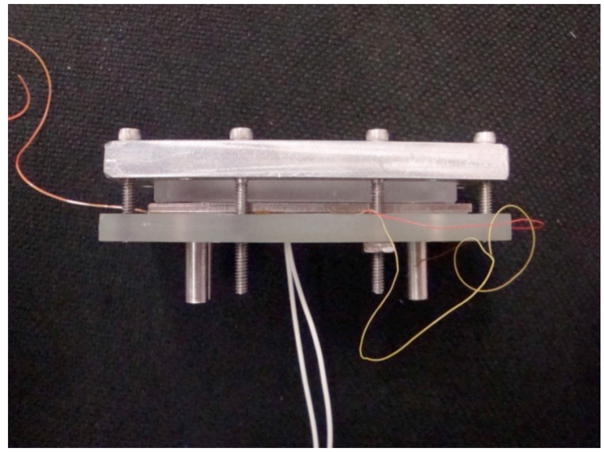

Figure 19. Side view of the desorber.

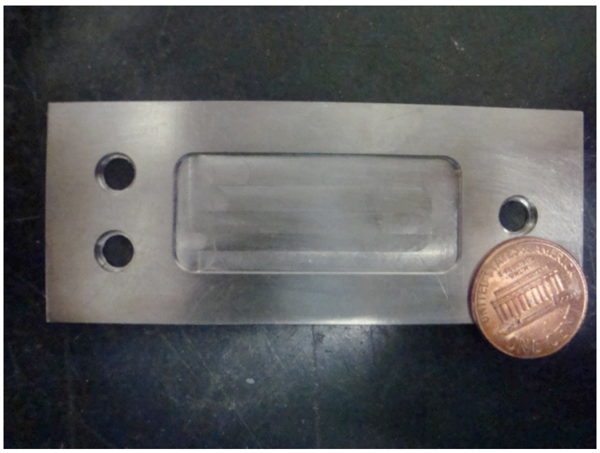

Figure 20. Lower surface of the brass plate.

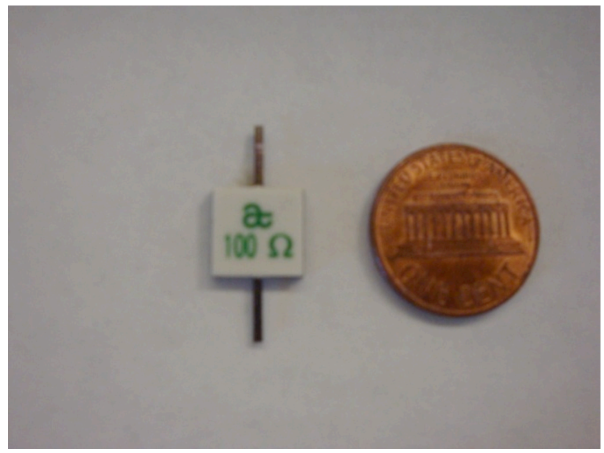

Figure 21. Thin film heater.

A 100Ω thin film heater is used for supplying heat to the desorber. The heater required for desorption is placed in the lower surface of the brass.

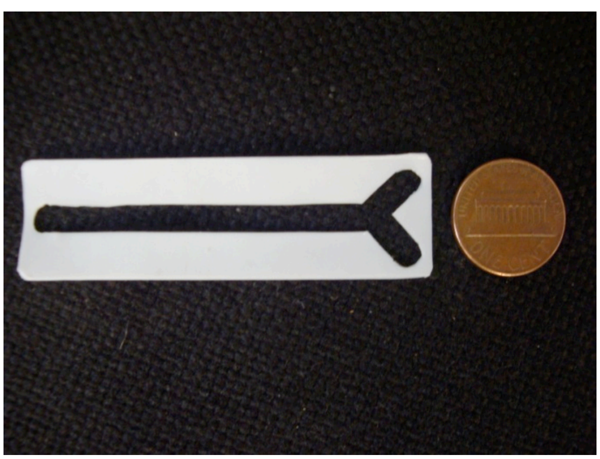

Figure 22. Teflon microchannel used for mixing/separation.

Figure 23. Glass plate.

Figure 22 shows a preliminary design for the mixing/separation channel. The following list of the properties is for the Teflon which is used for the microchannel [18]:

- High melting point: varies for different types of Teflon (260-327C˚)
- Low coefficient of friction (0.04-0.1): No particles of the working fluid to stick to the channel
- Good vapor transmission: (0.4 g/100in2) for Teflon® FEP Film, 25 μm (1 mil) thickness/per ASTM E-96 (modified)

Figure 24 shows the glass plate that is used for the visualization of the absorption/desorption processes. Figure 29 shows a diagram of the experimental setup.

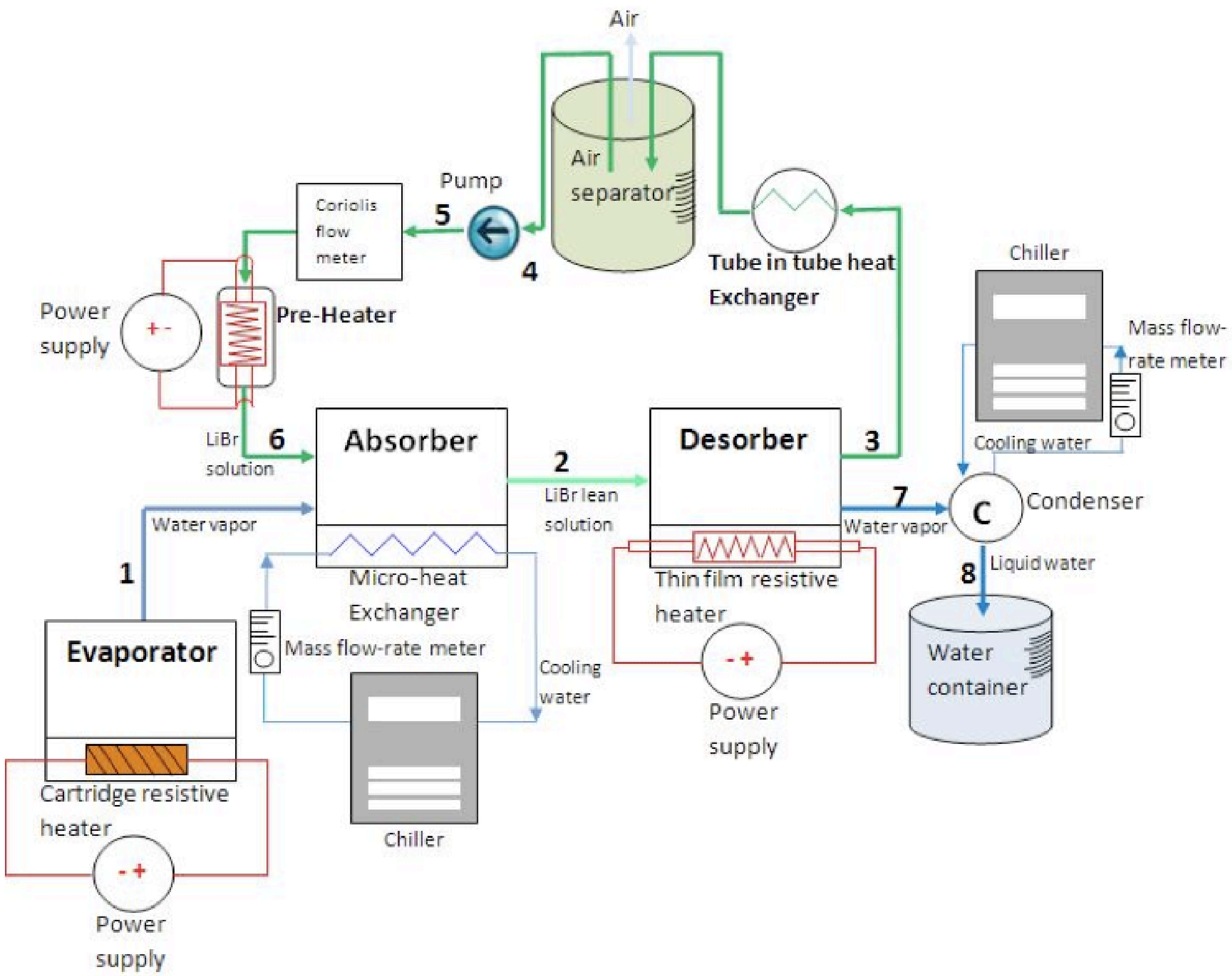

Figure 24. Block diagram of the experimental setup.

The numbers in the diagram indicate the different variables for eight regions: temperature, pressure, concentration, mass flow and enthalpy. Engineering Equation Solver (EES) was used for modeling the energy balance, mass balance and concentration and mass balance for the experiment.

Methane and oxygen production

In order to determine reactions suitable for the petrochemical industry, an extensive literature survey was performed. The initial literature review focused on microreactor technologies and their working principles. KP Brooks et al [1] discussed the adsorption, absorption, Sabatier reaction (SR), reverse water gas shift (RWGS) and separation reactions in microreactors.

The Sabatier reaction is given as

$2H_2O \rightarrow O_2 + 2H_2 \rightarrow$ (respiration) $\rightarrow CO_2 + 2H_2 + 2H_2$ (added) $\rightarrow 2H_2O + CH_4$ (discarded)

The RWGS reaction is given by:

$CO + H_2O \rightarrow CO_2 + H_2$

In absorption reactions it was found that the overall mass transfer coefficient was as much as 2.6 times greater than for the conventional packed column for the thinnest microwick [1].

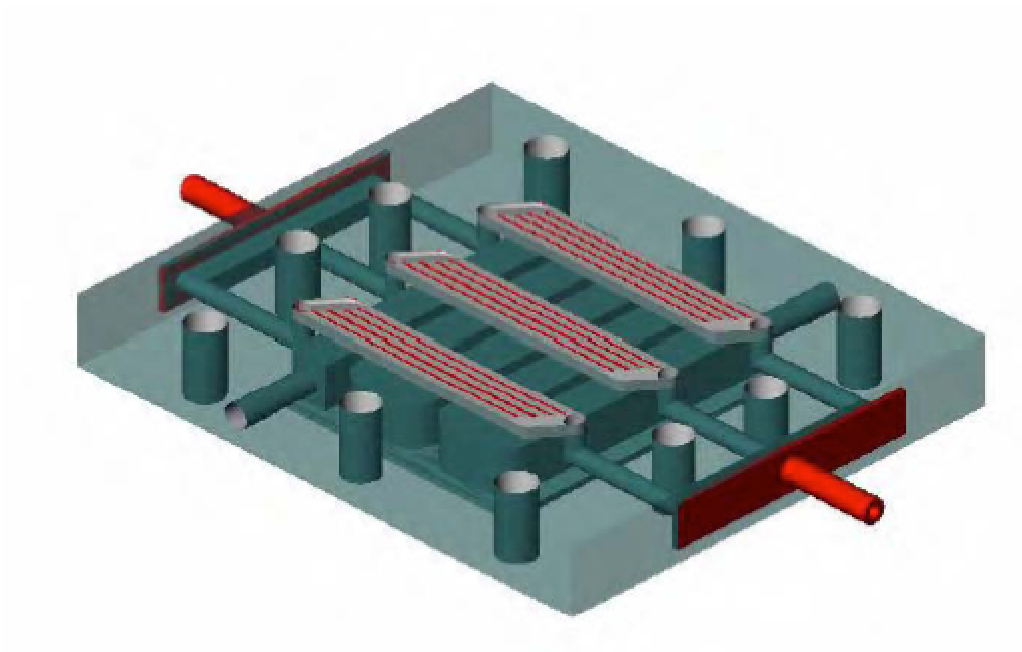

Figure 25. A semi-transparent rendering of one section of the three-parallel microchannel membrane contactor absorber. The red lines are membrane support ribs; the red tubes on the ends of the unit are headers feeding the 3-parallel channels; and the gray tubes on the sides of the structure are fluid ports for the serpentine heat-exchange channel.

Experimental work was performed in a single-channel adsorber to assess the adsorber system based on microchannels. A temperature cycle between 12 and 77°C could be achieved in less than two minutes with greater than 90% of theoretical working capacity. It was found that a diurnal cycle thermal-swing adsorption system requires more than 100-times more adsorbent than a microchannel sorption pump operating on 2-minute cycles [1].

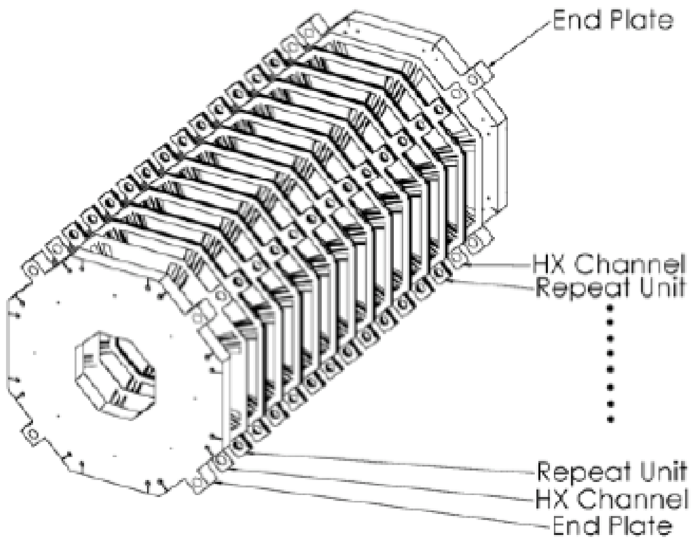

Figure 26. An exploded view of multiple repeat units, capping heat-exchange shims, and endplates arranged for bonding.

Testing with the RWGS and SR units was encouraging. Overall, 60 % conversion was achieved using a two-stage RWGS reactor in which water was removed between two stages [1].

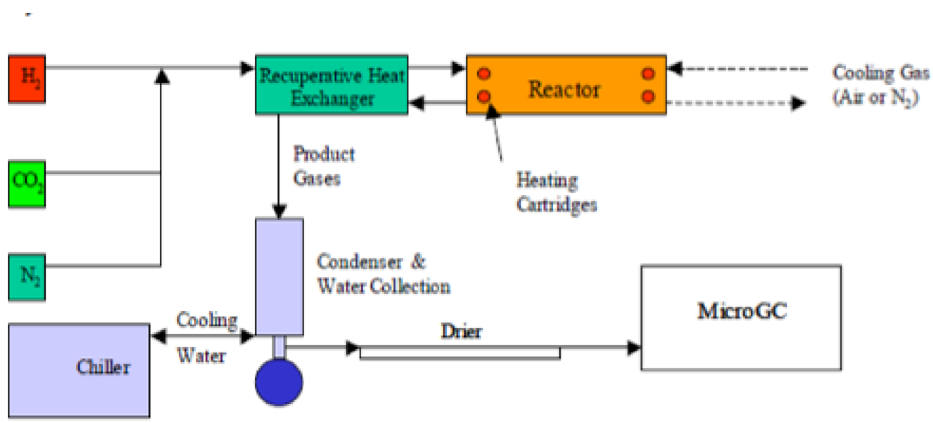

Figure 27. Generic equipment layout for RWGS & SR reactor testing.

This paper provided us with the perspective of the nature of reactions that can be performed in microreactors.

Hydrogen Peroxide Synthesis

H_2O_2 can be produced in two ways:

1) Direct conversion of H_2 and O_2 into H_2O_2
2) Auto oxidation of anthraquinone.

The process of direct conversion of H_2 and O_2 into H_2O_2 is shown below. This process is known as the Riedl-Pfleiderer process, having been first discovered by them in 1936. The overall equation for the process is deceptively simple:

$$H_2 + O_2 \rightarrow H_2O_2$$

Initially synthesis of hydrogen peroxide in a microreactor was considered for as a possible candidate for research. Hydrogen peroxide is the strongest oxidant that can be used in petrochemical industry for oxidation of carbohydrates. The catalytic synthesis of hydrogen peroxide with direct conversion method was looked at by S. Maehara et al [2]. In the study it was found that the concentration of hydrogen peroxide was very low, 0.204 g/kg. In another similar study by Voloshin et al, [3], they tried to get higher Hydrogen peroxide concentrations by adding 1% (w/w) H_2SO_4 and 10 ppm NaBr. The addition of 1% (w/w) H_2SO_4 and 10 ppm NaBr stabilizes H_2O_2 from further decomposition. They also tried to increase the H_2O_2 concentration by increasing selectivity of H_2O_2 by maintaining the H_2 conversion rate as low 2%. However, they still could manage to produce hydrogen peroxide with very low concentrations. So the production of H_2O_2 by direct conversion is not a feasible method for industries where H_2O_2 concentration required is very high.

The auto-oxidation process is shown by the reaction below.

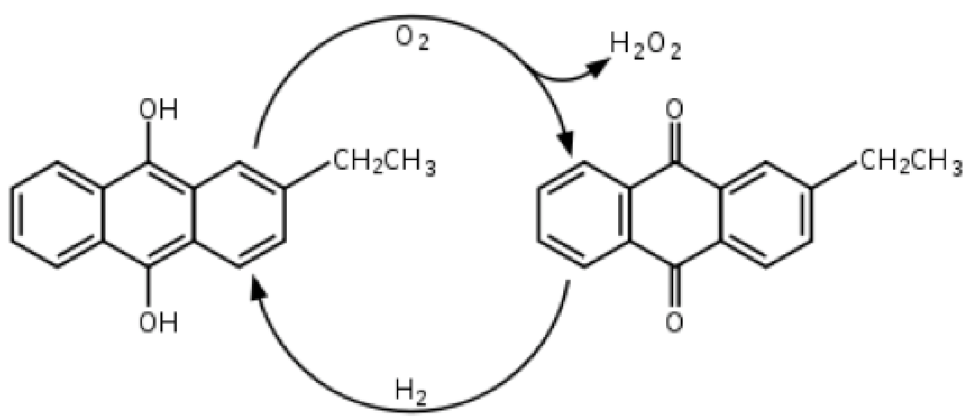

Figure 28. The auto-oxidation process.

Auto oxidation (AO) of anthraquinone is another method which is currently in use in the industry for H_2O_2 synthesis. Conventional methods require a very high inventory of reagent, as has been discussed by [4,5]. In addition to this, the conventional method results in degradation of hydrogenated anthraquinone due to overt reduction reactions [4,5] and formation of epoxides due to excessive oxidation [4,5]. This results in loss of expensive anthraquinone [4,5]. Also, the residence time for reactants is very high for the conventional method, and they require more expensive material to design the entire process [4,5]. Auto oxidation, being a well-tested method for the synthesis of H_2O_2 if performed in microreactors, would result in higher efficiency, high conversion rate and low residence time [4,5].

Steam Methane Reforming

Steam reforming reactions are endothermic in nature and involve five species in two reversible reactions.

$CH_4 + H_2O \Leftrightarrow CO + 3H_2$ $\Delta H298 = 206$ kJ/ mol

$CO + H_2O \Leftrightarrow CO_2 + H_2$ $\Delta H298 = -41$ kJ /mol

Overall reaction:

$CH_4 + 2H_2O \Leftrightarrow CO_2 + 4H_2$ $\Delta H298 = 165$ kJ /mol

Multiple reactors are connected in parallel to achieve plant-scale capacity, as shown in Figure 34 below, where a full-scale unit (3.9m × 5.8m × 3.9m) produces $10m^3$ of hydrogen per second by manifolding 30 commercial-scale microchannel reactors housed evenly between six reactor assemblies [20].

Microchannel process technology advantages are based on the use of small diameter channels to improve both heat and mass transfer rates by one to two orders of magnitude. Critical channel dimensions typically range from 50 to 5000 µm, and flow regimes are usually laminar. Transport rates are inversely proportional to channel diameters. Further, microchannels allow for an increase in the amount of surface area per unit volume—thus also increasing the overall productivity per unit volume [20].

Conventional methane steam reforming catalysts based on extruded pellets have reaction times on the order of seconds. Inserted engineered structures described in this paper are based on catalyst-coated FeCrAlY felts that are adjacent to the heat transfer wall and facilitate reaction rates on the order of milliseconds.

One particular technical challenge addressed in this paper surrounds the stable operation of combined reforming and combustion with low excess air in adjacent reaction microchannels.

In this study the combustion of methane/natural gas was carried out in parallel to the SMR reaction. Shown below is the experimental setup:

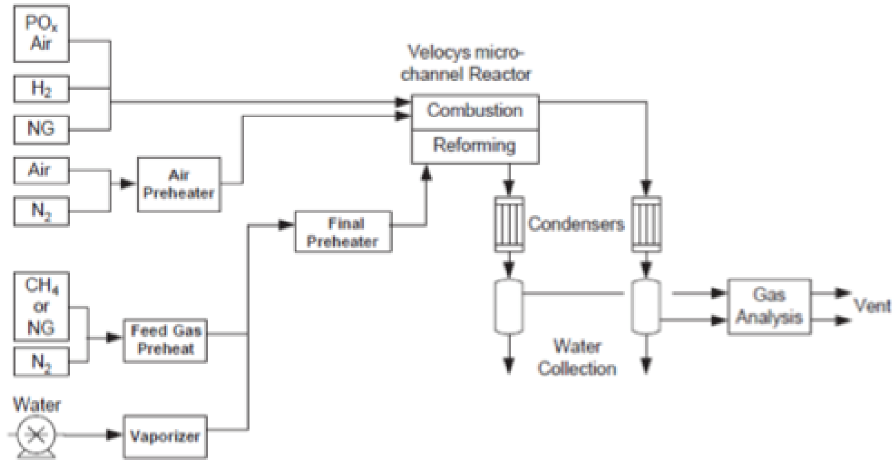

Figure 29. Experimental setup for microchannel reformer.

Water was vaporized at pressure in a resistance-heated microchannel heat exchanger and mixed with preheated methane or natural gas. The resulting mixture was then preheated to the desired reactor inlet temperature (280–310 ˚C) with the aid of an electrical microchannel preheater. An external resistance-heated microchannel heat exchanger was also used to preheat the inlet combustion air to 150–160 ˚C.

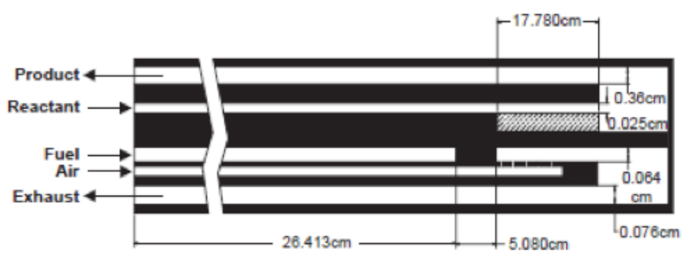

Figure 30. Microchannel steam reforming reactor with integrated partial oxidation.

A catalyst was washcoated on the walls of combustion chamber, while for the SMR reaction the catalyst was solution-coated on a porous metal foam (40 pore/cm) and inserted in the reactor. The reforming catalyst was prepared as a powder, which was then made into slurry and deposited on a FeCrAlY felt substrate (0.25 mm nominal thicknwaa, 75% porosity). The SMR catalyst was 10% Rh on a gamma alumina support modified with 4.5% MgO (w/w).

Methane conversion of >90% was achieved at >150kPa pressure and 850°C with contact time as low as 6 ms. Internal heat transfer flux was 17 W/cm^2. Volumetric heat transfer flux was more than 65 W/cm^3, which is very high compared to conventional SMR reactor volumetric heat transfer value of 1 W/cm^3.

For these tests, combustion of methane or natural gas was conducted with low rates of excess air (25%), an important requirement for plant scaleup to reduce the cost of blowers or compressors. Heat was transferred as it was generated to drive the endothermic reforming reaction. The average area heat flux exceeded 17 W/cm^2 while maintaining acceptable metal wall temperatures (< 900 ◦C), an important consideration for mechanical integrity.

4. Difficulties Encountered/Overcome

- Identifying a reaction that is of interest to ADNOC which also can be experimented with in the lab.

5. Planned Project Activities for the Next Quarter

- Continuing work on the literature survey.
- Further evaluations of potential reaction and reactor fabrication technologies.

Appendix

Justification and Background

Microreactors form a basis for the potential future downscaling of existing chemical processes, allowing tremendous reductions in capital and operating cost. They provide finer control of conditions, allow for faster process times, and improve safety in operation. Also, they should not encounter a significant problem scaling from laboratory-sized systems to commercial-sized systems, since their operating principle will simply allow them to be stacked together modularly.

Of critical importance to the microreactors' capability to make the jump into industrial applications is the mixing efficiency, which controls the reaction rates and the yield expected from a reactor. Due to the scale of the systems, laminar flow is almost always encountered, which means that the vortices typically associated with turbulent flow are often missing. Instilling vortices into the flows to encourage mixing is accordingly a matter of construction of mixer channels.

Approach

- Literature survey of the microreactor technologies as well as microchannel fabrication technologies.
- Selection of the target process for realization in microreactors with maximum benefit.
- Selection of microchannel fabrication technology suitable for microchannel mass production.
- Design and fabrication of a microreactor using microchannel fabricating technology suitable for mass production.
- Microreactor demonstration.

Two-Year Schedule

<u>Year 1:</u>
- Conduct literature review to study current technologies for micoreactors, micromixers, and incorporation of catalysts into microreaction technology.
- Evaluate existing microchannel formation techniques and their applications to microreactor construction.
- Selection of the target process for realization in microreactors with maximum benefit to ADNOC.
- Selection of microchannel manufacturing process most suitable for mass production.
- Preparation of a microreactor testing facility.
- Visualization study of mixing in microchannels.

<u>Year 2:</u>
- Continue selection of the target process for realization in microreactors with maximum benefit to ADNOC.
- Continue selection of microchannel manufacturing process most suitable for mass production.
- Continue visualization study of mixing in microchannels.
- Continue preparation of a microreactor testing facility.
- Design and fabricate microreactors using microchannel fabricating technology selected.

References

[1] Bertsch, Arnand & Stephan Heimgartner & Peter Cousseau & Phillippe Renand, 3D Micromixer – Downscaling Large Scale Industrial Micromixers; Swiss Federal Institute of Technology: 2001; pp 507-510.

[2] Cha, Junghun & Jinseak Kim & Suk-Kyu Ryu & Jungyul Park & Yongwan Jeang & Sewan Park & Sukhe Park & Hyean Cheol Kim & Kukjin Chun, A Highly Efficient 3D Micromixer Using Soft PDMS Bonding; Journal of Micromechanics and Microengineering, vol. 16: 2004; pp 1778-1782.

[3] Engler, Michael & Norbert Keeckman & Thomas Kiefer & Peter Weiss, Numerical and Experimental Investigations on Liquid Mixing in Static Micromixers; Chemical Engineering Journal, vol. 101: 2004; pp 315-322.

[4] Hessel, Volker & Holyer Löwe & Friedhelm Schönfeld, Micromixers – A Review on Passive and Active Mixing Principles; Chemical Engineering Science, vol. 60: 2005; pp 2479-2501.

[5] Jiang, F. & K. S. Drese & S. Hardt & M. Küpper & F. Schönfeld, Helical Flows and Chaotic Mixing in Curved Micro-channels; AIChE Journal, vol. 50 (9): 2004; pp 2297-2305.

[6] Karnik, Sooraj V & Miltiadis K. Hatalis & Mayuresh V. Kothare, Palladium Based Micro-Membrane for Wafer Gas Shift Reaction; IMRET 5: Proceedings of the Fifth International Conference on Microreactor Technology: 2001; pp 295-302.

[7] Mansur, Elmabruck A. & Y. E. Mingxing & Wang Yundong & Dai Youyan, A State-of-the-Art Review of Mixing in Microfluidic Mixers; Chinese Journal of Chemical Engineering, vol. 16 (4): 2008; pp 503-516.

[8] Mengeand, Virginie & Rrosario Ferrigne & Jacques Josserend & Hubert H. Girault, Mixing Simulation of a ZigZag Microchannel: A Step towards the Methoxylation of Methyl-2-Furate; IMRET 5: Proceedings of the Fifth International Conference on Microreactor Technology: 2001; pp 350-358.

[9] Stroock, Abraham C. & Stephan K. W. Dertinger & Armand Ajdari & Igor Mezié & Howard A. Stone & George M. Whitesides, Chaotic Mixer for Microchannels; Science, vol. 295 (25): 2002.

[10] Stroock, Abraham & Stephan K. Dertinger & George M. Whitesides & Armand Ajdari, Patterning Flows Using Grooved Surfaces Analytical Chemistry, vol. 74 (20): 2002; pp 5306-5312.

[11] Xu, B. & K. T. Ooi & C. Mavriplis & M. E. Zaghloul, Evaluation of Viscous Dissipation of Liquid Flow in Microchannels, Journal of Micromechanics and Microengineering, vol. 13: 2003; pp 53-57.

Thrust 3
Energy System Management

Integration of Engineering and Business Decisions for Robust Optimization of Petrochemical Systems

UMD Investigators: Shapour Azarm, P.K. Kannan
PI Investigators: Ali Almansoori, Saleh Al Hashimi
UMD GRAs: Weiwei Hu, Phillipe Kamaha
PI GRA: Naveen Al Qasas
Acknowledgement: Mian Li
Start Date: April 2009

1. Objective/Abstract

The overall objective of this project is to develop a framework for integrating engineering and business decisions. Towards that objective, a Robust Decision Support System (RDSS) will be developed that can be used for multi-objective and multi-disciplinary optimization and sensitivity analysis, under uncertainty, of oil, gas and petrochemical systems. Since the last quarterly report of Phase II, we have identified the connections between the business and engineering decisions in the context of a petrochemical system case study. Based on the decomposition of business and engineering disciplines, we have proposed a preliminary framework which can be used to integrate business and engineering decisions. We have refined the integration framework in this quarter and applied it to our case study. A collaborative optimization technique is used to solve the case study models and obtain optimal business and engineering decisions. The optimal decisions indicate that the overall profits can be significantly increased. Initial work on the development of a dashboard has also been started in this quarter. It will be demonstrated in this report that the decision making process through the use of dashboards for management can be simplified, and the quality of decisions can be significantly enhanced.

2. Deliverables for the Completed Quarter

- Continue the focus on integrating business and engineering decisions in the context of oil, gas and petrochemical systems.
- Apply a collaborative optimization (ref. [13]) technique to decompose business and engineering problems and obtain optimal decisions for a simple case study model.
- Study the optimal decisions from the case study that provide insights into both business and engineering problems.
- Begin research on the decision support role of dashboards for the management in the integration framework and develop a preliminary dashboard using Matlab Graphical User Interface (GUI).
- Four papers based on the collaboration were co-authored and will appear in publication outlets or are working papers under preparation. Among these papers, as listed below, Paper (a) is a publication from the results in Phase I, which finally appeared as a journal publication. Paper (b) is a Phase I to Phase II transition publication. The remaining papers are related to Phase II progress:
    a. Li, G., M. Li, S. Azarm, S. Al Hashimi, T. Al Ameri, and N. Al Qasas, 2009, "Improving Multi-Objective Genetic Algorithms with Adaptive Design of Experiments and Online Meta-modeling," *Structural and Multidisciplinary Optimization*, Vol. 37, No. 5, pp. 447-461.
    b. Li, M., S. Azarm, N. Williams, S. Al Hashimi, A. Almansoori, and N. Al Qasas, 2009, "Integrated Multi-Objective Robust Optimization and Sensitivity Analysis with Irreducible and Reducible Interval Uncertainty," Engineering Optimization, Vol. 41, No. 10, pp. 889–908.
    c. Hu, W., M. Li, S. Azarm, S. Al Hashimi, A. Almansoori, and N. Al Qasas, "On

Improving Multi-Objective Robust Optimization Under Interval Uncertainty Using Worst Possible Point Constraint Cuts," *CD-ROM Proceedings of the ASME 2009 International Design Engineering Technical Conferences*, Aug. 30 – Sep. 2, 2009, San Diego, CA, USA (forthcoming). (Also, under revision in *Journal of Mechanical Design*.)

d. Kamaha, P., W. Hu, A. Almansoori, S. Al Hashimi, P.K. Kannan and S. Azarm, 2009, "Corporate Dashboards for Multi-Unit Firms: An Agent-Based Approach for Supply Chain Optimization" (*working paper: under preparation*).

3. Summary of Project Activities for the Completed Quarter

Meetings and Video Conferences

Visits between UMD and PI faculty have been successfully completed.

- Prof. Almansoori (PI) visited UMD and the Design Decision Support Laboratory (DDSL) of Mechanical Engineering Department during the third and fourth week of July, 2009. During his visit, Prof. Almansoori participated in a number of group meetings with the UMD's research team and provided valuable recommendations for the collaborative research and education.

- Prof. Azarm (UMD) and Prof. Kannan (UMD) visited PI and several ADNOC companies during the third week of August. The ADNOC companies that had meetings with Profs Azarm and Kannan included: ADGAS, ADCO, ZADCO, Takreer, and Borouge. Their talks on "integrating business and engineering decisions for optimization of petrochemical systems" were well received during their visit. A few of the ADNOC companies expressed interests in future collaborations.

Teleconference meetings (via Windows Live Messenger) were held between UMD and PI project collaborators on August 5 and September 11. A summary of the highlights of minutes from these meetings is given below:

- During the meeting on August 5, the UMD's research team discussed the presentation prepared for the visit to PI and finalized it during the meeting on August 5. Items regarding Prof. Azarm and Prof. Kannan's visit to PI and some ADNOC companies were discussed.

- During the meeting on September 11, Prof. Azarm and Prof. Kannan summarized their visit at PI and the ADNOC companies. Preliminary plans on working with TAKREER to optimize CO_2 emission through meta-modeling were discussed.

An EERC PI-UMD Video Conference meeting was held on September 14, during which both PI (Prof. Almansoori) and UMD (Profs Azarm and Kannan) gave a summary of their interaction during their respective visits to the attending audience of both institutions.

Integrating Business and Engineering Decisions

Multi-unit enterprises are defined as systems that are interconnected: (1) through the complementary product/service categories and markets they serve and (2) through a common ownership of the enterprises that renders the problem of overseeing/managing these enterprises as a whole complex task. In this context the need for greater manageability is coupled with pressures for financial success that forces managers at all levels to cooperate and continually look for optimum operating conditions. Unfortunately, due to the non-deterministic nature of the data typically available to managers, deterministic approaches cannot be used to obtain optimum operating conditions. Managing a multi-unit firm involves making decisions that will have impacts across the firm and will affect the operations at every level of the company, whether at the engineering process level or business level. The objective is to show that even in the midst of fluctuating demand or uncertain engineering parameters, business and engineering departments can work as a team to achieve optimal operations and financial returns for the organization.

The schematic of integrating business and engineering decisions is shown through a roadmap in Figure 1. At the top of the figure is “management with dashboard” block. The role of management is to focus on setting goals for the firm in order to make good decisions within constraints. When setting these goals, management should not only consider inventory and finance but also product quality derived from customer requirements. The decision-making process of management is supported by the dashboard, through which the management is able to easily watch key performance indicators and improve performance by way of optimization. Information that is fed to the dashboard is obtained from the integration of business and engineering decisions, as shown at the bottom of the roadmap. The objectives in the business discipline include improving the firm’s profit, meeting market demand and maintaining inventory. Towards these objectives, the business leaders need to make decisions on raw material procurement and allocation, work in progress and the end product distribution. In the engineering discipline, the objectives are to support overall business goals and comply with product quality specifications. Typically, engineering decisions are characterized by operation settings in the plant such as material flow rate and temperature/pressure settings.

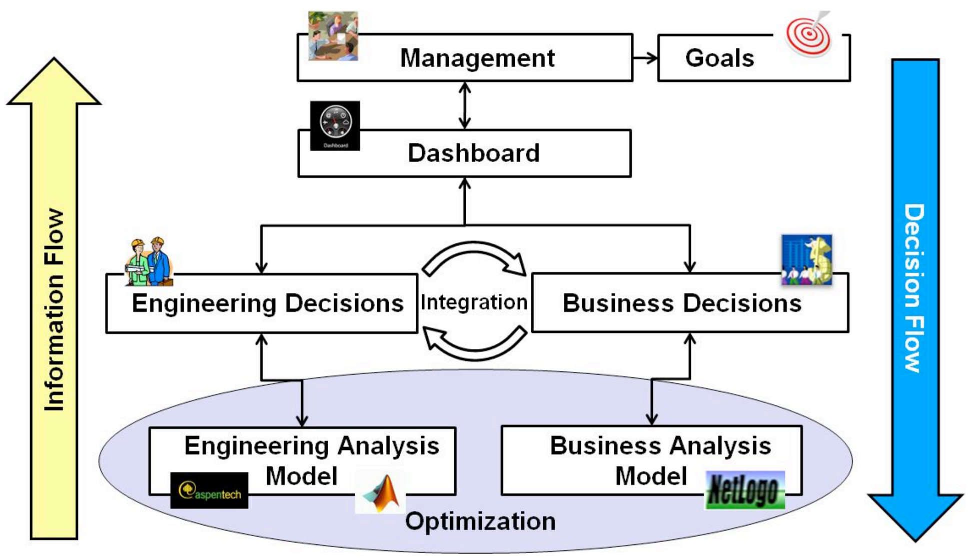

Figure 1. The roadmap on integrating business and engineering decisions.

.
In this study, both engineering and business decisions are made based on the analysis of simulation models. The business analysis model is developed using an agent-based simulation software called NetLogo as shown in Figure 1. NetLogo can be used to simulate firm-market interactions. Using the business analysis model, the business decision makers will be able to forecast market demand and predict impact of business decisions according to the expected value of key performance metrics. The engineering analysis model consists of a series of Matlab programs and functions which are used to simulate the complicated reactions and distillation processes in a real refinery plant. The engineering decision-makers rely on an analysis model to estimate how the product quality and energy consumption change with respect to different operating conditions.

As we discussed in the last quarterly report, a Collaborative Optimization (CO) (ref. [13]) framework is applied to solve the integrated decision-making problem. CO is a bi-level optimization method developed for multidisciplinary applications. The business decisions are made at the system level, and the engineering decisions are made at the sub-system level. The connections between business and engineering analysis models in the context of CO are shown in Figure 2. The business optimizer attempts to maximize the expected profit while satisfying consistency constraints. According to the business analysis model and engineering optimization results, the business optimizer determines the feed flow rate and sets the product quality and quantity targets. The feed flow rate and the expected targets from the business optimization are then sent to the engineering optimization. The engineering optimizer attempts to minimize the cost of energy consumption by changing the operation setting based on the engineering analysis model while matching those targets as closely as possible. In the proposed approach, if there are any discrepancies between the targets and actual values in the engineering optimization, the differences are reported to the business optimization. The process of business and engineering optimization iterates until the discrepancy on the target is smaller than a predefined tolerance value (which is typically very small).

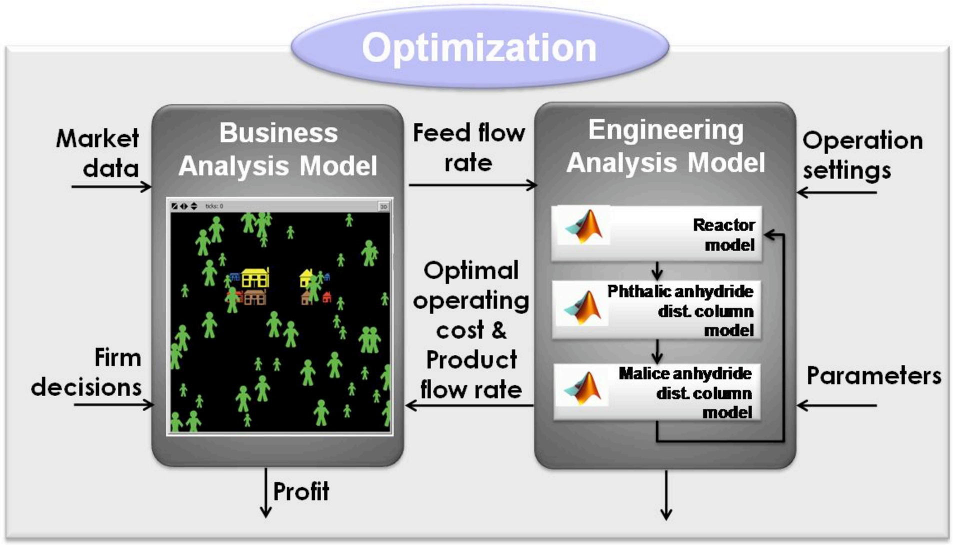

Figure 2. Schematic for the business decisions.

The Decision Support Role of the Dashboard

Essentially, the dashboard in the integrated business and engineering decision support framework will serve the following purposes:

- Display decision variables and expected value of performance measures based on an integrated optimization scheme. The optimization is performed based on the analysis models.
- Display the current value of performance measures based on the real firm-market interactions. The values of the decision variables in the real firm-market interactions are provided by the decision makers from the optimal decision variables.
- Visualize all data obtained during the management interface, enabling management to control and adjust the decision variables.

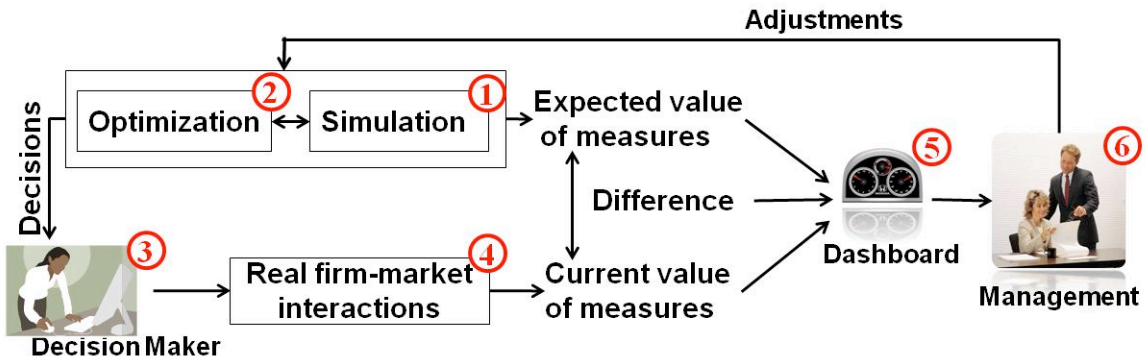

Figure 3. The decision support role of dashboard.

Figure 3 shows the dashboard as a decision support tool in the integration framework. The dashboard contains Key Performance Indicators (KPIs) such as profit and inventory. The expected values of KPIs are obtained from the simulation model and the optimization results. The decision-maker, based on the expected KPIs and his/her expertise in the related discipline, will try to make the best decisions for the firm. Those decisions will impact the current KPI values according to the real firm-market interactions. Both the expected and the current values of KPIs will be sent to the dashboard.

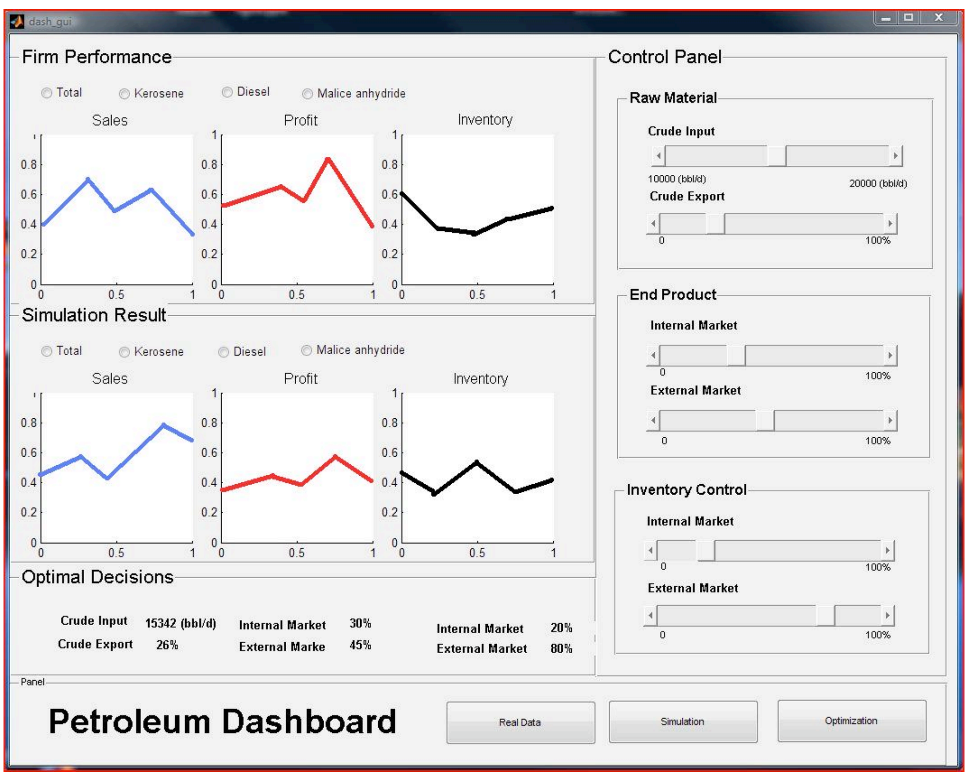

Figure 4. The preliminary dashboard for the proposed integration framework.

A preliminary dashboard using the Graphical User Interface has been developed in the Matlab programming environment. At the bottom of the dashboard, three push buttons are designed for the decision-maker to obtain the expected and current plant performance and make real-time decisions accordingly. When the "Simulation" button is clicked, the simulation models from the business and engineering disciplines are started. The simulated performance values are shown in the "Simulation Result" panel. The decision maker can then click the "Optimization" button, which will activate the collaborative optimization scheme in the backstage, based on the business and engineering analysis models. After business and engineering optimization converge, the optimization results are obtained and shown in the "Optimal Decisions" panel. The decision-maker can obtain the real-time firm performance data by clicking on the "Real Data" button. The current performance data will be shown under the "Firm Performance" panel on the dashboard. In case the real-time and expected performances are different, the decision-maker will make decisions on the raw material procurement, end-product distribution and inventory level based on his/her experience. These decisions can be fulfilled using the sliders in the "Control Panel" of Figure 4.

Case Study

The case study considers a simplified refinery which sells one refined product and one raw product (crude oil) to market. The goal is to maximize profit over a time horizon while satisfying inventory policy and customer needs. To meet that goal, management needs to obtain information concerning real-time and estimated key plant metrics that will help them to make and adjust decisions. Those key plant metrics are provided through the dashboard, which has been introduced in the previous section. The dashboard contains KPIs such as profit, sales, inventories and so on.

For the case study, it is presumed that the market is composed of two different product-market types, i.e., the crude product-market and the phthaline product-market, as shown in Figure 5. The crude/murban can only be sold to the external market, while phthaline is sold both locally and internationally. In the crude market, the company sells some of its crude directly. This is an external market characterized by fluctuating prices with 100% chance of purchasing, and the consumption is guaranteed to be equal to the supply. That is, no matter how much the company decides to sell to the crude external market, it will get purchased by external customers. The local and external phathaline markets each have 5 customers, which could be distributors, or other firms that purchase the end product locally. Their consumption is presumed to be normally distributed, just as their probability of purchase. The local phathaline prices are fixed in time. Phathaline prices in the external market are not fixed and vary in time by a normal distribution process.

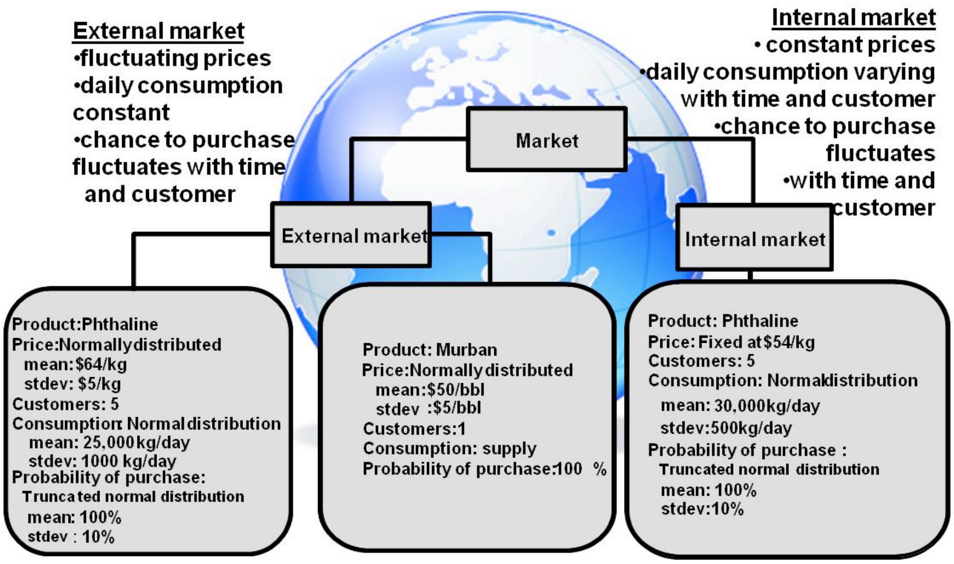

Figure 5. Market description in business case study model.

For the case study, we are considering the profit that the refinery is generating through the sale of the product: phthaline anhydride. The business schematic is shown in Figure 6. The corresponding engineering optimization problem is shown in Figure 7. Murban oil is processed in the crude distillation unit (CDU). The output of CDU includes, among other products, some naphtha. That naphtha is sent to a reactor that converts it into the finished product phthaline anhydride. As shown in Figure 6 and Table 1, the decisions the company has to make, i.e., the variables in the business optimization, are to find how much crude to purchase (specified by x_1), what percentage of that crude should be sold to the crude external market, what percentage of end product should be stored in inventories, what percentage of end product should be sold to the external market, and what percentage should be sold in the local market (specified by x_2 to x_6). The goal is to maximize the profit while meeting customer demand and a goal of zero inventory.

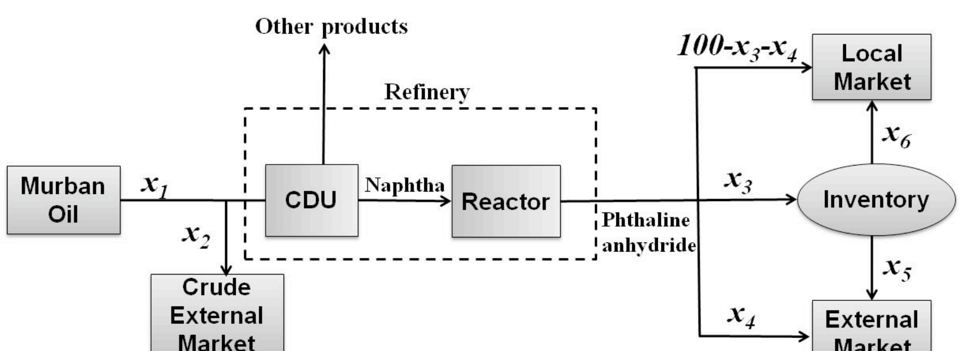

Figure 6. Business schematic and variables in the case study.

Table 1. Design variables and description in business optimization

Variable	Description
x_1	Daily crude oil purchase (bbl/d)
x_2	Percentage of crude oil sold to external market : fixed at 10%
x_3	Percentage of finished product sent to inventory
x_4	Percentage of finished product sent to external market
x_5	Percentage of inventory released to external market
x_6	Percentage of inventory released to local market

Engineering Optimization

Minimize: Operating cost $= f(y_1,\ldots,y_5)$

Subject to: purity of products ≥ minimum specifications

Variable:
y_1 - air feed flow rate (kmol/hr)
y_2 - recycled o-xylene flow rate (kmol/hr)
y_3 - minimum reflux ratio for phthalic distillation
y_4, y_5 - reflux/boil up ratio for malice distillation

Parameters: o-xylene feed flow rate (kmol/hr)

Figure 7. Engineering optimization problem of the case study.

The entire optimized variables, for business and engineering, are shown in Table 2. It has been observed that the yield of naphtha affects the flow rate of oxylene, which could have an impact on engineering constraints. The product purity required by the customers in the business discipline has an impact on engineering optimization results. The profit obtained with optimum decisions should not vary from expected value beyond an acceptable tolerance level.

Table 2. Optimized decisions from the integrated optimization in the case study

Variables	After optimization
x_1: crude input (bbl/day)	400,000
x_2: percentage of murban to external market	10
x_3: percentage of phthaline to inventory	0
x_4: percentage of phthaline to external market	0.6
x_5: percentage of inventory sent to external market	32.2
x_6: percentage of inventory sent to local market	0
y_1: air feed flow rate (kmol/hr)	987.8
y_2: recycled o-xylene flow rate (kmol/hr)	383.4
y_3: minimum reflux ratio for phthalic distillation	5.0
y_4: reflux/boil up ratio for malice distillation	5.0
y_5: reflux/boil up ratio for malice distillation	6.0
Average daily profit after 1000 cycles (planning horizon)	$16 Million

4. Difficulties Encountered/Overcome

One challenge for implementing the CO framework is that it could take a large number of iterations before the subsystem (engineering) optimization variables to converge to the targets set by the system level (business) optimization. In the case study, both business and engineering optimizations are based on simulation models. This could require extended computational time if both optimization problems need to iterate many times. Moreover, the computational cost of the optimization problem grows dramatically as the size of the business and engineering domains grows: for example, as the number of subsystems increases or as the number of decision variables grows. To overcome this difficulty, an approximation-assisted, multi-objective, multi-disciplinary robust optimization approach is currently being developed.

5. Planned Project Activities for the Next Quarter

- Extend the current single-objective collaborative optimization framework to multi-objective optimization problems, meaning all system and subsystem optimization problems could have more than one objective.
- Consider input uncertainties in the optimization problems and develop a robust integration framework for the refinery systems.
- Continue current research on approximation-assisted optimization techniques and improving computational efficiency of MORO using approximation methods.
- Study the impact of customer interaction on company performance.
- Continue investigation on the metrics for Key Performance Indicators.
- Start collecting data from partner companies in Abu Dhabi for the case study.

Appendix

Justification and Background

Many oil, gas and petrochemical systems involve numerous coupled subsystems. These systems and their subsystems usually have uncertain inputs and thus it can be difficult to make the “best” engineering and business decisions in terms of independent operations of these complex systems. It becomes even more difficult to make those decisions when the system consists of many units or plants producing different products. This difficulty presents an opportunity taken on in this project; a review of mainstream literature has revealed that previous models in management of petrochemical systems have been in majority based on either engineering or business decisions but not both. There is a significant gap in the literature as to how these two types of decisions should be devised and integrated. To address this important gap, the focus of this investigation is to develop an integrated robust decision support framework considering both engineering and business models under uncertain conditions. Our overall objective has several underlying research issues or objectives, including: (i) how to develop business models that include management decisions in a multi-unit organization and at the same time account for engineering aspects; (ii) how to determine the relative importance and effects of uncertain system and/or subsystem input parameters on subsystem and/or system outputs (e.g., system performance); (iii) defining a set of metrics, a dashboard, that will serve as a visualization tool to keep track of the company’s financial status and provide for easy communication between various levels in the company, and (iii) how to extend our current single-level robust optimization method to multi-subsystem problems and maintain reasonable computational complexity for the method. These underlying objectives will be organized into tasks throughout the time frame allocated to the project. The details of the tasks are explained in the next section.

Approach

There are two main tasks in this investigation as detailed in the following.

<u>Task 1 (PI):</u>
Develop and implement engineering analysis models, in a Matlab (or Matlab compatible) environment, for a crude distillation unit case study model.

- Task 1.1: Develop a multi-input multi-output analysis model for a representative petrochemical system with corresponding subsystem analysis models.
- Task 1.2: Extend the analysis model in Task 1.1 to include: (i) additional complexity, (ii) subsystem details and uncertainty to include reasonable representation of engineering side of a plant. The ultimate goal is to develop an integrated multi-subsystem petrochemical analysis model for a plant or a group of units in a plant.

<u>Task 2 (UMD):</u>
Develop and implement a Robust Decision Support System (RDSS).

Engineering Tasks
- Task 2.1: Develop a single level (all-at-once) approximation-assisted robust optimization technique that is able to significantly reduce the computational efforts of making robust decisions.
- Task 2.2: Demonstrate an application of the approach from Task 2.1 with a case study in petrochemical systems which will be developed by PI as a part of Task 1.
- Task 2.3: Develop an approximation assisted multi-objective multi-disciplinary robust optimization approach, which is an extension to Task 2.1.
- Task 2.4: Demonstrate an application of the approach from Task 2.3 with a case study in petrochemical systems which will be developed by PI as part of Task 1.

Business Tasks

- Task 2.5: Develop business models in Netlogo and solve a simplified refinery supply chain optimization problem with Matlab.

- Task 2.6: Develop a Dashboard and test the robustness and sensitivity of the Dashboard's elements for the model in Task 2.5.

Integration Tasks

- Task 2.7: Inspect engineering and business problems to determine coupling variables between two problems.

- Task 2.8: Integrate Tasks 2.1 to 2.4 with Tasks 2.5 to 2.6 to formulate a refinery optimization problem that considers both engineering and business objectives and constraints.

- Task 2.9: make the supply chain management problem more realistic by considering more decision levels, more finished products and a wider market, and by increasing the size of the refinery's internal network and then repeat Task 2.8.

- Task 2.10: Verify and validate the integrated model.

Key References

[1] Douglas, J.M., 1988, "Conceptual Design of Chemical Processes", McGraw-Hill, New York, USA.
[2] Forbes, R.J., 1948, "Short History of the Art of Distillation", Brill, Leiden, Holland.
[3] Gargeya, V., 2005, "Plant Level Performance Measurement: An Exploratory Case Study of a Pharmaceutical Encapsulation Company", Technovation, 25(12), 1457-1467.
[4] Gattu, G., Palavajjhala, S., and Robertson, D. 2003, "Are Oil Refineries Ready for Non-Linear Control and Optimization?" International Symposium on Process Systems Engineering and Control, Mumbai, India.
[5] Grossmann, I. E., 2005, "Enterprise-Wide Optimization: A New Frontier in Process Systems Engineering," AIChE Journal, 51(7), p. 1846-1857.
[6] Halemane K. P., Grossmann I. E., 1983, "Optimal Process Design under Uncertainty," AIChE Journal, 29(3), 425-433.
[7] Inamdar, S. V., Gupta, S. K. and Saraf, D. N, 2004, "Multi-Objective Optimization of an Industrial Crude Distillation Unit Using the Elitist Non-Dominated Sorting Genetic Algorithm," Chemical Engineering Research and Design, 82(5), 611-623.
[8] Jackson, J., Hofmann, J., Wassick, J. and Grossmann, I., 2003, "A nonlinear multi-period process optimization model for production planning in multi-plant facilities", Proceedings FOCAPO2003, 281-284..
[9] Janak, L., Lin, X. and Floudas, C. A., 2007, "A New Robust Optimization Approach for Scheduling Under Uncertainty: II. Uncertainty with Known Probability Distribution," Computers and Chemical Engineering, 31(3), 171-195.
[10] Kaplan, R. and Norton, D., 1996, "Using the Balanced Scorecard As a Strategic Management System", Harvard Business Review, 74(1), 75-85.
[11] Kleijnen, J. and Smits, M., 2003, "Performance metrics in supply chain management". Journal of the Operational Research Society, 54(5), 507–514.
[12] Lin, X., Janak, S. L. and Floudas, C. A., 2004, "A New Robust Optimization Approach for Scheduling Under Uncertainty: I. Bounded Uncertainty," Computers and Chemical Engineering, 28(6-7), 1069-1085.
[13] Li, M. and S. Azarm, 2008, "Multi-objective Collaborative Robust Optimization With Interval

Uncertainty and Interdisciplinary Uncertainty Propagation," Journal of Mechanical Design, 130(8), 081402.1-081402.11.
[14] Micheletto, S. R., Carvalho, M. C. A. and Pinto, J. M., 2008, "Operational Optimization of the Utility System of an Oil Refinery," Computers and Chemical Engineering, 32(1-2), 170-185.
[15] Netlogo, http://ccl.northwestern.edu/netlogo/
[16] Pinto, J., Joly, M. and Moro, L., 2000, "Planning and scheduling models for refinery operations", Computers and Chemical Engineering, 24(9), 2259–2276.
[17] Robins, J. and Wiersema, M., 1995, "A Resource-Based Approach to the Multi-business Firm: Empirical Analysis of Portfolio Interrelationships and Corporate Financial Performance", Strategic Management Journal, 16(4), 277-299.
[18] Sahdev, M., Jain, K., Srivastava, P., "Petroleum Refinery Planning and optimization Using Linear Programming", The Chemical Engineers' Resource Page, http://www.cheresources.com/refinery_planning_optimization.shtml
[19] Suresh, S. Pitty, Li, W., Adhitya, A., Srinivasan, R., Karimi, A., 2008, "Decision support for integrated refinery supply chains", Computer and Chemical Engineering, 32, 2767–2786.
[20] Zhang, N. and Zhu, X., 2000, "A novel modeling and decomposition strategy for overall refinery optimization." Computers and Chemical Engineering, 24(2), 1543- 1548.

Dynamics and Control of Drill Strings

UMD Investigator: Balakumar Balachandran
PI Investigators: Hamad Karki and Youssef Abdelmagid
GRA: Chien-Min Liao (started in Spring 2007)
Start Date: December 2006 (Phase I) and April 2009 (Phase II)

1. Objective/Abstract

Drill-string dynamics need to be better understood to understand drill-string failures, control drill-string motions, and steer them to their appropriate locations in oil wells. Although a considerable amount of work has been carried out on understanding drill-string vibrations (for example, Leine and van Campen, 2002; Melakhessou *et al*., 2003; Spanos *et al*., 2003), the nonlinear dynamics of this system are only partially understood, given that the drill string can undergo axial, torsion, and lateral vibrations, and operational difficulties include sticking, buckling, and fatiguing of strings. In addition, the prior models focus on either bending or torsion or axial motions. Hence, it is important to consider coupled axial-bending-torsion vibrations and contact instability in oil and gas well drilling.

The overall goal of the proposed research is to understand the nonlinear dynamics of the drill string and develop a control-theoretic framework for its stabilization enabling energy efficient drilling with longer life-span for the equipment. Specific research objectives of this project are the following: i) building on Phase I efforts, develop and study control-oriented models for the drill strings through analytically and numerically methods, ii) investigate the control of an under-actuated nonlinear system (drill string) with complex interactions with the environment, and iii) use the drill-string test-beds constructed at the Petroleum Institute & the University of Maryland to validate the analytical findings and suggest possible strategies to mitigate drill-string failures in fixed and floating platform environments.

2. Deliverables for the Completed Quarter

- Conducted experiments to examine the system behavior and compare it with predictions obtained through the Hamiltonian formulation.
- Collaborated with Professor S.P. Singh on fundamental studies on the stick-slip interactions and reduced-order models.

3. Summary of Results

In the first quarter, the Hamiltonian formulation was constructed and preliminary results were obtained (Liao *et al*., 2009). This formulation allows for longer time-domain simulations compared to those realized with prior formulations, and this would be important for examining long-term system behavior. In this quarter, a set of related experiments has been carried out to examine the system behavior and compare it with predictions obtained through the Hamiltonian formulation. In addition, in collaboration with a visiting faculty member (Professor S. P. Singh from the Indian Institute of Technology, Delhi, India), fundamental studies have been carried out to better understand the stick-slip interactions and enhance the reduced-order models developed in the current work.

The rest of this section is organized as follows. In Section 3.1, the experimental setting is presented along with the experimental results obtained for different system settings such as the unbalanced mass and the driving torque. In Section 3.2, results of numerical investigations are presented and comparisons are made with the experimental result as system identification. In Section 3.3, fundamental investigations into stick-slip interactions are presented.

3.1 Experimental Studies

From the results of numerical simulations, the investigators have inferred that the system dynamics are influenced appreciably by the rotating mass imbalance and contact interactions between the drill string and outer shell. It has been discussed in earlier reports that with the developed reduced-order models, different types of rotor motions, including bumping and sticking motions, can be obtained for different drive speeds. To better understand this, a series of experiments with different unbalanced massed were conducted, and the results are reported here.

3.1.1 System Description and Torsion Motions

The experimental arrangement is the same as the one that has been previously reported. In the present set of experiments, in addition to the encoders, triaxial accelerometers have also been used as shown in Figure 1. These accelerometers are mounted at the two ends of the drill string to measure the acceleration levels along the different directions, and the encoders have been used as before to measure rotational motions.

The torsion motion at the end of the drill string is determined as the difference between the rotational motions measured at the two ends of the drill string. Two unbalanced masses are used in the experiments, with one of them being 10 grams and the other being 70 grams. The former is referred to as a small unbalanced mass, while the latter is referred to as a large unbalanced mass.

In Figure 2, representative experimental results are shown for the cases of no unbalanced mass, small unbalanced mass, and large unbalanced mass. These results are shown in the form of time histories and frequency spectra. The system is driven with a motor, whose speed is 300 rpm. In the case of the system with no unbalanced mass, there is a prominent response peak at 11 Hz, and this peak drops to 8 Hz and 7 Hz in the cases of the small unbalanced mass and the large unbalanced mass, respectively. These experiments indicate that the principal torsion response frequency drops in value as the unbalanced mass is increased.

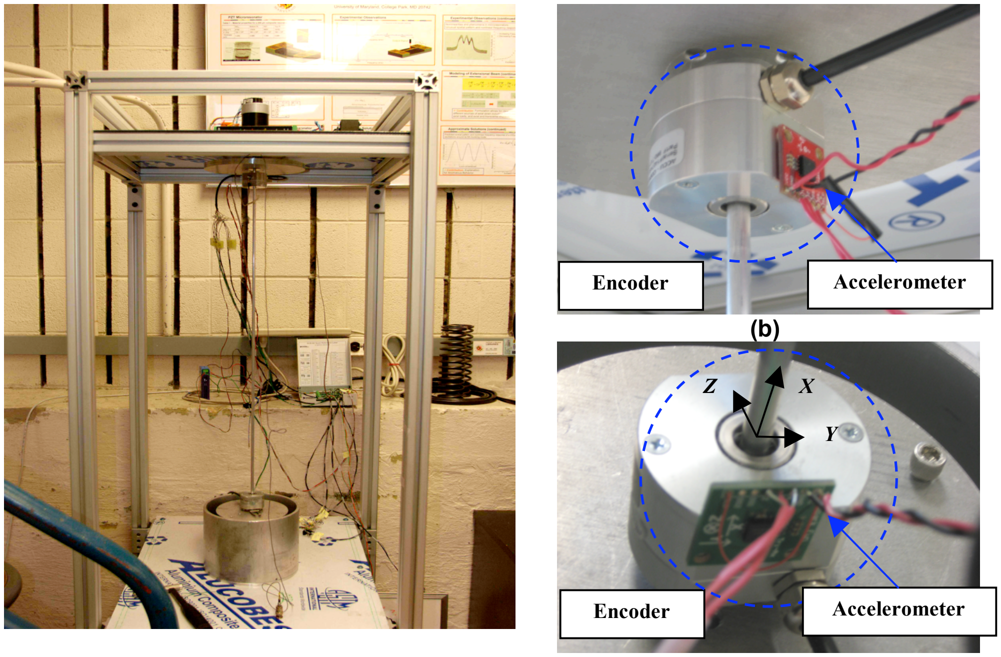

(a) (c)

Figure 1. Experimental setup: (a) side view of overall experimental arrangement, (b) accelerometer along with encoder at the top end of the drill string, and (c) accelerometer along with encoder at the bottom end.

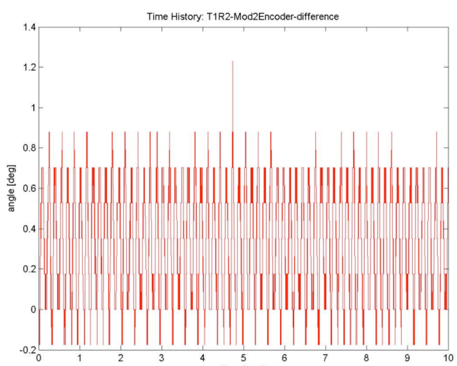

(a) Time history with no unbalanced mass.

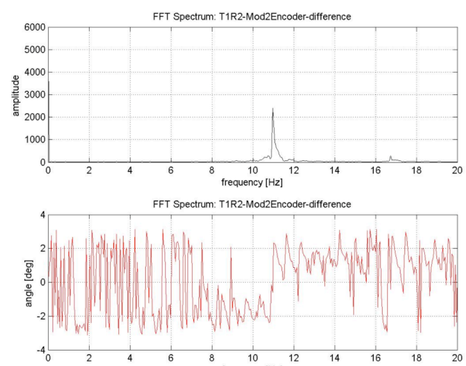

(b) Frequency and phase spectrum with no unbalanced mass.

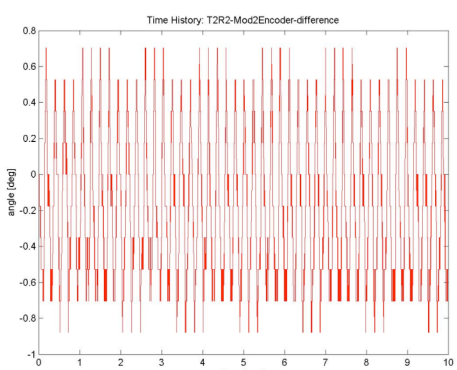

(c) Time history with small unbalanced mass.

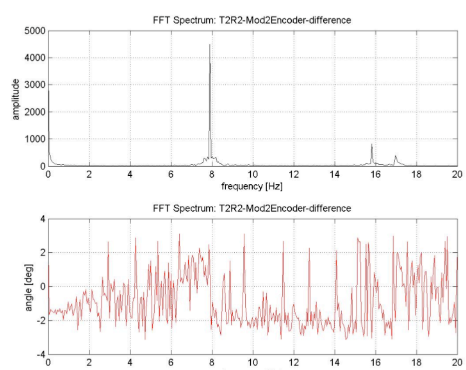

(d) Frequency and phase spectrum with small

unbalanced mass.

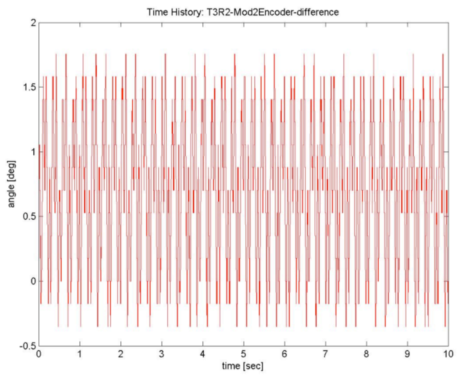

(e) Time history with large unbalanced mass.

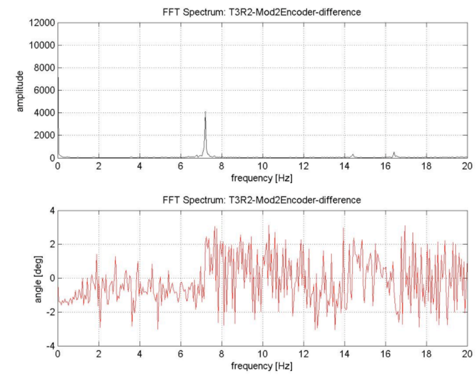

(f) Frequency and phase spectrum with large unbalanced mass.

Figure 2. Torsion response of system with and without unbalanced mass.

3.1.2 Examination of Lateral Response Characteristics

In the previous subsection, the torsion response of the system was examined for different unbalanced masses. In this subsection, lateral response characteristics of the system are examined. The system is excited either by a drive motor torque at the top of the drill string or through an impact hammer hit at the bottom disc along the lateral direction.

In Figure 3, the accelerometer response spectra obtained along three orthogonal directions are shown for cases with a small unbalanced mass and a large unbalanced mass. In each of these cases, the system is excited by a drive motor at a frequency of 4.5 Hz. In the case of the system with the small unbalanced mass, apart from the drive frequency peak, peaks at 1.7 Hz and 15.9 Hz can be seen. The peak at 1.7 Hz corresponds to the pendulum mode of the system. The response results are similar in the case of the system with the large unbalanced mass, except that there is a response peak at 13.7 Hz instead of the 15.9 Hz peak observed previously. In Figure 4.1.4, the results obtained when the system is excited by an impact hammer are shown. Again, the pendulum response component can be observed. In addition, the lateral response of the drill string leads to a response peak at 11 Hz.

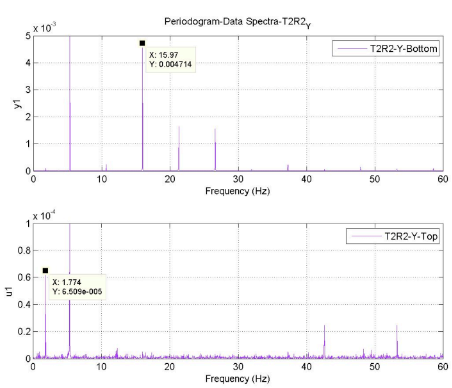

(a) Acceleration spectra along Y-axis with small unbalanced mass.

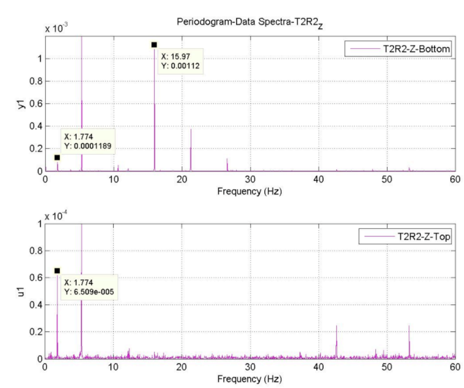

(b) Acceleration spectra along Z-axis with small unbalanced mass.

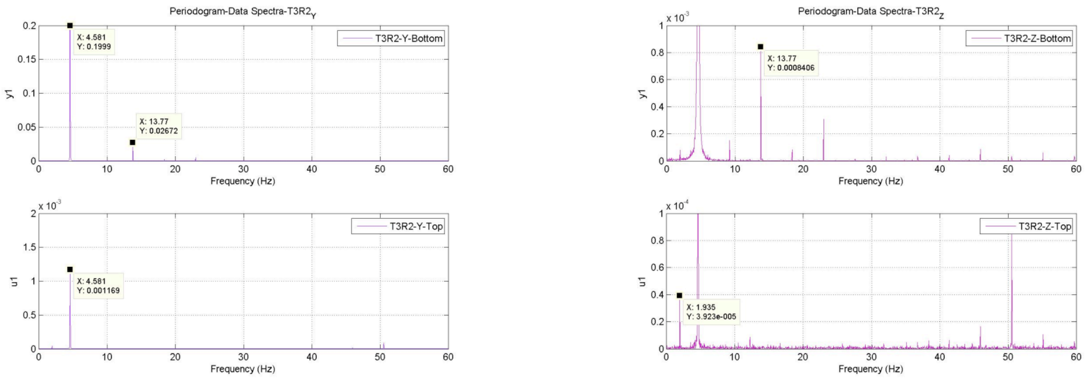

(c) Acceleration spectra along Y-axis with large unbalanced mass.

(d) Acceleration spectra along Z-axis with small unbalanced mass.

Figure 3. Lateral response characteristics for different unbalanced masses.

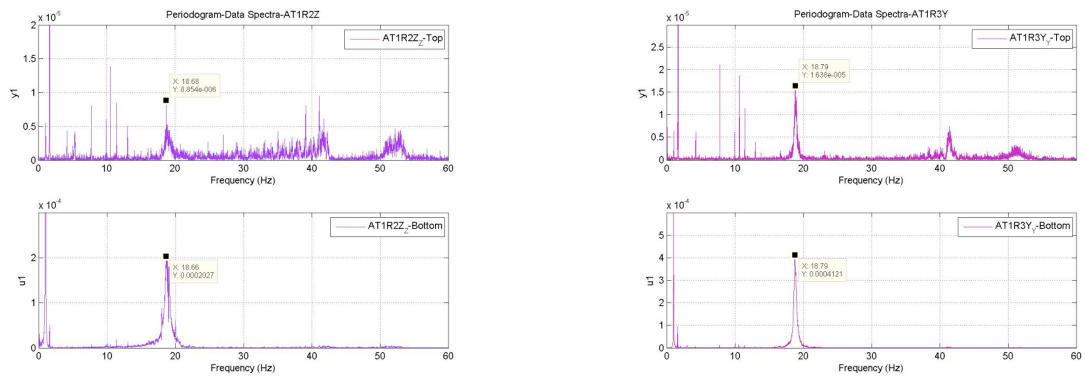

(a) Acceleration response spectra along Z-axis.

(b) Acceleration response spectra along Y-axis.

Figure 4. Lateral response characteristics for system with small unbalanced mass.

3.2 Comparison of Numerical Results with Experimental Results

To generate the numerical results, the system parameter values shown in Table 1 are used.

Table 1. Parameter values corresponding to experimental arrangement

Parameters	Variable	Value	units
Mass of Rotor	m	$7.08 * 10^{-1}$	Kg
Unbalanced Mass on Rotor	m_b	$7 * 10^{-3}$	Kg
Stator Moment of Inertia	I_1	$5.9 * 10^{-3}$	Kgm^2
Rotor Moment of Inertia	I_2	$1.9 * 10^{-3}$	Kgm^2
Bending Stiffnesses I	K_r	27.2	Nm^{-1}
Bending Stiffnesses II	K_t	27.2	Nm^{-1}
Torsional Stiffnesses	K_{TOR}	4.69	$\mathrm{Nm}*rad^{-1}$
Stiffnesses of Outer Shell	K_p	$2.7 * 10^5$	Nm^{-1}
Outer Shell Inner Diameter	D	$1.91 * 10^{-1}$	m
Rotor Diameter	d	$1.52 * 10^{-1}$	m
Initial Position of Rotor	ρ_0	$1.9 * 10^{-2}$	m
Motor Torque	τ	$2.05 * 10^{-2}$	Nm

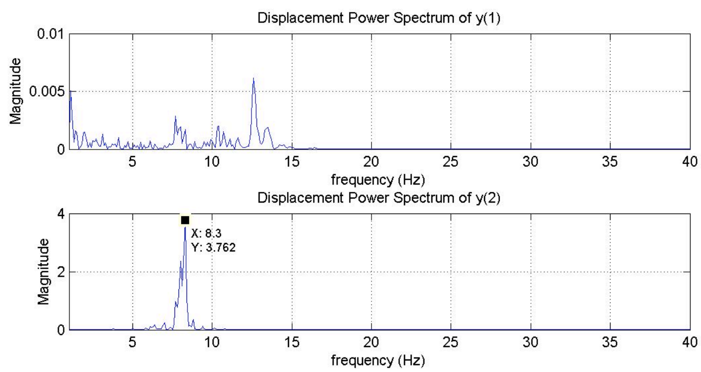

(a) Displacement spectrum along Z-axis with small unbalanced mass.

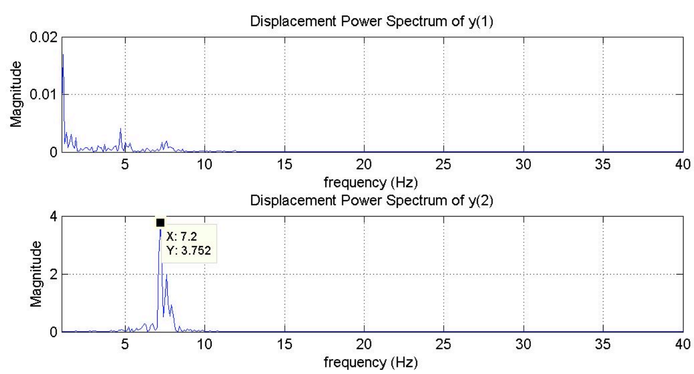

(b) Displacement spectrum along Z-axis with large unbalanced mass.

Figure 5. Displacement response spectra predicted through simulations.

The numerical results are obtained based on the Hamiltonian formulation, and to determine the torsion response, the four degree-of-freedom formulation is reduced to a three degree-of-freedom formulation and attention is focused on the difference between the angular motions of the rotor and stator; that is, $(\theta - \alpha)$. Along with this angle, the lateral motion captured by ρ and the tangential motion captured by φ constitute the other coordinates used to describe the system. The numerically obtained response spectra are shown in Figure 5. The results of Figure 5(a), which correspond to the system with small unbalanced mass, compare well with the experimental results in terms of the torsion response and lateral motion response peaks. For the case of the system with the large unbalanced mass, the numerical results show reasonable agreement with the experimental results, but the difference in the lateral response requires further examination. The differences could be due to components such as encoders not included in the model.

3.3 Fundamental Investigations into Stick-Slip Interactions: Rub and Roll Model

In collaboration with visiting faculty member Professor S. P. Singh from the Indian Institute of Technology, Delhi, India, stick-slip interactions were examined to better capture such interactions in the drill-string system. To this end, the stick-slip model shown as Figure 6 was studied. In this model, rotational friction is also accounted for, unlike the situation in the previous models. In this fundamental system, a disk O is restrained by a linear spring along the lateral direction, and the rotational motions are described by using the variable Φ . The external force and the drive torque are represented by F_{ext} and τ_{ext} , respectively. Point P of the disc makes contact with the point Q on the ground. The friction force acting at this point is represented by F_s and friction associated torsion

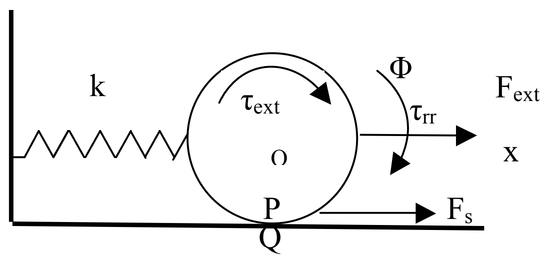

Figure 6. Simultaneous rub and roll of flexibly connected disk.

resistance is represented by τ_{rr} in the model of this system. To obtain representative numerical results, the disk is chosen to have a mass of 1Kg and a radius of 0.2m, the spring stiffness is chosen as 1 N/m, the rotational friction coefficient is chosen to be equal to 0.02, and the sliding friction force coefficient is given a value of 0.2. The generated results are shown in Figure 7, when the system is excited by a ramp force, which reaches a peak value of 2.5 N in 10 seconds. It is clear from the results that the system displays rolling motion along with sliding after 0.78 seconds or so, after the rolling resistance is overcome. There is also pure sliding after 7.8 seconds. The system returns to an oscillatory state, after removal of the external loading. Based on this fundamental study, such interactions can be expected in the drill-string system.

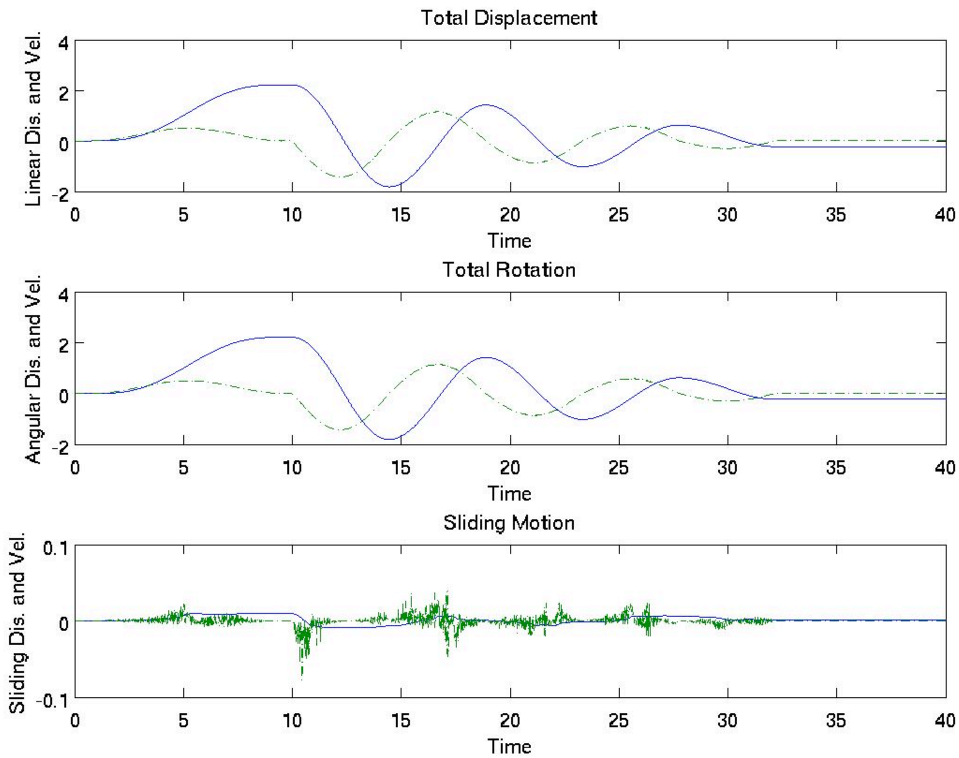

Figure 7. Response of the disk subjected to ramp force excitation: (a) total travel distance of the disc, (b) rotation of the disc, and (c) sliding of the disc. Solid lines are used to depict the displacement responses and dashed lines are used to represent the velocity responses.

3.4 Concluding Remarks and Future Work

In this phase of the project, torsion and lateral response characteristics of the drill string system have been examined experimentally and numerically. Good agreement is observed between the experimental results and the results obtained from the reduced-order models.

4. Difficulties Encountered/Overcome

None to report.

5. Planned Project Activities for the Next Quarter

Fundamental studies into stick-slip interactions have been initiated. These studies will be continued in future studies along with the experimental work and analysis and simulations with the reduced-order models.

Appendix

Approach

A combined analytical, numerical, and experimental approach is being pursued at the University of Maryland and the Petroleum Institute. Specifically, the drill string is being modeled as a reduced-order nonlinear dynamical system. Appropriate attention is also to be paid to the interactions with the environment. The experiments at UMD and PI are tailored to address specific aspects of the drill-string dynamics as well as complement each other. Actuator and sensor choices are also to be explored to determine how best to control the system dynamics. The studies will be initiated with drill strings located on fixed platforms, and later extended to systems located on floating platforms.

Three-Year Schedule

Phase II:

January 1, 2009 to December 31, 2009: Carry out quantitative comparisons between experimental results and predictions of reduced-order models for open-loop studies; understand stick-slip interactions and explore continuum mechanics based drill-string models for fixed platform environments and experimental results; examine different configurations including horizontal drilling

January 1, 2010 to December 31, 2010: Construct control schemes; carry out experimental, analytical, and numerical studies; and identify appropriate schemes; study horizontal drilling configurations through experiments and analysis; initiate drill-string models for off-shore environments including floating platforms

January 1, 2011 to December 31, 2011: Carry out experiments, analysis, and numerical efforts with a focus on drill-string operations in off-shore environments.

Key References

[1] Akgun, F. 2004, "A Finite Element Model for Analyzing Horizontal Well BHA Behavior," J. of Petrol. Sci & Eng., Vol. 42, pp. 121-132.

[2] Bednarz, S., 2004, "Design and Exploitation Problems of Drill Strings in Directional Drilling," Acta Montanistica Slovaca, Vol. 9, pp. 152-155.

[3] Downtown, G., 2009, "*New Directions in Rotary Steerable Drilling*", Oilfield Review, pp. 18-29.

[4] Leine, R. I., van Campen, D. H., and Keultjes, W. J. G. (2002). "Stick-Slip Whirl Interaction in Drill String Dynamics," *ASME Journal of Vibration and Acoustics*, Vol. 124 (2), pp. 209-220.

[5] Liao, C.-M., Balachandran, B., and Karkoub, M., (2009). "Drill-String Dynamics: Reduced Order Models," To appear in Proceedings of ASME IMECE 2009, Nov. 13-19 Lake Buena Vista, FL, USA, 2009; Paper No. IMECE2009-10339.

[6] Melakhessou, H., Berlioz, A., and Ferraris, G. (2003). "A Nonlinear Well-Drillstring Interaction Model," *ASME Journal of Vibration and Acoustics*, Vol. 125, pp. 46-52.

[7] Mihajlović, N., van Veggel, A. A., van de Wouw, N., and Nijmeijer, H. (2004) "Analysis of Friction-Induced Limit Cycling in an Experimental Drill-String System," *ASME Journal of Dynamic Systems, Measurement, and Control*, Vol. 126(4), pp. 709-720.

[8] Mihajlović, N., van de Wouw, N., Rosielle, P.C.J.N., and Nijmeijer, H. (2007) "Interaction between torsional and lateral vibrations in flexible rotor systems with discontinuous friction," *Nonlinear Dynamics*, Vol. 50, pp. 679-699.

[9] Nayfeh, A. H. and Balachandran, B. (1995). *Applied Nonlinear Dynamics: Analytical, Computational, and Experimental Methods*, Wiley, New York.

[10] Spanos, P. D., Chevallier, A. M., Politis, N. P., and Payne, M. L. (2003). “Oil and Gas Well Drilling: A Vibrations Perspective,” *Shock and Vibration Digest* Vol. 35(2), pp. 85-103.
[11] Short, J. A. “Introduction to Directional and Horizontal Drilling ” Pennwell Pub, 1993.

Studies on Mobile Sensor Platforms

UMD Investigators: Balakumar Balachandran, Nikil Chopra
PI Investigator: Hamad Karki, Sai Cheong Fok
GRAs: Hesham Ishmail (to start in Fall 2009)
Start Date: April 2009

1. Objective/Abstract

Mobile sensor platforms can be employed in a variety of operations, including environmental and structural health monitoring operations in harsh and remote environments. In the proposed work, cooperating sensor platforms will be studied for potential use in oil storage tanks, which are periodically tested for corrosion, cracks, and leaks. These platforms are envisioned for estimating geometrical profile parameters such as, for example, the tank bottom thickness. To this end, a simultaneous localization and mapping (SLAM) algorithm for cooperating sensor platforms operating in harsh environments will be investigated. Although one can use a single sensor system to carry out a geometrical profile measurement in a large structure, cooperating platforms can provide redundancy to sensor failures as well as superior localization and mapping capabilities. Although the SLAM problem has been studied in open terrestrial and aerial environments (e.g., Durrant-Whyte and Bailey, 2006), the same is not true for environments such as those encountered in an oil tank (e. g., Sogi *et al*., 2000). These submerged environments pose a significant challenge due to the complex dynamics of the sensor platforms, as well as related issues of motion control, cooperative path planning, and information fusion.

The overall objective of this project will be to carry out a combined analytical, numerical, and experimental effort to develop mobile sensor platforms and appropriate simultaneous localization and mapping (SLAM) algorithms for cooperative sensor platforms to operate in harsh environments. Research objectives are the following: i) develop SLAM algorithms based platforms taking into account system constraints such as constrained communications, the type of sensors considered, allowable dynamics, and factors such as sensor failures and reliability of the considered sensors, and ii) carry out experimental and supporting simulation studies using mobile platform test platforms at the University of Maryland and the Petroleum Institute.

2. Deliverables for Completed Quarter

- A numerical simulation was carried out to examine the extended Kalman filter SLAM algorithm.
- PI faculty investigator, Prof. Karki, visited ADCO to get a better understanding of the inspection system, the ultrasonic and magnetic flux sensors used as a part of the inspection system, the harshness of the environment, and the complexity of it

3. Summary of Project Activities for the Completed Quarter

In this section, results obtained through numerical simulations to gain fundamental insights are presented along with some details collected through visits to industry.

3.1 Numerical Simulation Results

A numerical simulation was carried out to examine the ***extended Kalman filter (***EKF) SLAM algorithm with the following kinematic model of a mobile sensor platform (see Figure 1), which can be used to describe the translations in a plane and rotation in this plane. This first-order system is written as

$$\begin{Bmatrix} \dot{x} \\ \dot{y} \\ \dot{\phi} \end{Bmatrix} = \begin{Bmatrix} v\cos\phi \\ v\sin\phi \\ v/L \tan\alpha \end{Bmatrix}$$

where *x* and *y* are the Cartesian coordinates associated with the sensor platform, α is the steering angle, ϕ is the angle that the moving platform makes with the x direction, v is the speed of the sensor platform along the direction of motion, and *L* is the distance between the front and the rear wheels. The observation (sensor) model is given by

$$\begin{bmatrix} z_r \\ z_\beta \end{bmatrix} = \begin{bmatrix} \sqrt{(x_i - x)^2 + (y_i - y)^2} \\ \tan^{-1}\left(\dfrac{y_i - y}{x_i - x}\right) - \phi + \dfrac{\pi}{2} \end{bmatrix}$$

where z_r and $z_ß$ are the object range and the heading angle, respectively, and (x_i, y_i) are the coordinates of a location or landmark to be mapped.

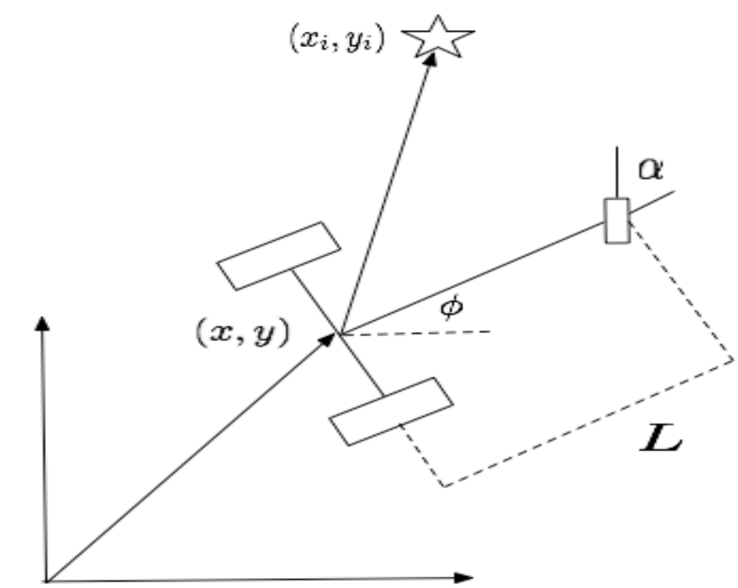

Figure 1. Conceptual illustration of mobile sensor platform.

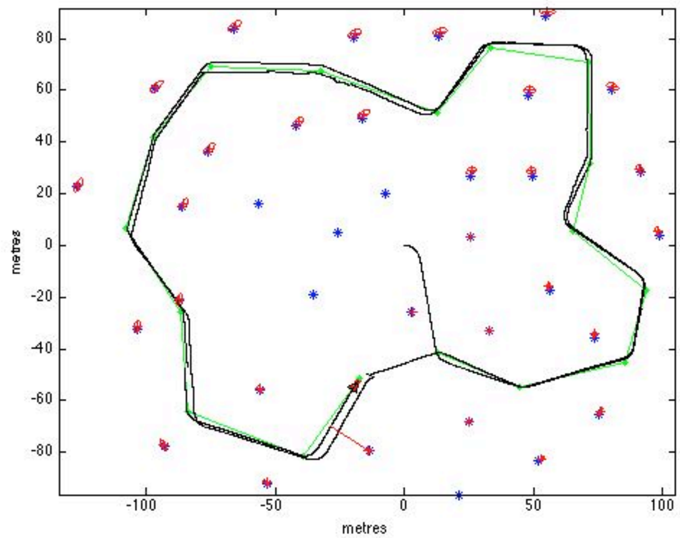

Figure 2. Results with low noise in range sensing. Good localization and mapping are realized even with noise in sensor information.

Both the kinematics and the sensor information can have noise in them. To understand how this noise can affect the system performance, simulations were carried out for different levels of noise using widely publicly available MATLAB scripts for SLAM algorithms. As the numerical results presented next illustrate, noise can have deleterious effects on the estimation process for map building as well as for localization in the environment. With low noise levels, as seen in Figure 4.2, the path that the sensor platform actually tracks (in green) and what it believes it is tracking (in black) are relatively close. The blue stars indicate the landmarks, and the red objects indicate where the mobile sensor thinks the landmarks are in its map. As the noise levels are increased in the sensor and kinematics information (Figures 4.3-4.5), the level of uncertainty in the mobile sensor platform map and localization is increased.

As seen in Figures 3 to 5, with increasing noise in the sensor and eventually in the angular speed, there is divergence between the actual path of the mobile platform and its map. Additionally, there is localization error as well as imprecision in locating the positions of the landmarks. Hence, it is evident that with this particular SLAM algorithm, increasing noise leads to increased uncertainty in the system response.

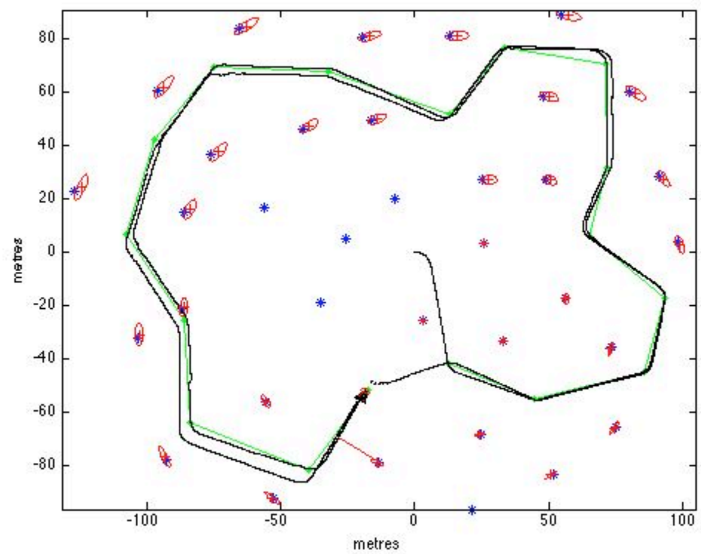

Figure 3. Results with high noise in range sensing.

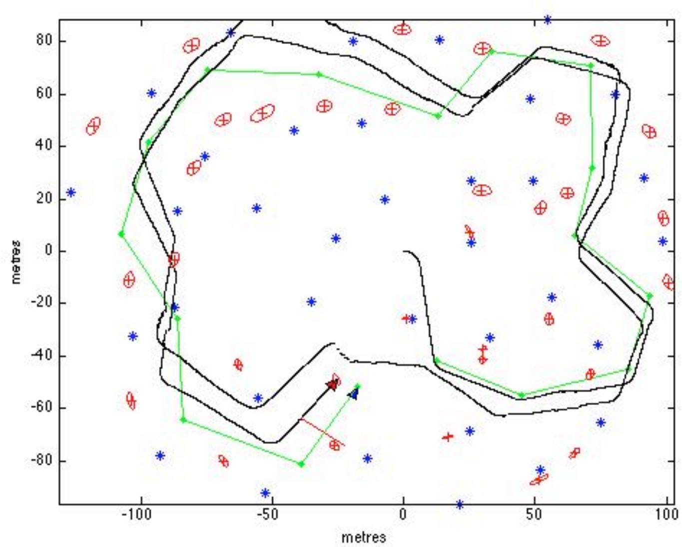

Figure 4. Results with high noise levels in range sensing and kinematics (angular speed) information.

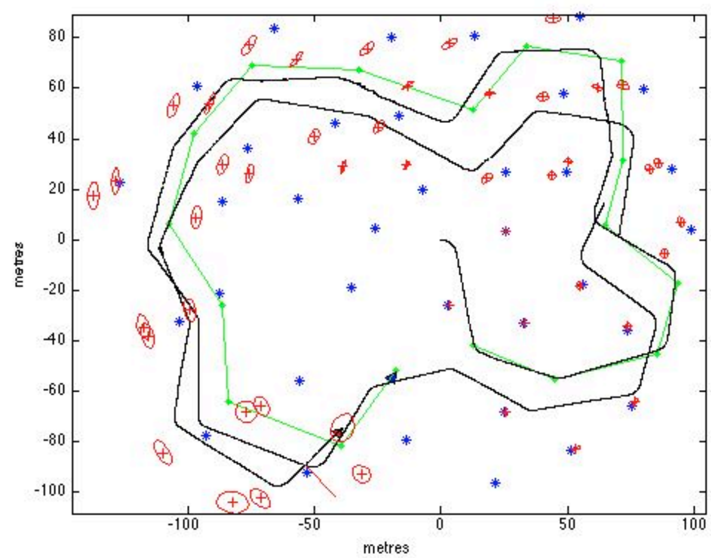

Figure 5. Results with high noise levels in kinematics information and low noise levels in sensor information.

The above numerical experiments will guide future physical experiments planned at the University of Maryland and the Petroleum Institute.

3.2 Visits to and Interactions with Industry

The graduate student who started at the University of Maryland this fall had started interactions with Abu Dhabi Oil Company for Onshore Operations (ADCO) earlier this year, and the investigators are examining this information to develop appropriate experimental arrangements. This month, the PI faculty investigator, Prof. Karki, visited ADCO to get a better understanding of the inspection system, the ultrasonic and magnetic flux sensors used as a part of the inspection system, the harshness of the environment, and the complexity of it.

4. Difficulties Encountered/Overcome

None to report.

5. Planned Project Activities for the Next Quarter

A graduate student from the Petroleum Institute, Mr. Hesham Ishmail, has recently joined the research group and will start working on the project from the next quarter. In the coming quarter, standard SLAM algorithms in the literature will be analyzed and numerically verified. The idea behind this approach is to identify the strengths and weaknesses of various algorithms and to analyze their suitability for use in fluid environments. The fluid environment constrains the motion of the sensor platform, while preventing use of common localizing devices such as the global positioning system. The acoustic medium constrains the inter-sensor platform communication and complicates the information fusion process. In addition, while most studies for SLAM have focused on single platforms, numerical verification will give useful insights into their extension for cooperating sensor platforms.

A scaled experimental setup is being planned at the University of Maryland. The setup will be based on data collected by the student (Section 4.2), during his undergraduate studies at PI. Once the scaling laws have been established, suitable underwater sensor platforms will be acquired and a scaled tank will be constructed. In collaboration with PI, appropriate sensing modalities for the sensor platform will also be studied.

Appendix

Approach

In the SLAM problem, one fundamentally seeks a solution where a sensor platform can incrementally develop a map of the unknown environment while simultaneously localizing itself within the map. In the particular problem at hand, while the topology of the oil tank floor may be well known, the map of tank thickness along the tank floor is an unknown map to be estimated by the sensor platform. The challenges are primarily due to the fluid environment, which constrains the motion of the sensor platform while preventing use of common localizing devices such as global positioning systems. The acoustic medium constrains the inter-sensor platform communication and complicates the information fusion process. These challenges will be addressed as part of the proposed approach, which is expected to evolve as a better definition of the problem is made. (Additional details are provided in Section 4.) Sensors that make use of wave physics (for example, acoustic emission sensors) will be studied along with other sensors for possible use in these mobile platforms. In addition, appropriate actuation mechanisms to realize the desired mobility of these platforms will also be investigated. The experimental test platforms to be developed as a part of the work will be used to examine and develop different mobile platform architectures.

Three-Year Schedule

Phase II:

April 1, 2009 to December 31, 2009: Carry out analytical and numerical investigations into SLAM algorithm-based mobile platforms for representative geometrical profile measurements, construction of experimental test platforms, and preliminary experimental findings

January 1, 2010 to December 31, 2010: Continue analytical, experimental, and numerical efforts, with focus on the development of appropriate communication and motion planning protocols for operations in harsh environments

January 1, 2011 to December 31, 2011: Continuation of experimental and numerical studies and formulation of recommendations for appropriate sensor and mobile platform configurations for use in oil tanks.

References

[1] Durrant-Whyte, H. and Bailey, T., 2006, “Simultaneous localization and mapping: part I," IEEE Robotics & Automation Magazine, Vol.13, no.2, pp. 99-110, June.

[2] Schempf, H., Chemel, B., and Everett, N., 1995, “Neptune: Above-ground storage tank inspection robot systems,” IEEE Robotics & Automation Magazine, pp. 9-15, June.

[3] Sogi, T., Kawaguchi, Y., Morisaki, H., Ohkawa, K., Kai, N., and Hayakawa, H., 2000, “Inspection robot for spherical storage tanks,” Industrial Electronics Society, IECON 2000. 26th Annual Conference of the IEEE, Vol. 1, pp. 393–398, 22-28 October.

[4] Thrun, S., 2002, Robotic mapping: a survey, School of Computer Science Report CMU-CS-02-111, Carnegie-Mellon University, Pittsburgh, PA, USA.

Development of a Probabilistic Model for Degradation Effects of Corrosion-Fatigue Cracking in Oil and Gas Pipelines

UMD Investigator: Mohammad Modarres
PI Investigators: Abdennour Seibi
GRA: Mohammad Nuhi

- **Objective/Abstract**

This research continues Phase-I mechanistic modeling of the *corrosion-fatigue* phenomenon for applications to pipeline health, risk and reliability management. The objective of this study is to perform additional mechanistic-based probabilistic models derived from physics of failure studies and validate them using the state-of-the-art experimental laboratory being developed at the PI as part of the Phase I of this study. Where possible, observed field data from ADNOC operating facilities will be used to supplement observations from the laboratory experiments based on the well-established Bayesian approach to mechanistic model updating and validation developed in Phase I. Uncertainties about the structure of the mechanistic models as well as their parameters will also be characterized and accounted for when such models are applied. The proposed models will allow the end-users (e.g., maintenance analysts and inspection crew) to integrate observed performance data from a wide range of pipelines and selected refinery equipment, such as pumps, compressors and motor-operated valves. Admitting the fact that modeling all degradation mechanisms would be a challenging undertaking, the proposed research will additionally address the following degradation phenomena related to the petroleum industry: pitting corrosion, stress cracking corrosion (SCC), and creep-fatigue

- **Approach**

The test rig, which is currently installed at UMD and is expected to be installed at PI later, will be used by the GRA, Mr. Mohammad Nuhi, to conduct an experimental study reflecting field conditions for model validation developed in EERC Phase I and II. The equipment needed would include corrosion test cells, autoclaves, multiphase flow loops, and testing machines for slow strain rate and crack-growth testing. This activity also requires a complete line of monitoring equipment for evaluation of corrosion, scaling, and chemical treatment for field and laboratory. This test rig will be a useful tool for teaching, research, and possibly training field engineers from operating companies.

- **Background**

A number of deterministic models have been proposed to assess reliability and life-remaining assessment of pipelines. Among these models is the ASME B31G code, which is most widely used for the assessment of corroded pipelines. However, these models are highly conservative and lack the ability to estimate the true life of the pipelines and other equipment used in the oil industry. To address this shortcoming one needs to develop a best-estimate assessment of the life (to assess reliability and risk imposed) by these structures and equipment and assess the uncertainties surrounding such estimates. The proposed probabilistic mechanistic models, when fully developed, would integrate the physics-of-failure of the leading failure degradation phenomena in the oil industry into the formal risk and reliability assessments. Such physical models will be validated using a state-of-the-art reliability assessment laboratory (being developed at PI). Uncertainties about the model structures and parameters will also be quantified. Such models will incorporate inspection data (characterizing limited and uncertain evidence). The rate of degradation is influenced by many factors such as pipeline materials, process conditions, geometry and location. Based on these factors, a best estimate of the structure (pipeline) or equipment (primarily valves, pumps and compressors) service life (reliability and remaining life) is to be calculated and uncertainties associated with the service life quantified.

This estimate would serve as a basis that guides decisions regarding maintenance and replacement practices.

Phase I of this research focused on developing a corrosion-fatigue model. It successfully proposed such a model and developed an advanced laboratory for testing this phenomenon at PI. The current research continues in the same line of research by investigating and developing additional degradation phenomena (SCC, pitting corrosion, and creep-fatigue) and integrates these phenomena with reliability and risk assessment through four different tasks. The long-term objective of this research is to develop a comprehensive library of probabilistic mechanistic models for all degradation phenomena pertinent to structures (piping, and pressure vessels) used in the oil industry.

- **Summary of Results**

The following tasks have been completed in the last three months:

Theoretical Investigation

A paper, entitled “A probabilistic physics of failure model for prognostic health monitoring of piping subject to pitting and corrosion fatigue,” has been revised and modified for submission to a journal. The developed model by Dr. M. Chookah has been further assessed and justified. Graphs, calculations, and results have been checked and modified. The computer programs written in MATLAB have been double-checked. WinBugs and Weibull analysis programs have been used again to add more data and further justify the results. The paper will be sent to the *Journal of Reliability Engineering and System Safety*.

The empirical model developed by Dr. Chookah that contains the critical environmental physical parameters of the load frequency (v), the applied stress load (σ), the temperature of the fluid (T), inside the pipe, and the corresponding corrosion current (I_p) of the fluid has the following:

$$
\begin{aligned}
&a = A \cdot (\sigma^{0.182} \cdot \nu^{-0.288} \cdot I_p^{\ 0.248}) \cdot N^{1/3} + B \cdot (\sigma^{3.24} \cdot \nu^{-0.377} \cdot I_p^{\ 0.421}) \cdot N^2 \cdot \exp[(4 \times 10^{-10} \cdot \sigma^{2.062} \cdot \nu^{0.024}) \cdot N] \\
&where: \\
&A = C_1 \cdot (\sigma^{0.182} \cdot \nu^{-o.288} \cdot I_p^{\ 0.248})^{-1}, \\
&B = C_2 \cdot (\sigma^{3.24} \cdot \nu^{-0.377} \cdot I_p^{\ 0.421})^{-1}, and \\
&\varepsilon = (4 \times 10^{-10} \cdot \sigma^{2.062} \cdot \nu^{0.024}).
\end{aligned}
$$

where A and B are constants which depend on material properties only. The proposed model in the above empirical model has two terms; the first term represents the pitting corrosion and the second term represents the fatigue enhanced by corrosion. Assuming a lognormal distribution to characterize crack-size uncertainty with a log-standard deviation of s, the Bayesian estimation model using WinBugs is used to combine prior information on A, B, and s along with the experimental data to arrive at posterior distributions of A, B, and s.

For example, assuming prior estimates of A and B discussed earlier along with a non-informative prior estimate of s, the posterior marginal distributions of A, B, and s were estimated using experimental data to build the likelihood function. In the following posterior, marginal distributions of A, B and s are shown assuming Weibull distributions for A, lognormal distributions for B, and s:

A = LN (μ_A = 9.34, s_A^* = 0.0062),

B = LN (μ_B = -34.52, s_B^* = 0.47), and

s = LN (μ_s = 1.50, s_s^* = 0.03)

The above posterior distributions were estimated in the WinBUGs Bayesian updating process given the experimental data and the appropriate distribution parameters. By changing frequency, corrosion current and loading stress (using harsher environment) for an application to the refinery data, it was shown that the loading stress is the dominant factor for the degradation of pipeline compared to the corrosion current and frequency.

While the distributions of A and B were obtained from the benchmark model, the underlying premise for the simplified model was based on field observations or experiments. For this reason pitting corrosion tests were performed in the Mechanical System PoF Laboratory at the University of Maryland. The experiment, which uses the CORTEST corrosion-fatigue equipment to apply a stress of 150 MPa, frequency of 0.0017Hz and at a temperature of 383K (110 ^{0}C), is now being completed. The test results from the specimen were evaluated according to the Johnson Equation using the direct current potential drop (DCPD) method. The plot of the data is show below in Figure 1.

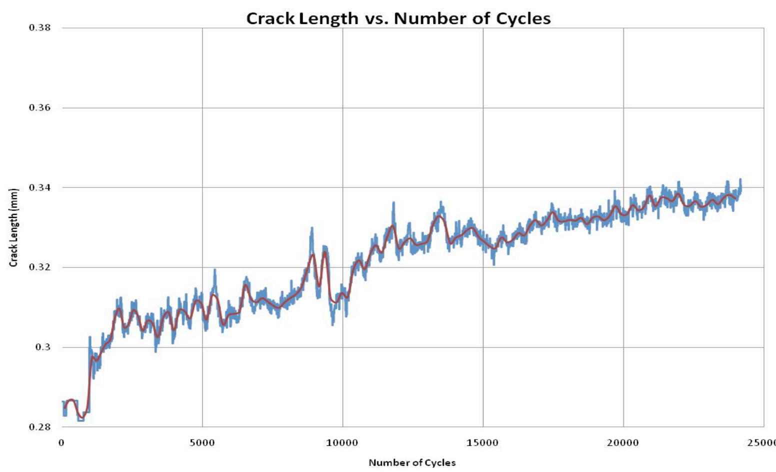

Figure 1. Crack length vs. number of cycle from Cortest corrosion-fatigue testing systems, in seawater of 250 ppm $Na_2S_2O_3$ -5H_2O at 383 K, and 150- MPa.

Two PI summer interns completed their study of pitting corrosion, and their report has been independently checked for accuracy. Following ongoing editing, it will be published at a conference proceeding (conference to be decided).

Corrosion experiments for estimation of pit depth and number of pit distribution were made on X70 carbon steel specimens for different chloride and H_2S concentrations. Specimens were prepared in part by the physics workshop and in part by two students from the PI. The material science laboratory at the University of Maryland was used to evaluate the results. The first step involved building a model for pitting size and distribution. These experiments were made by two PI students in a summer workshop task at the University of Maryland, conducted from the Reliability department. The experiments were focused mainly on measuring the pit depth, pit density and the mass loss after exposing the samples to different corroding environments with different concentrations and different time periods. The experiments were divided into three main stages, performed in 5, 10 and 24-hour periods, and in each period, the test was done using approximately five different chloride and H_2S concentrations of 100ppm, 150ppm, 200ppm, 300ppm and 400ppm.

The following results were estimated from the experiments:

- Pit depths increased with the concentration, according to a power law and with times according to the $t^{1/3}$-law (justified by the literature [10]).
  Pit depths followed Weibull distributions.
- Pit densities followed the lognormal distributions.

Literature surveys of creep and stress corrosion cracking (SCC) degradation mechanisms are 80% completed and will be classified for finding the relevant models. Identification of the generic form of the physics of failure model for these two mechanisms is under way.

Experimental Investigation

1. Pitting corrosion experiments were made in a small-scale corrosion-fatigue chamber that has been designed, made and tested for Dog-bone specimens and checked for its workability in a corrosion-fatigue experiment for an aluminum prototype sample. Another more sophisticated test is designed for CT-specimens and will be tested in Q3 of this research.
2. Information about requirements for a heating chamber for creep experiments has been gathered from supplier and manufacturers; the most appropriate supplier will be chosen for the laboratory in Q3.
3. The Cortest rig was used to run an additional experiment to further verify and reduce epistemic uncertainties associated with the corrosion-fatigue model developed by Dr. M. Chookah.

Near Future Plans:

1. Develop the mechanistic models (PoF models) for creep-fatigue and SCC.
2. Design a corresponding simulation tool to help both model development and field applications after classifying the models and choosing the appropriate one.
3. Expand the UMD PoF-based laboratory to include creep capabilities. A Plexiglas chamber designed (outside of this project) by Mr. Nuhi and Dr. Modarres will be installed on the MTS machines in the PoF laboratory.
4. Prepare the Cortest rig for shipment by the Cortest Corporation to PI.

5. Two-Year Schedule

This project involves three distinct tasks. The first task is the development of the mechanistic models, development of a corresponding simulation tool to help both model development and field applications. The second task focuses on experimental activities to generate relevant data to validate the proposed models of Task 1. Finally, the third task involves the actual validation of the models proposed in Task 1 with the experimental results obtained in Task 2, including Bayesian estimation of the model parameters.

Task 1: Develop the best estimate mechanistic (physics of failure) empirical models for pitting corrosion, SCC, and fatigue-creep. The model development involves the following activities.

Task1.1: Gather, review and select most promising physics-of-failure based methods and algorithms proposed in the literature.

- Literature surveys for creep and stress corrosion cracking (SCC) degradation mechanisms are almost completed and will be classified for finding the relevant models (80% done).

Task1.2: Select, develop or adopt a detailed mechanistic model (one deterministic model for each phenomenon) that properly describes the degradation process.

- Development of the mechanistic models and of a corresponding simulation tool to help both model development and field applications after classifying the models and choosing the appropriate will be done in the near future (20% complete).

Task 1.3: Develop a Monte-Carlo based mathematical simulation routine on Matlab depicting the detailed mechanistic model of each degradation phenomenon (far faster than real-time).

- This was completed for the empirical model developed based on the works of the PI interns for pitting corrosion. After proposing the similar models for SCC and creep-fatigue, it will be repeated (30% completed).

Task 1.4: Based on the results of the simulation, a simplified empirical model that best describes the results of simulation will be proposed. Such a model relates the degradation (e.g., depth of the pit or the crack growth rate) to applied loads, such as pipeline internal pressure and chemical composition of the product inside the pipeline, as a function of time or cycle of load application.

- This part is completed for the pitting corrosion and corrosion-fatigue, but further work will be done for the other failure mechanisms (30% complete).

Task 2: A PoF reliability analysis laboratory has been designed and being developed at PI. Currently, the advanced corrosion-fatigue purchased by the PI was installed at the University of Maryland (the Cortest Rig) is being prepared for shipment to PI.

Task 2.1 Completing the remaining corrosion-fatigue tests being conducted by Mr. Nuhi and Chookah. (100% Completed)

Task 2.2 Pitting corrosion experiments (develop test plan, prepare samples and the facility, perform the test, and evaluate the test results) (100% Completed).

Task 2.3 SCC Experiments (develop test plan, prepare samples and the facility, perform the test, and evaluate the test results). (Not started yet)

- This task will be performed in the near future. The SCC specimen holders are being designed according to the recent patents and ASTM standards. They will be fabricated in the physics workshop of the University of Maryland.

Task 2.4 Creep-Fatigue Experiments (develop test plan, prepare samples and the facility, perform the test, and evaluate the test results). (10% completed)

- A small-scale corrosion-fatigue (or creep) chamber has been designed (not as part of this project), fabricated and tested for dog-bone specimens and checked for its workability on the UMD MTS machines using an Aluminum alloy sample. Another more sophisticated one is being designed for CT-specimens and will be tested in the near future.
- Information about heating chambers for creep experiments has been gathered from supplier and manufacturers; the most appropriate one is going to be chosen for the laboratory.

Task 3: This task involves modification, advancement and use of the WinBugs' Bayesian formalism for model validation using experimental data and integration of the field data and information including sensor-based data (acoustics and/or optical) to update the empirical models and estimate the remaining life of oil pipelines and structures. (30% Complete)

- The WinBugs' Bayesian formalism for model estimation and validation was developed as part of Dr. Chookah's work. This formalism is being updated and new applications of the formalism have been performed using past experimental data and new data on corrosion-fatigue obtained since the departure of Dr. Chookah. Further work with this software for integration the experimental data will be done in future.

6.Schedule/Milestones/Deliverables

Tasks 1.1-1.3 (5/1/09-12/15/09)
Task 1.4 (12/15/09-3/1/10)
Task 2.1 (completed 7/1/09)
Task2.2 (7/1/09-12/15/09)
Task 2.3 (12/15/09 – 6/1/10)
Task 2.4 (6/1/10-2/1/11)
Task 3 (12/15/09-3/15/11)

The project is ahead of schedule and there is no issue or delay at this point.

7. Visits

- Dr. A.Seibi visited UMD in July 2009.
- Two PI students, Abdullah Al Tamimi and Mohammad Abu Daghah, took parts at summer internship (2009).
- Dr. M. Chookah successfully defended and completed his PhD degree in Mechanical Engineering at the University of Maryland.

8. Papers Published and prepared for publishing by the Team

1- M. Chookah, M. Nuhi, and M. Modarres, "Assessment of Integrity of Oil Pipelines Subject to Corrosion-Fatigue and Pitting Corrosion," presented by Prof. Modarres at the International Conference of Integrity- Reliability-Failure (IRF) in Porto, Portugal, July 20-24 2009**.** (The cost of the conference and associated travels was not covered by EERC)
2- M. Chookah, M. Nuhi, and M. Modarres, A. Seibi "A Probabilistic Physics of Failure Model for Prognostic Health Monitoring of Piping Subject to Pitting and Corrosion –Fatigue" is sent for publication to the "Journal of Reliability Engineering and System Safety."
3- A paper on "Development of a Database of Mechanistic Models of Failure for Application to Pipeline and Equipment Risk, Reliability and Health Management (Pitting Corrosion- Pit Depth and Density)," is being prepared for publication at a conference. We are studying the possibility that the PI interns present the paper.

Appendix

Justification and Background

A number of deterministic models have been proposed to assess reliability and life-remaining assessment of pipelines. Among these models is the ASME B31G code, which is most widely used for the assessment of corroded pipelines. However, these models are highly conservative and lack the ability to estimate the true life of the pipelines and other equipment used in the oil industry. To address this shortcoming, it is necessary to develop a best-estimate assessment of the life (to assess reliability and risk imposed) of these structures and equipment and to assess the uncertainties surrounding such estimates. The proposed probabilistic mechanistic models, when fully developed, would integrate the physics of failure of the leading failure degradation phenomena in the oil industry into the formal risk and reliability assessments. Such physical models will be validated using a state-of-the-art reliability assessment laboratory (being developed at PI). Uncertainties about the model structures and parameters will also be quantified. Such models will incorporate inspection data (characterizing limited and uncertain evidence). The rate of degradation is influenced by many factors, such as pipeline materials, process conditions, geometry and location. Based on these factors, a best estimate of the service life (reliability and remaining life) of the structure (pipeline) or equipment (primarily valves, pumps and compressors) is to be calculated and uncertainties associated with the service life quantified. This estimate will serve as a basis for decisions regarding maintenance and replacement practices.

Phase I of this research focused on developing a corrosion-fatigue model. It successfully proposed such a model and developed an advanced laboratory for testing this phenomenon at PI. The current research continues in the same line of research by investigating and developing additional degradation phenomena (SCC, pitting corrosion, and creep-fatigue) and integrates these phenomena with reliability and risk assessment through four different tasks. The long-term objective of this research is to develop a comprehensive library of probabilistic mechanistic models for all degradation phenomena pertinent to structures (piping and pressure vessels) used in the oil industry.

Approach

The test rig, which is installed at UM, will be used by the GRA, Mr. Mohammad Nuhi, to conduct an experimental study reflecting field conditions for the model validation developed in EERC Phases I and II. The equipment needed would include corrosion test cells, autoclaves, multiphase flow loops, and testing machines for slow strain-rate and crack-growth testing. This activity will also require a complete line of monitoring equipment for evaluation of corrosion, scaling, and chemical treatment for the field and laboratory. This test rig will be a useful tool for teaching, research, and possibly training field engineers from operating companies.

Phase II Two-Year Schedule

This project involves three distinct tasks. The first task is to develop the mechanistic models, and develop a corresponding simulation tool to help both model development and field applications. The second task focuses on experimental activities to generate relevant data to validate the proposed models of Task 1. Finally, the third task involves the actual validation of the models proposed in Task 1 with the experimental results obtained in Task 2, including Bayesian estimation of the model parameters.

Task 1: Develop the best estimate mechanistic (physics of failure) empirical models for bulk corrosion, SCC, and fatigue-creep. The model development involves the following activities.
Task1.1: Gather, review and select the most promising physics of failure-based methods and algorithms proposed in the literature.
Task1.2: Select, develop or adopt a detailed mechanistic model (one deterministic model for each phenomenon) that properly describes the degradation process.
Task 1.3: Develop a Monte Carlo-based mathematical simulation routine on Matlab depicting the detailed mechanistic model of each degradation phenomenon (far faster than real-time).
Task 1.4: Based on the results of the simulation, propose a simplified empirical model that best describes the results of the simulation. Such a model will relate the degradation (e.g., depth of the pit or the crack growth rate) to applied loads such as pipeline internal pressure and chemical composition of the product inside the pipeline, as a function of time or cycle of load application.

Task 2: A physics of failure-based reliability analysis laboratory has been designed and is being developed at PI. Currently, the advanced corrosion-fatigue purchased by the PI was installed at the University of Maryland and will be used at UMD until the lab at PI is ready and the ongoing experiments of Phase I end. The CORTEST test equipment includes corrosion test cells, autoclaves, multiphase flow loops, and testing machines for slow strain rate and crack-growth testing. While the test rig can be used for the additional failure phenomena, the following equipment should be added to the laboratory to allow model development and validation tests for the new phenomena:
i) Slow strain-rate test systems with constant extension rate tests from 10^{-5} to 10^{-8} in/sec, including a variety of environmental chambers and controls.
ii) Sensors for measuring corrosion load: steam, pH, O_2, H_2 and other measurements.
iii) High-pressure autoclaves for handling high pressure tests (up to 5,000 psi and 600°F).
iv) Advanced data acquisition systems.
Task 2.1 Complete the remaining corrosion-fatigue tests being conducted by Mr. Nuhi and Mr. Chookah.
Task 2.2 Perform pitting corrosion experiments (develop test plan, prepare samples and the facility, perform the test, and evaluate the test results)
Task 2.3 Perform SCC experiments (develop test plan, prepare samples and the facility, perform the test, and evaluate the test results)
Task 2.4 Perform creep-fatigue experiments (develop test plan, prepare samples and the facility, perform the test, and evaluate the test results)

Task 3: This task involves modification, advancement and use of the WinBugs Bayesian formalism for model validation using experimental data and integration of the field data and information, including sensor-based data (acoustics and/or optical), to update the empirical models and estimate the remaining life of oil pipelines and structures.

Tasks 1.1-1.3 (5/1/09-12/15/09);
Task 1.4 (12/15/09-3/1/10);
Task 2.1 (completed 7/1/09);
Task2.2 (7/1/09-12/15/09);
Task 2.3 (12/15/09 – 6/1/10);
Task 2.4 (6/1/10-2/1/11);
Task 3 (12/15/09-3/15/11).

Visits Planned

A. Seibi visit UMD to attend Ph.D. defense of M. Chookah and research planning 7/5/09-7/13/09.
M. Modarres visit to PI 10/09
M. Chookah visit UMD 12/09
M. Modarres visits PI 3/10
M. Chookah and A. Seibi visit UMD 6/10

M. Modarres Attends PI Workshop 11/10

Phase I Publications

1. Submitted paper titled "Development of a Probabilistic Model for Mechanistic Evaluation of Reliability of Oil Pipelines Subject to Corrosion-Fatigue Cracking" for presentation & publication in the "ASME DAC 2008" conference to be held in New York, NY in the period 3-6 Aug 2008. (paper presented and published in the conference proceedings).

2. Submitted paper titled "Development of a Probabilistic Model for Mechanistic Evaluation of Reliability of Oil Pipelines Subject to Corrosion-Fatigue Cracking" "Probabilistic Safety Assessment & Analysis (PSA) 2008" conference, Knoxville, Tennessee 7-11 Sep 2008. (paper presented and published in the conference proceedings).

3. A poster is exhibited at the "PHM-International Conference on Prognostics and Health Management (affiliated with the IEEE Reliability Society)" Denver, CO, in October 2008. (presented).

4. A poster is exhibited at the "Second International Energy 2030 Conference" Abu Dhabi, UAE, from 4-5 November 2008.

Phase I Visits

1. M. Modarres visited PI in March 2-5, 2007 to discuss the Phase I research with Dr. Seibi and meet other PI faculty.

2. Mohamed Chookah visited Ruwais & Abu Dhabi Refineries of Takreer to collect data in Oct 2007. He also visited PI to meet Dr. Seibi to discuss the data collection process.

3. Dr. Modarres and M. Chookah participated in the first Energy Education and Research Collaboration (EERC) Workshop held at the PI in Abu Dhabi from 4-5 January, 2008.

4. Dr. Seibi was hosted in Nov 2007 to attend M. Chookah’s Ph.D. thesis proposal and discuss the project's different aspects.

5. Dr. Seibi visited UMD in Sept 2008 to discuss the latest progress in the project and finalize the testing equipment shipment destination to UMD.

References

[1] Harlow, D. G., and Wei, R. P. (1993). A Mechanistically Based Approach to Probability Modeling for Corrosion Fatigue Crack Growth. *Engineering Fracture Mechanics*, 45, 1, 79-88.

[2] Wei, R. P., and Harlow, D. G. (2005). Mechanistically Based Probability Modeling, Life Prediction and Reliability Assessment. *Modeling Simulation Material Science Engineering*, 13, R33-R51.

[3] Harlow, D. G., and Wei, R. P. (2001). Probability Modeling and Statistical Analysis of Damage in the Lower Wing Skins of Two Retired B-707 Aircraft. *Fatigue Fracture Engineering Material Structure*, 24, 523-535.

[4] Wei, R. P., Masser, D., Liu, H., and Harlow, D. G. (1994). Probabilistic Considerations of Creep Crack Growth. *Material Science and Engineering*, A189, 69-76.

[5] Wei, R. P. (2001). A Model for Particle Induced Pit Growth in Aluminum Alloys. *Scripta Materialia*, 44, 2647-2652.

[6] Dolley, E. J., Lee, B., and Wei, R. P. (2000). The Effect of Pitting Corrosion on Fatigue Life. *Fatigue Fracture Engineering Material Structure*, 23, 555-560.

[7] Wei, R. P. (2002). Environmental Considerations for Fatigue Cracking. *Fatigue & Fracture of Engineering Materials & Structures*, 25, 8/9, 845-854.

[8] Trethewey, K. R., and Chamberlain, J. (1995). Corrosion for Science and Engineering. Longman, England.

[9] Harlow, D. G., and Wei, R. P. (1994). Probability Approach for Prediction of Corrosion and Corrosion Fatigue Life. *AIAA Journal*, 32, 10, 2073-2079.

[10] Kondo, Y. (1989). Prediction of Fatigue Crack Initiation Life Based on Pit Growth. *Corrosion*, 45, 7-11.

[11] Atkins, P. W. (1994). Physical Chemistry. W. H. Freeman and Company, NY.

[12] Dowling, N. E. (1993). Mechanical Behavior of Materials. Prentice Hall, NJ.

[13] Wei, R. P., and Gao, M. (1983). Reconsideration of the Superposition Model for Environmentally Assisted Fatigue Crack Growth. Scripta Metallurgica, 17, 959-962.

[14] State Structures Research Laboratory, and State Materials Office – Corrosion Research Laboratory (2002). Galvanic Testing of Stressed Strands Inside Carbon Steel Pipe – Final Report. Florida Department of Transportation.

[15] H.N. Chen, L.S. Chen, Q.H. Lin and X. Long, *Corrosion* **55** (1999), p. 626.

[16] A. Pardo, E. Otero, M.C. Merino, M.D. López, M.V. Utrilla and F. Moreno, *Corrosion* **56** (2000), p. 411.

[17] M. Romero, Z. Duque, O. Rincón, O. Pérez, I. Araujo and A. Martinez, *Corrosion* **56** (2000), p. 867.

[18] I.B. Singh, *Corrosion* **57** (2001), p. 483.

[19] T. Laitinen, *Corros. Sci.* **42** (2000), p. 421.

[20] G. Gabetta, *Corrosion* **53** (1997), p. 516.

[21] K. Yamakawa and R. Nishimura, *Corrosion* **55** (1999), p. 24.

[22] R.C. Sierra, E. Sosa, M.T. Oropeza and I. González, *Electrochim. Acta* **47** (2002), p. 2149.

[23] R.A. Carneiro, R.C. Ratnapuli and V.F.C. Lins, *Mater. Sci. Eng. A* **357** (2003), p. 104.

[24] G.M. Omweg, G.S. Frankel, W.A. Bruce, J.E. Ramirez and G. Koch, *Corrosion* **59** (2003), p. 640.

[25] F.D. Moraes, F.L. Bastina and J.A. Ponciano, *Corros. Sci.* **47** (2005), p. 1325.

[26] C. Ren, D. Liu, Z. Bai and T. Li, *Mater. Chem. Phys.* **93** (2005), p. 305.

[27] A.N. Kuzyukov, Y.Y. Nikhayenko, V.A. Levchenko, V.A. Borisenko and V.G. Moisa, *Int. J. Hydrogen Energy* **27** (2005), p. 813.

[28] Y.Y. Chen, Y.M. Liou, H.C. Shih., "Stress corrosion cracking of type 321 stainless steels in simulated etrochemical process environments containing hydrogen sulfide and chloride," *Materials Science and Engineering*, **A 407**, pp.114–126, (2005).

[29] Gutzeit, J. et al. Corrosion in Petroleum Refining and Petrochemical Operations. *Metals Handbook*, 9th Ed., **13**, Corrosion Metals Park, Ohio 44073.

[30] Gutzeit, J. (2000). Effect of Organic Chloridecontamination of Crude Oil on Refinery Corrosion. *Corrosion*, Paper No. 00694.
[31] www.nace.org/nacestore/assets/ConferencePapers/2000/00694.pdf
[32] Lin, C. J., et,al. Scanning Micoelectrode Studies of Early Pitting Corrosion of 18/8 Stainless Steel,Corrosion, Vol 54, No.4, pp.265-270.
[33] Chapter 9. Pitting Corrosion, KAIST, http://corrosion.kaist.ac.kr
[34] Andijani, I., ,et.al. (1999). Studies on corrosion of carbon steel in deaerated saline solutions in presence of scale inhibitor. Presented at the WSTA IV Golf Conference, Bahrain.
[35] Petek, A., et.al. (2007). Localized Dissolution Kinetics of Low Carbon Steel. *Acta Chim Slov*. 54, pp 725-729.
[36] Huisert, M. Electrochemical Characterisation of Filiform. Corrosion on Aluminium Rolled Products. www.iospress.nl/html/9789040722363.php
[37] Joseph, C., Farmer, et.al. (1997) Crevice Corrosion & pitting of High-Level Waste Containers: Integration of Deterministic & Probabilistic Models, UCRL_JC_127980 Part 1.
[38] Sardisco, J. B., ,et.al. (1965). Corrosion of iron in an H_2S-CO_2-H_2O system composition and protectiveness of the ssulfide film as a function of pH. *Corrosion*, Vol 21, pp 350-354.
[39] Brossia, C. S., and Cragnolino, G. A. (2000). Effect of EnvironmentalVariables on localized Corrosion of Carbon Steel. *Corrosion*, Vol 56, No 5, pp 505-514.
[40] Mack, L. P., ,et.al. (1984). Effect of Bromide Ions on the Electrochemical Behavior of Iron. *Corrosion*, Vol 40, No 5.
[41] Sorell, G., and Hoyt, W. B., (1956). Collection and Correlation of High Temperature Hydrogen Sulfide Corrosion Data. The 12th Annual NACE Conference. The M. W. Kellogg Co., New York, N. Y.
[42] Corrosion Doctors (2008). Corrosion Rate Conversion. http://corrosion-doctors.org/Principles/Conversion.htm
[43] Shannon, D. W., and Boggs, J. E. (1958). Factors Affecting the Corrosion of Steel By Oil-Brine-Hydrogen Sulfide Mixtures. NACE, Vol. 15, pp. 299t-302t.
[44] Shannon, D. W., and Boggs, J. E. (1958). An Analytical Procedure for Testing the Effectiveness of Hydrogen Sulfide Corrosion Inhibitors. NACE, Vol. 15, pp. 303t.
[45] Carroll, J. J. (1998). Software for Phase Equilibria in Natural Gas-Water Systems, A Discussion of the Effect of pH on the Solubility of Hydrogen Sulfide. AQUAlibrium, http://www.telusplanet.net/public/jcarroll/ION.HTM.
[46] Backnesto, E. B., Drew, R. E., and Stapleford, C. C. (1956). High Temperature Hydrogen Sulfide Corrosion. Corrosion, Vol. 12, No. 1, pp. 22-31.
[47] Ma, H.Y., Cheng, X.L., Chen, S.H., Li, Chen, G.Q., X., Lei, S.B., and Yang, H.Q. (1998). Theoretical Interpretation on Impedance Spectra for Anodic Iron Dissolution in Acidic Solutions Containing Hydrogen Sulfide. CORROSION–Vol. 54, No. 8.
[48] Lauvstad, G. Ø. (2007). BREAKDOWN IN PASSIVITY OF AUSTENITIC STAINLESS STEELS IN Cl- AND H2S – MODELING AND CHARACTERIZATION OF THE PIT INITIATION PROCESS. NACE Corrosion. Paper No.07660.
[49] Wei, S., and Nesic S. (2007). A MECHANISTIC MODEL OF H2S CORROSION OF MILD STEEL. NACE Corrosion. Paper No. 07655.
[50] ASME-B31G (1991). Manual for Determining the Remaining Strength of Corroded Pipelines: A Supplement to ASME B31G Code For Pressure Piping. New York: American Society of Mechanical Engineers.
[51] Lee, O. S., Kim, D. H. and Choi, S. S. (2006). Reliability of Buried Pipeline Using A Theory Of Probability Of Failure. *Solid State Phenomena*, 110, 221-230.

Some additional references:

A- Modeling of the evolution of stress corrosion cracks from corrosion pits.

[1] Kondo Y. Corrosion 1989; 45:7.
[2] Wei RP. Material aging and reliability of engineered systems, in: Proceedings of conference on Environmentally Assisted Cracking: Predictive methods for risk assessment and

evaluation of material, equipment and structures, editor R.D. Kane, ASTM STP1401, 2000, pp. 3–19.
[3] Engelhardt G, Macdonald DD, Zhang Y, Dooley B. Power Plant Chem 2004;6:647.
[4] Engelhardt G, Macdonald DD. Corros Sci 2004; 46:2755.
[5] Turnbull A., McCartney LN, Zhou S. A deterministic model of pitting corrosion and the pit- to-crack transition, Corros Sci, in press, 2005.
[6] Zhou S, Turnbull A. Environment assisted cracking of steam turbine disc and blade steels—Description of test procedure and preliminary results, NPL Report MAT(C) A41, 2001.
[7] Zhou S, Turnbull A. Effect of Stress Transients on the Crack Propagation Rate in Steam Turbine Disc Steel, Corrosion, accepted for publication.
[8] Turnbull A., Zhou S, Orkney L, McCormick N. Visualisation of Stress Corrosion Cracks Emerging from Pits, Corrosion, submitted for publication.
[9] Turnbull A, Zhou A. Corros Eng Sci Technol 2003; 38:177.

B- Creep

[1] “Creep and stress rupture” www.materialsengineer.com/CA-Creep-Stress-Rupture.htm.
[2] Xiao-Chi Nin et.al.” Creep damage prediction of the steam pipelines with high temperature and high pressure. International Journal of Pressure Vessels and Piping 86 (2009) 593–598ure”.
[3] T.H. Hyde, A. Yaghi and M. Proctor, Use of the reference stress method in estimating the life of pipe bends under creep conditions, *Int J Press Vessels and Piping* **75** (2) (1998), pp. 161–169.
[4] W. Sun, T.H. Hyde, A.A. Becker and J.A. Williams, Comparison of the creep and damage failure prediction of the new, service-aged and repaired thick-walled circumferential CrMoV pipe welds using material properties at 640 °C, *Int J Press Vessels and Piping* **77** (7) (2000), pp. 389–398.
[5] W. Sun, T.H. Hyde, A.A. Becker and J.A. Williams, Steady-state creep reference rupture stresses for internally pressurised pipes for use in life prediction, *Int J Press Vessels and Piping* **79** (2) (2002), pp. 135–143.
[6] S.-T. Tu, R. Wu and R. Sandstrom, Design against creep failure for weldments in 0.5 Cr 0.5 Mo 0.25 V pipe, *Int J Press Vessels and Piping* **58** (3) (1994), pp. 345 – 354.
[7] J.M. Gong, S.T. Tu and X. Ling, Research of welding effect on creep damage of high temperature furnace tubes, *Key Eng Mat* **171–174** (2000), pp. 189–196.
[8] Chen JJ. Investigation of design criterion and welding repair principle of high temperature components using continuum damage mechanics based finite element method. Ms. D thesis. Nanjing University of Technology: Nanjing; 2002 [in Chinese].
[9] T.H. Hyde, W. Sun and J.A. Williams, Prediction of creep failure life of internally pressurized thick walled CrMoV pipes, *Int J Press Vessels and Piping* **76** (14–15) (1999), pp. 925–933.
[10] S.T. Tu, P. Segle and J.M. Gong, Creep damage and fracture of weldments at high temperature, *Int J Press Vessels and Piping* **81** (2) (2004), pp. 199–209.
[11] S.T. Tu, P. Segle and J.M. Gong, Strength design and life assessment of welded structures subjected to high temperature creep, *Int J Press Vessels and Piping* **66** (1–3) (1996), pp. 171–186.
[12] D.R. Hayhurst, P.R. Dimmer and C.J. Morrison, Development of continuum damage in the creep rupture of notched bars [J], *Philos Trans R Soc Lond* **A311** (1984), pp. 103–129.